

Nuclear and Radiation Physics

Dr D. Margarone

2021-2022

PRELIMINARIES

A. THE IMPORTANCE OF NUCLEAR PHYSICS

Nuclear physics, i.e. the study of the nucleus of the atom, is a fundamental discipline to understand the universe. Nuclear physics provides key answers both to problems from the infinitely small and the extremely large. Few examples are listed below:

- The nuclear strong force is one of the fundamental forces in nature.
- Nuclear fusion powers the stars, such as the Sun.
- Radioactivity warms the core of the Earth and has implication in the delaying the cooling process of the Earth and protection from solar wind (Earth magnetic field).
- Nuclear power plants, both fission and (potentially) fusion, are important energy production methods.
- Radiotherapy is important in cancer treatment and cancer diagnostics (imaging).
- Carbon dating, based on radioactive decay, is very useful in geology and palaeontology.

B. OBJECTIVES AND OUTCOMES

The objectives and learning outcomes for the nuclear physics part of the module are:

- Knowing the terminology and notation of nuclear physics.
- Understanding physical reasoning behind models of the nucleus.
- Understanding processes such as radioactive decay, fission, fusion.
- Becoming aware of applications of nuclear physics in science, technology, and medicine.

C. SYLLABUS

1. Nuclear Properties
2. The Inter-Nucleon Potential
3. Nuclear Models
4. Nuclear Decays and Reactions
5. Interaction of Radiation with Matter
6. Applications of Nuclear Physics

D. SUGGESTED READING

Eisberg and Resnick: Quantum Physics of Atoms, Molecules, Solids, Nuclei and Particles (Wiley 2nd Edition):

Chapter 15; Chapter 16, sections 16-1,16-2,16-3,16-5,16-9 and 16-10

KS Krane: Introductory Nuclear Physics (Wiley):

Chapter 1; Chapter 3; Chapter 4, sections 4.1 and 4.4; Chapter 5, sections 5.1 and 5.2; Chapter 7 up to section 7.6 inclusive; Chapter 8, sections 8.1-8.4; Chapter 9, section 9.1; Chapter 13, sections 13.1-13.3 and sections 13.5,13.6; Chapter 14, Chapters 19 and 20.

1. NUCLEAR PROPERTIES

1.1 General Nuclear Properties

Although *nuclear forces* are known, a comprehensive theory of nuclei able to explain their properties in terms of the nuclear forces acting between their protons and neutrons is not available yet. Therefore, several models are used to explain a certain limited range of nuclear properties, using arguments that do not involve all the details of nuclear forces.

A pronounced difference between experimental studies of atoms and of nuclei arises from the difference between their characteristic energies. The characteristic energy of nuclei is of the order of 1 MeV, while for atoms it is of the order of 1 eV. Thus, nuclei require very special circumstances to be excited because of their very high characteristic energy. In fact, in our environment atomic nuclei typically exist only in their ground state, and most of the interesting nuclear phenomena occur only under special conditions created by accelerating machines, or in certain region of the universe such as the centre of a star.

To a considerable extend, we can describe a nucleus by a relatively small number of parameters: electric charge, radius, binding energy, angular momentum, parity, magnetic dipole and electric quadrupole moments, and characteristic energies of excited states. These are known as *static properties* of nuclei. However, additional nuclear properties exist such as decay, fission and fusion, and are known as *dynamic properties*.

Nuclei are composed of two types of nucleons: protons and neutrons. The *neutron* is an uncharged particle nearly the same mass as the *proton*. A nucleon with mass number A and atomic number Z contains A nucleons of which Z are protons and $A - Z$ are neutrons. Some years before its discovery, Rutherford suggested the existence of a particle having the properties of what we now call neutron. The neutron, being uncharged, was difficult to detect since it does not easily ionize atoms when it passes through matter, and most devices for detecting particles depend on ionization. In 1932 Chadwick succeeded in detecting neutrons emitted from beryllium nuclei when bombarded with α -particles produced from a radioactive source, as illustrated in Fig.1.1. For this measurement he used a Geiger counter behind a layer of paraffin. The neutrons collide with protons in the paraffin and transfer a fraction of their kinetic energy to the protons. The protons then penetrate the Geiger counter, where they are detected with high efficiency since they are charge particles.

The first artificially produced nuclear reaction discovered by Rutherford in 1919 was the following:



A bombarding ${}^4\text{He}$ (α -particle) interacts with a target nucleus ${}^{14}\text{N}$ to produce a residual nucleus ${}^{17}\text{O}$ and a product particle ${}^1\text{H}$ (proton). The 7.7 MeV α -particles were produced from a radioactive source. In general, mass and energy are not separately conserved in nuclear reactions. Instead, there is a conservation of total relativistic energy, $E + K = mc^2$, where K is kinetic energy and m is used here for rest mass. Thus, for the general case:

$$\text{a} + \text{A} \rightarrow \text{B} + \text{b} \quad (1.2)$$

the conservation of total relativistic energy in the laboratory frame of reference reads:

$$(K_a + m_a c^2) + m_A c^2 = (K_B + m_B c^2) + (K_b + m_b c^2) \quad (1.3)$$

After the reaction takes place, the product particle b is emitted at the angle θ , and the residual nucleus B recoils in such a way that momentum is conserved.

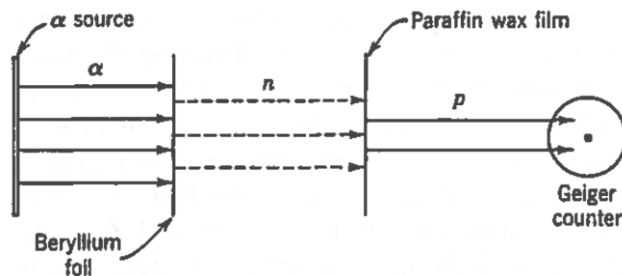


Figure 1.1 A schematic description of the experimental arrangement used Chadwick in the discovery of the neutron (from Eisberg & Resnick)

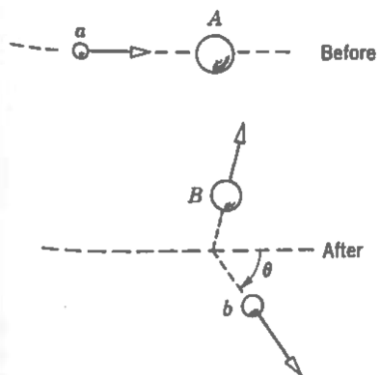


Figure 1.2 Schematic representation of a nuclear reaction (from Eisberg & Resnick)

1.2 The Nuclear Radius and Density

Like the radius of an atom, the radius of a nucleus is not a precisely defined quantity. Neither atoms nor nuclei are solid spheres with abrupt boundaries. It is relatively natural to characterize the nuclear shape with two parameters: the *mean radius*, where the density is half its central value, and the *skin thickness*, over which the density drops from near its maximum to near its

minimum. However, the density distribution that is measured depends on the kind of experiment that is performed. In some experiment, such as high-energy electron scattering, we measure the Coulomb interaction of charged particles with the nucleus, thus we determine the ***distribution of nuclear charge*** (primarily the distribution of protons but also involving the distribution of neutrons because of their internal constituents). In other experiments, such as Rutherford scattering (with α -particles), we measure the strong nuclear interaction of nuclear particles, thus we determine the distribution of nucleons (protons and neutrons), called ***distribution of nuclear matter***.

The usual means to determine the size and shape of an object is to examine the radiation scattered from it, similarly to a diffraction pattern generated by a plane wave incident into a circular object. To see an object and its details, the wavelength of the radiation must be smaller than the dimensions of the object. For nuclei with diameter of about 10 fm, we require $\lambda < 10 \text{ fm}$, i.e. $p > 100 \text{ MeV}/c$. Beams of electrons with energies of 0.1-100 MeV can be easily produced with a conventional linear accelerator, and can be analysed with a precise energy spectrometer to select only those electrons that are elastically scattered from the nuclear target. A result from this kind of experiment is shown in Fig.1.3. The first minimum in the diffraction-like pattern can be clearly distinguished. For diffraction by a circular disk of diameter D , the first minimum should appear at $\theta = \sin^{-1}(1.22/D)$. Fig.1.4 shows the result of elastic electron scattering from a heavy nucleus, ^{208}Pb . Several minima in the diffraction pattern can be seen. They do not fall to zero like diffraction minima seen with light incident on an opaque disk, because the nucleus does not have a sharp boundary.

The central nuclear charge density is nearly the same for all nuclei. Nucleons do not seem to congregate near the centre of the nucleus, but instead have a fairly constant distribution out to the surface. Thus, the number of nucleons per unit volume is roughly constant:

$$\frac{A}{\frac{4}{3}\pi R^3} \sim \text{constant} \quad (1.4)$$

where R is the mean nuclear radius. Thus, defining the proportionality constant R_0 gives:

$$R = R_0 A^{1/3} \quad (1.5)$$

where $R_0 \approx 1.2 \text{ fm}$.

Fig.1.5 shows how diffuse the nuclear surface appears to be. The charge density is roughly constant out to a certain point and then drops relatively slowly to zero. The distance over which this occurs is nearly independent of the size of the nucleus, thus is usually assumed to be constant. The skin thickness parameter can be precisely defined as the distance over which the charge density falls from 90% of its central value to 10% (typically $\approx 2.3 \text{ fm}$).

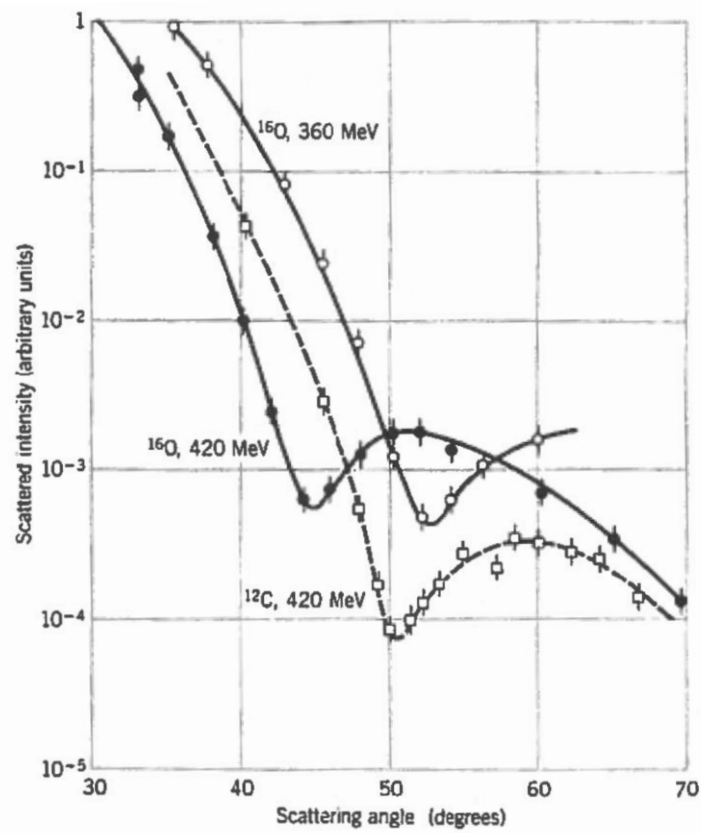


Figure 1.3 Elastic electron scattering from ^{16}O and ^{12}C (from Krane)

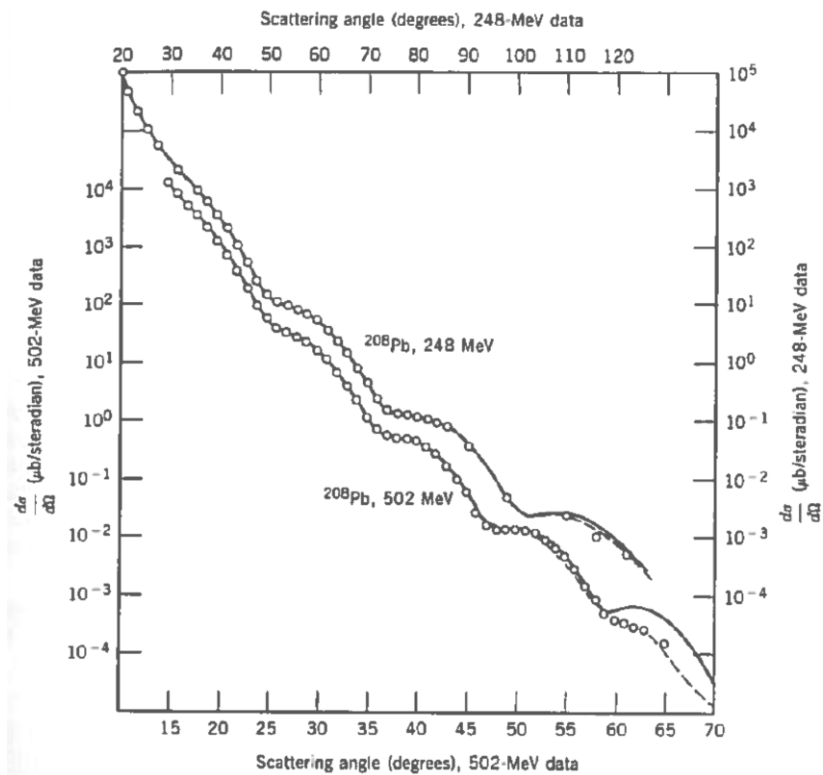


Figure 1.4 Elastic electron scattering from ^{208}Pb (from Krane)

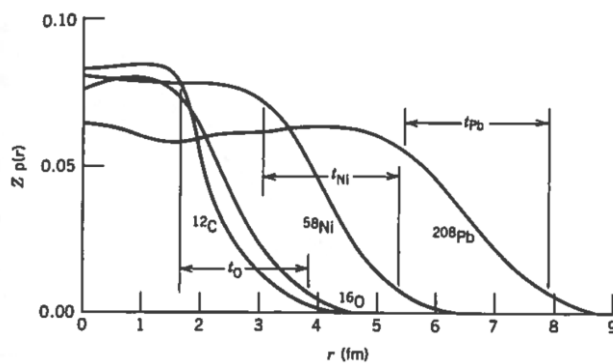


Figure 1.5 Radial charge distribution of several nuclei determined from electron scattering (from Krane)

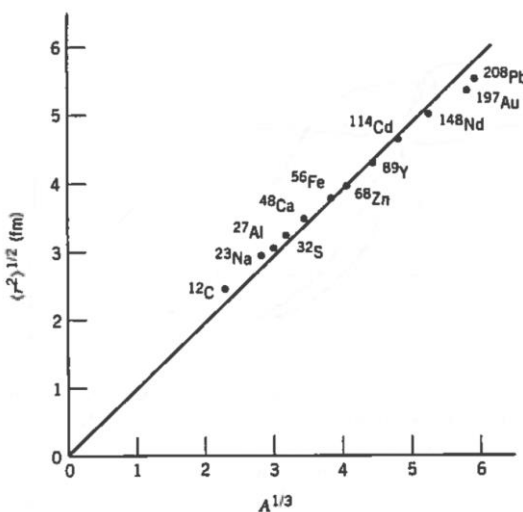


Figure 1.6 Nuclear radius determined from electron scattering experiments (from Krane)

Fig.1.6 shows a more quantitative determination of eq. (1.5), based on electron scattering results. The root mean square (rms) radius, $\langle r^2 \rangle^{1/2}$, is deduced directly from the distribution of scattered electrons. The slope of the straight line gives $R_0 = 1.23$ fm (the error bars are smaller than the size of the experimental points).

An experiment that involves the nuclear force between two nuclei will often provide a measure of the nuclear radius. The determination of the spatial variation of the force between nuclei enables the calculation of the nuclear radii. In this case the radius is characteristic of the nuclear, rather than the Coulomb, force. This radius therefore reflects the distribution of all nucleons in a nucleus, not only the protons. An example of experiments that can be performed to determine the size of the nuclear matter distribution is the scattering of an α -particle (${}^4\text{He}$ nucleus) from a much heavier target of ${}^{197}\text{Au}$. If the separation between the two nuclei is always greater than the sum of their radii, each is always beyond the range of the other's nuclear force, thus only the Coulomb force acts (this setup is known as Rutherford scattering). The probability of scattering at

a certain angle depends on the energy of the incident particle exactly as predicted by the Rutherford formula, when the energy of the incident particle is below a certain value. As the energy of the incident α -particle is increased, the Coulomb repulsion of the nuclei is overcome, and they may approach close enough to allow the nuclear force to act. In this case the Rutherford formula no longer holds, as shown in Fig.1.7.

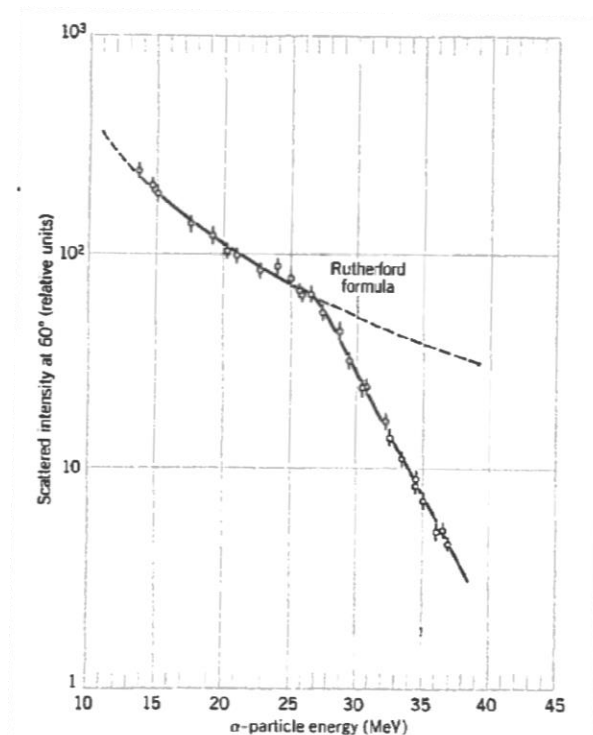


Figure 1.7 Breakdown of the Rutherford scattering formula (from Krane)

1.3 Mass and Abundance of Nuclides

Measured values of the masses and abundances of neutral atoms of various stable and radioactive nuclei are tabulated and available from different sources. Even though we must analyse the energy balance in nuclear reactions and decays using nuclear masses, it is conventional to tabulate the masses of neutral atoms. It may therefore be necessary to correct for the mass and binding energy of the electrons.

As we probe deeper into the constituents of matter, the nuclear binding energy becomes greater in comparison with the rest energy of the bound system. In a simple nucleus, such as deuterium (one proton and one neutron), the binding energy of 2.2 MeV is 1.2×10^{-3} of the total mass energy. The deuterium is weakly bound and thus this number is rather low compared with other nuclei, for which the fraction will be more like 8×10^{-3} . It is therefore not possible to separate a discussion of nuclear mass from a discussion of nuclear binding energy.

To determine the nuclear masses and relatively abundances in a sample of ordinary matter, which even for a pure element may be a mixture of different isotopes, we must have a way to separate the isotopes from one another by their masses. Typically, instruments known as mass spectrograph or mass spectrometers (see Fig.1.8) are used to separate masses with high precision (order of 10^{-6}), and this allowed to map the entire scheme of stable isotopes. All mass spectrometers begin with an ion source, which produces a beam of ionized atoms. Often a vapour of a material under study is bombarded with electrons to produce the ions, or they can be produced as a result of a spark discharge between electrodes coated with the material. Ions emerging from the source have a broad range of velocities, as might be expected for a thermal distribution, and different mass range. The next element is a velocity selector, consisting of perpendicular electric (E) and magnetic (B) fields. The E field would exert a force qE that would tend to divert the ions upward (see Fig.1.8); the B field would exert a downward force qvB . Ions pass through undeflected if the forces cancel, thus:

$$qE = qvB \quad (1.6)$$

$$v = \frac{E}{B} \quad (1.7)$$

The final element is a momentum selector, which is essentially a uniform magnetic field that bends the beam into a circular path with radius r determined by the momentum:

$$mv = qBr \quad (1.8)$$

$$r = \frac{mv}{qB} \quad (1.9)$$

Since q , B , and v are uniquely determined, each different mass m appears at a particular r .

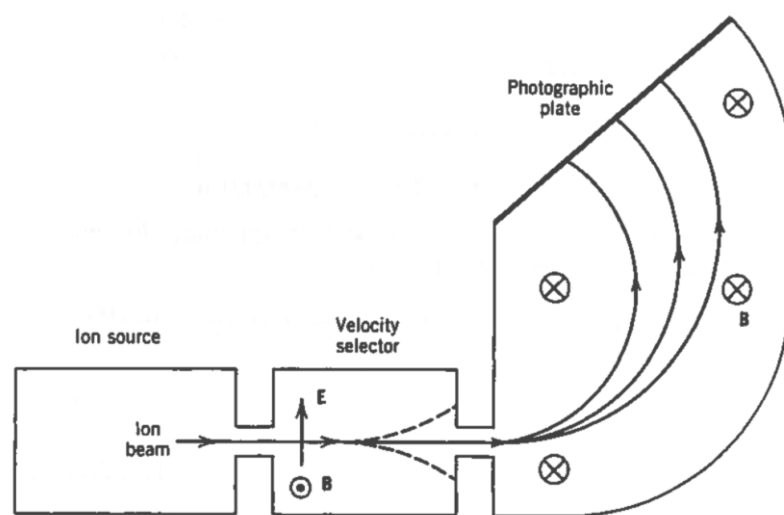


Figure 1.8 Schematic diagram of a mass spectrograph (from Krane)

Mass spectrometry also allows us to measure the relative abundances of the various isotopes of an element. In fact, as we scan the mass range by varying E or B , we can measure the current passing through an exit slit, thus we can reconstruct a mass-spectrum with different peaks corresponding to different masses. A two-dimensional graph of isotopes of the elements, in which one axis represents the number of neutrons (symbol N) and the other represents the number of protons (atomic number, symbol Z) in the atomic nucleus, is known as Segrè chart (see Fig.1.9). The distribution of stable nuclei for even and odd $A/N/Z$, where $A = N + Z$, is shown in Table 1.1. At high Z we have $N > Z$ such that $Z/A \sim 2/5$.

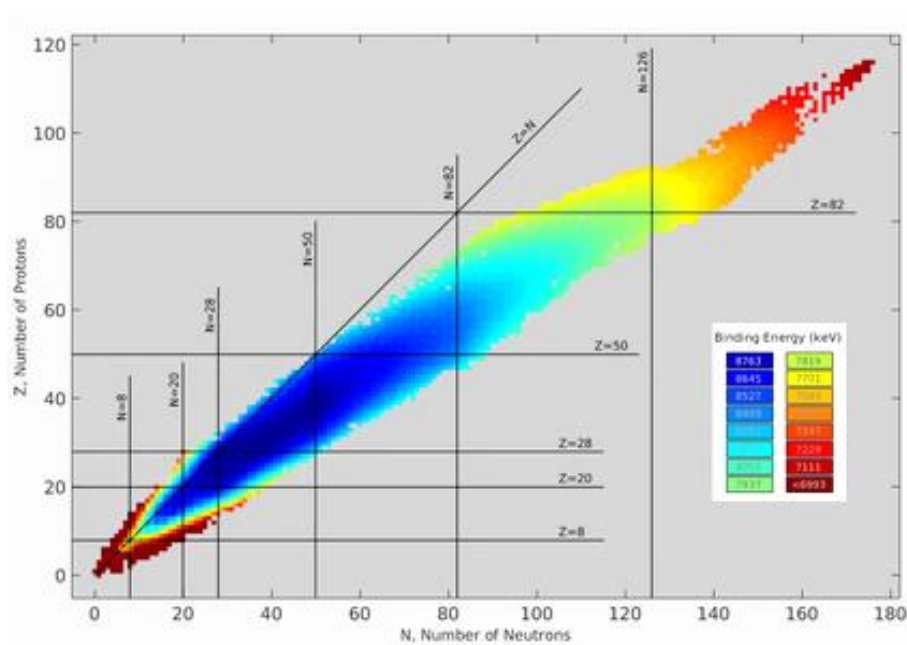


Figure 1.9 The Segrè chart: two-dimensional graph of isotopes of the elements, in which one axis represents the number of neutrons and the other represents the number of protons in the atomic nucleus

A	N	Z	Number of Stable Nuclei
Even	Even	Even	166
	Odd	Odd	8
Odd	Even	Odd	57
	Odd	Even	53

Table 1.1 The distribution of stable nuclei (*from Eisberg & Resnick*)

1.4 Nuclear Binding Energy

The mass energy $m_{Nucl}c^2$ of a certain nuclide is its atomic mass energy $m_A c^2$ less the total mass energy of Z electrons and the total electronic binding energy:

$$m_{Nucl}c^2 = m_A c^2 - Z m_e c^2 + \sum_{i=1}^Z B_i \quad (1.10)$$

where B_i is the binding energy of the i^{th} electron. Electronic binding energies are of the order of 10-100 keV in heavy atoms, while atomic mass energies are of the order $A \times 1 \text{ GeV}$, thus to a precision of about 10^{-6} we can neglect the last term of eq. (1.10). Furthermore, since in nuclear physics we usually work with “differences” in mass energies, the effect of electron binding energies tends to cancel in such differences.

The *binding energy* B of a nucleus is the difference in mass energy between a nucleus ${}^A_Z X_N$ and its constituents Z protons and N neutrons:

$$B = \{Zm_p + Nm_n - [m({}^A X) - Zm_e]\}c^2 \quad (1.11)$$

where we have dropped the subscript from m_A since from now on, we will be dealing with atomic masses. Proton and neutron masses are similar but not identical. The masses are often expressed in MeV and this is shorthand for the mass-energy, which is given by mc^2 . Grouping the Z proton and electron masses into Z neutral hydrogen atoms, we can rewrite eq. (1.11) as:

$$B = [Zm({}^1 H) + Nm_n - m({}^A X)]c^2 \quad (1.12)$$

With the masses generally given in atomic mass units, it is convenient to include the unit conversion factor in $c^2 = 931.50 \text{ MeV/u}$.

We occasionally find atomic mass tables in which, rather than $m({}^A X)$, what is given is the mass defect $\Delta = (m - A)c^2$. Thus, given the mass defect it is possible to use eq. (1.12) to deduce the atomic mass.

Other interesting and useful properties that are often tabulated are the neutron and proton separation energies. The *neutron separation energy* S_n is the amount of energy that is needed to remove a neutron from a nucleus ${}^A_Z X_N$, equal to the difference in binding energies between ${}^A_Z X_N$ and ${}^{A-1}_Z X_{N-1}$:

$$\begin{aligned} S_n &= B({}^A_Z X_N) - B({}^{A-1}_Z X_{N-1}) \\ &= [m({}^{A-1}_Z X_{N-1}) - m({}^A_Z X_N) + m_n]c^2 \end{aligned} \quad (1.13)$$

In a similar way we can define the *proton separation energy* S_p as the energy needed to remove a proton:

$$\begin{aligned} S_p &= B({}^A_Z X_N) - B({}^{A-1}_{Z-1} X_N) \\ &= [m({}^{A-1}_{Z-1} X_N) - m({}^A_Z X_N) + m({}^1 H)]c^2 \end{aligned} \quad (1.14)$$

The neutron and proton separation energies are analogous to the ionization energies in atomic physics. They tell us about the binding of the outermost or valence nucleons. Just like the atomic ionization energies, they show evidence for nuclear shell structure that is similar to atomic shell structure. Table 1.2 reports the mass defects and separation energies for some nuclides.

Since the binding energy increases more or less linearly with A , it is general practice to show the average binding energy per nucleon, B/A , as a function of A (see Fig.1.10). The curve is relatively constant except for the very light nuclei. The average binding energy of most nuclei is, to within 10%, about 8 MeV per nucleon. Furthermore, it is important to note that the curve reaches a peak near $A = 60$, where the nuclei are most tightly bound (e.g. maximum stability). This suggests that we can “gain” (i.e. release) energy into two ways: (i) *below* $A = 60$ by assembling lighter nuclei into heavier nuclei, or (ii) *above* $A = 60$ by breaking heavier nuclei into lighter nuclei. In either case we “climb the curve” of binding energy and liberate nuclear energy. The first method is known as *nuclear fusion*, while the second as *nuclear fission*.

Nuclide	Δ (MeV)	S_n (MeV)	S_p (MeV)
^{16}O	-4.737	15.66	12.13
^{17}O	-0.810	4.14	13.78
^{17}F	+1.952	16.81	0.60
^{40}Ca	-34.847	15.64	8.33
^{41}Ca	-35.138	8.36	8.89
^{41}Sc	-28.644	16.19	1.09
^{208}Pb	-21.759	7.37	8.01
^{209}Pb	-17.624	3.94	8.15
^{209}Bi	-18.268	7.46	3.80

Table 1.2 Mass defects and separation energies of some nuclides (from Krane)

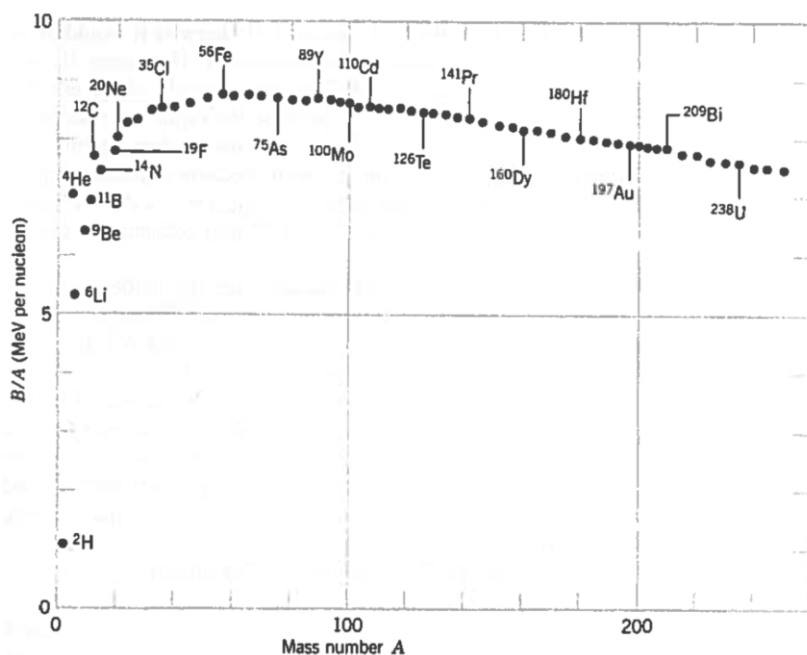


Figure 1.10 The binding energy per nucleon (from Krane)

1.5 Nuclear Angular Momentum and Parity

The coupling of orbital angular momentum \mathbf{L} and spin \mathbf{S} gives a total angular momentum \mathbf{J} ($\mathbf{J} = \mathbf{L} + \mathbf{S}$). In the quantum mechanical sense, we can therefore label every nucleon with the corresponding quantum numbers L, S, J . The total angular momentum of a nucleus containing A nucleons would then be the vector sum of the angular momenta of all the nucleons. This total angular momentum is usually called the *nuclear spin* and is represented by the symbol I . The angular momentum I has all the usual properties of quantum mechanical angular momentum vectors: $I^2 = \hbar I(I+1)$ and $I_z = m\hbar$ ($m = -I, \dots, +I$). For many applications involving angular momentum, the nucleus behaves as if it were a single entity with an angular momentum of I . To avoid confusion, we will use I to denote the nuclear spin (total angular momentum of a nucleus containing A nucleons) and J to represent the total angular momentum of a single nucleon. It will often be the case that a single valence particle determines all the nuclear properties, thus in that case $I = J$. In other cases, it may be necessary to consider two valence particles, thus $I = J_1 + J_2$, and several different resultant values of I may be possible.

One important restriction of the allowed values of I comes from considering the possible z components of the total angular momentum of the individual nucleons. Each J must be half-integral ($1/2, 3/2, 5/2, \dots$) and thus its only possible z-components are likewise half-integral ($\pm 1/2\hbar, \pm 3/2\hbar, \pm 5/2\hbar, \dots$). If we have an even number of nucleons, there will be an even number of half-integral components, with the result that the z-component of the total I can take only integral values. This requires that I itself be an integer. If the number of nucleons is odd, the total z-component must be half-integral and so must the total I . Therefore, the following rules are valid:

odd-A nuclei $\rightarrow I$ half-integer

even-A nuclei $\rightarrow I$ integer

The measured values of the nuclear spin can tell us a great deal about the nuclear structure. For example, of the hundreds of known (stable and radioactive) even-Z, even-N nuclei, all have spin-0 ground states. This is evidence for a nuclear pairing: the nucleons couple together in spin-0 pairs, giving a total I of zero. Consequently, the ground state spin of an odd-A nucleus must be equal to the J of the odd proton or neutron. Therefore, along with the nuclear spin, the *parity*, π , is also used to label nuclear states. The parity can take either + (even) or - (odd) values. Like the spin I , we regard the parity π as an “overall” property of the whole nucleus. It can be directly measured using a variety of techniques of nuclear decays and reactions. It is usually denoted by a + or a - superscript to the nuclear spin (e.g. $0^+, 2^-, 1/2^-, 5/2^+$). There is no direct theoretical relation between I and π , thus for any value of I , it is possible to have either $\pi = +$, or $\pi = -$.

1.6 Nuclear Electromagnetic Moments

Much of what we know about nuclear structure comes from studying not the strong nuclear interaction of nuclei with their surroundings, but instead the much weaker electromagnetic interaction. In fact, the strong nuclear interaction establishes the distribution and motion of nucleons in a nucleus, and we probe that distribution with the electromagnetic interaction. In doing so, we can use electromagnetic fields that have less effect on the motion of nucleons than the strong force of the nuclear environment, thus our measurements do not seriously distort the object we are trying to measure.

Electromagnetic theory gives us a recipe for calculating the various electric and magnetic multiple moments, and the same recipe can be carried over into the nuclear regime using quantum mechanics, by treating the multiple moments in operator form and calculating their expected values for various nuclear states. These expected values can then be directly compared with the experimental values measured in the laboratory. The simplest distributions of charges and currents give the lowest order multiple fields. A spherical charge distribution gives only a monopole (Coulomb) field, and the higher order fields all vanish. A circular current loop gives only a magnetic dipole field. In general, if a simple, symmetric structure is possible, then nuclei tend to acquire that structure. It is therefore usually necessary to measure or calculate only the lowest order multiple moments to characterize the electromagnetic properties of the nucleus.

A restriction on the multiple moments comes from the symmetry of the nucleus and is directly related to the parity of the nuclear states. Each electromagnetic multiple moment has a parity. The parity of electric moments is $(-1)^L$, where L is the order of the moment ($L = 0$ for monopole, $L = 1$ for dipole, $L = 2$ for quadrupole, etc.). For magnetic moments the parity is $(-1)^{L+1}$. All odd-parity static multiple moments must vanish (electric dipole, magnetic quadrupole, electric octupole, etc.).

The monopole electric moment is just the net nuclear charge Ze . The next nonvanishing moment is the **magnetic dipole moment** μ . A circular loop carrying current i and enclosing area A has a magnetic moment of magnitude $|\mu| = iA$. If the current is caused by a charge e , moving with speed v in a circle of radius r (with period $2\pi r/v$), then:

$$|\mu| = \frac{e}{2\pi r/v} \pi r^2 = \frac{evr}{2} = \frac{e}{2m} |\mathbf{L}| \quad (1.15)$$

where $|\mathbf{L}|$ is the classical angular momentum mvr . In quantum mechanics we define the observable magnetic moment to correspond to the direction of greatest component of \mathbf{L} , thus we can take eq. (1.15) directly into the quantum regime by replacing \mathbf{L} with the expectation value relative to the axis where it has maximum projection, which is $m_L\hbar$ with $m_L = +L$. Thus:

$$\mu = \frac{e\hbar}{2m} L \quad (1.16)$$

where now L is the angular momentum quantum number of the orbit.

The quantity $e\hbar/2m$ is called a “magneton”. For atomic motion we use the electron mass and obtain the Bohr magneton, $\mu_B = 5.7884 \times 10^{-5}$ eV/T. Putting in the proton mass we have the nuclear magneton, $\mu_N = 3.1525 \times 10^{-8}$ eV/T. Note that $\mu_N \ll \mu_B$ owing to the different in the masses, thus under most circumstances atomic magnetism has much larger effect than nuclear magnetism.

Protons and neutrons, like electrons, also have intrinsic (or spin) magnetic moments. The spin quantum number is indicated as S , where $S = \frac{1}{2}$ for protons, neutrons, and electrons. Interestingly, proton and neutron both have finite magnetic dipole:

$$\text{Proton: } \mu_p = +2.79 \mu_N$$

$$\text{Neutron: } \mu_n = -1.91 \mu_N$$

Thus, the uncharged neutron has a nonzero magnetic moment! Here is our first evidence that the nucleons are not elementary point particles like the electron, but have an internal structure, which must be due to charged particles in motion, whose resulting currents give the observed spin magnetic moments.

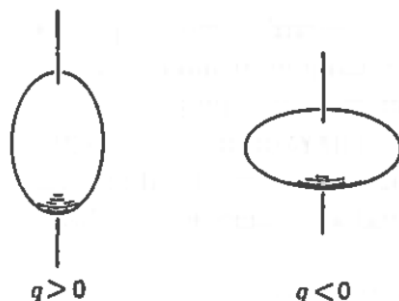


Figure 1.11 Prolate (left) and oblate (right) charge distributions for nucleons (from Eisberg and Resnick)

In nuclei, the pairing force favours the coupling of nucleons so that their orbitals angular momentum and spin angular momentum each add to zero. Thus, the pair nucleons do not contribute to the magnetic moment, and we need only consider a few valence nucleons. If this were not so, we might expect on statistical grounds alone to see a few heavy nuclei with a very large magnetic moment; however, no nucleon has been observed with a magnetic dipole moment larger than about $6\mu_N$.

The next nonvanishing moment is the **electric quadrupole moment**, Q_0 . For a classical point charge e , this is of the form $e(3z^2 - r^2)$. If the nuclear particle moves with spherical symmetry, then the quadrupole moment vanishes. If the nucleus does not have a spherical shape, then it will have an electric quadrupole moment. Examples of prolate (positive quadrupole moment) and oblate

(negative quadrupole moment) charge distributions of nucleons are shown in Fig.1.11. In general, the electric quadrupole moment of a nucleus is expressed as:

$$Q_0 = \int \rho(r)(3z^2 - r^2)dV \quad (1.17)$$

where ρ is the charge density distribution as a function of position r . Note that r has components in the x , y and z directions; thus, if the distribution is isotropic, the quadrupole moment is zero as $3z^2$ and r^2 average out to zero.

1.7 Nuclear Excited States

Just as we learn about atoms by studying their excited states, we study nuclear structure partially through the properties of nuclear excited states. In fact, in analogy to atomic excited states, nuclear excited states are unstable and decay rapidly to the ground state. In atoms, we make excited states by moving individual electrons to the higher energy orbits, and we can do the same with individual nucleons. Thus, the excited states of the nucleus can reveal something about the orbit of individual nucleons. Nuclei possess both single-particle and collective structure, thus we can produce excited states by adding energy to the core of paired nucleons. This energy can take the form of collective rotation or vibrations of the entire core, or it might even break one of the pairs, thereby adding two additional valence nucleons.

Part of the goal of nuclear spectroscopy is to observe the possible excited states and to measure their properties. The experimental techniques available include radioactive decay and nuclear reaction studies. Among the properties we should like to measure for each excited state there are: energy of excitation, lifetime and modes of decay, spin and parity, magnetic dipole moment, and electric quadrupole moment. A schematic representation of the potential and total energy of a nucleon is shown in Fig.1.12. The potential extends beyond the nuclear mass distribution by about the range of the nuclear force, and then it rapidly goes to zero. A few examples of level schemes showing the excited states of different nuclei are represented in Fig.1.13. Some nuclei, such as ^{209}Bi , show great simplicity, while others, such as ^{182}Ta , show great complexity.

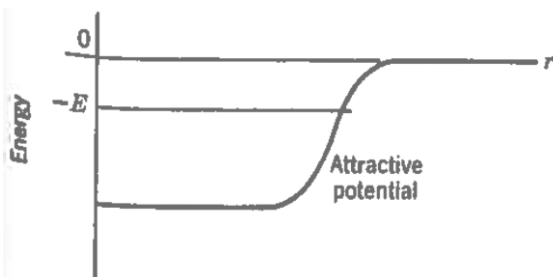


Figure 1.12 Schematic representation of the potential and total energy of a nucleon (*from Eisberg and Resnick*)

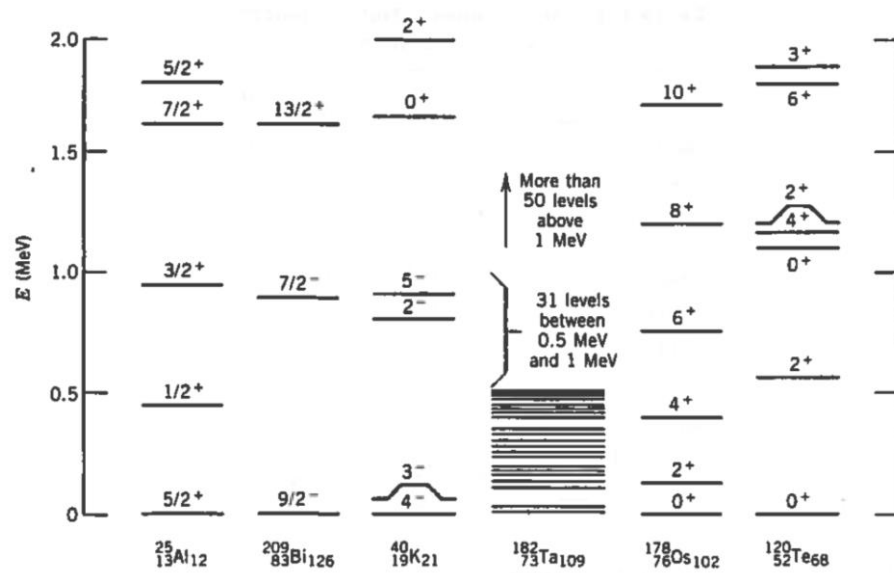


Figure 1.13 Examples of level schemes showing the excited states of different nuclei (from Krane)

2. THE INTER-NUCLEON FORCE

Based on intuitive considerations, we can list a few properties expected from the nucleon-nucleon force:

- It is stronger than the Coulomb force at short distances, i.e. the nuclear force can overcome the Coulomb repulsion of protons in the nucleus.
- It is negligible at long distances (order of atomic sizes), i.e. the interaction among nuclei in a molecule is based only on the Coulomb force.
- Some particles (e.g. electrons) do not feel the nuclear force.
- The nucleon-nucleon force is nearly independent of whether the nucleons are neutrons or protons (*charge independence*).
- The nucleon-nucleon force depends on whether the spins are parallel or antiparallel.
- The nucleons are kept at a certain average separation thanks to a repulsive term of the nucleon-nucleon force.
- The nucleon-nucleon force has a noncentral (tensor) component that does not conserve orbital angular momentum.

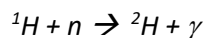
2.1 The Deuteron

A *deuteron* (2H nucleus) consists of a neutron and a proton (a neutral atom of 2H is called *deuterium*). This is the simplest bound state of nucleons; therefore, it is an ideal system for studying the nucleon-nucleon interaction. This problem is equivalent to the hydrogen atom in atomic physics.

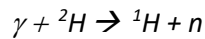
The **binding energy** of the deuteron is a very precisely measured quantity, which can be determined using three different methods. Spectroscopy allows directly determining the mass of the deuteron through eq. (1.12):

$$B = [m({}^1H) + m_N - m({}^2H)]c^2 = 2.22463 \pm 0.00004 \text{ MeV}$$

We can also determine this binding energy directly by bringing a proton and a neutron together to form 2H and measuring the energy of the γ -ray photon that is emitted:



The deduced binding energy, which is equal to the observed energy of the photon less a small recoil correction, is $2.224589 \pm 0.000002 \text{ MeV}$, thus in excellent agreement with the mass spectroscopic value. A third method uses the reversed reaction, known as *photodissociation*, in which a γ -ray photon breaks apart a deuteron:



The minimum γ -ray energy that accomplishes this process is equal to the binding energy (again corrected for the recoil of the final products). In this case, the observed value is 2.224 ± 0.002 MeV, which is in good agreement with the previous findings. As discussed in Chapter 1, the average binding energy per nucleon is about 8 MeV. Thus, the deuteron is very weakly bound compared to typical nuclei. In fact, there are no excited states of the deuteron but unbound systems consisting of a free proton and neutron.

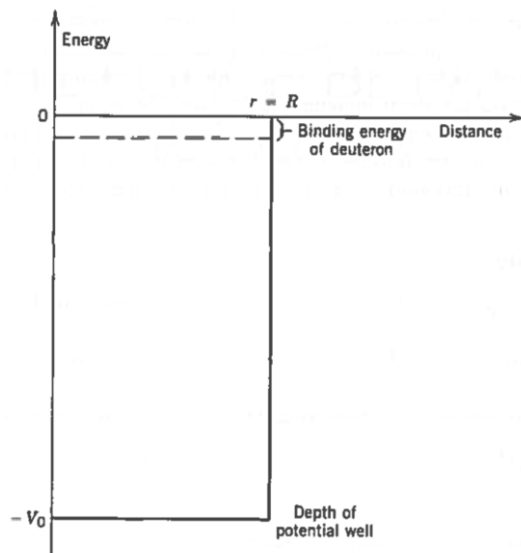


Figure 2.1 The spherical square-well potential

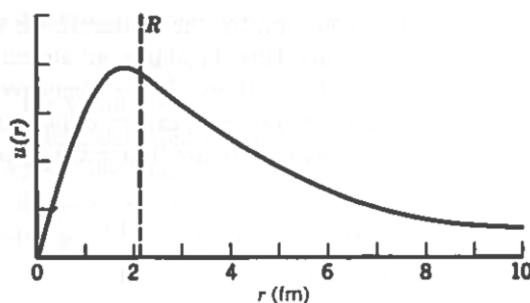


Figure 2.2 The deuteron wave function for $R = 2.1$ fm (the exponential joins smoothly the sine at $r = R$)

To simplify the analysis of the deuteron, we will assume the nucleon-nucleon potential as a three-dimensional square well, as shown in Fig.2.1:

$$\begin{aligned} V(r) &= -V_0 && \text{for } r < R \\ &= 0 && \text{for } r > R \end{aligned} \quad (2.1)$$

This is an oversimplification, but it is sufficient for qualitative conclusions. Here r represents the separation between the proton and the neutron, and R is a measure of the deuteron diameter.

Furthermore, we will assume that the lowest energy state of the deuteron has a spherical symmetry, i.e. the angular momentum is zero ($L = 0$). The next step is to solve the Schrödinger equation:

$$\left(-\frac{\hbar^2}{2m}\nabla^2 + V\right)\Psi = E\Psi \quad (2.2)$$

by defining the radial part of Ψ as $u(r)/r$, hence:

$$-\frac{\hbar^2}{2m}\frac{d^2u}{dr^2} + V(r)u(r) = Eu(r) \quad (2.3)$$

For $r < R$, the solution to eq. (2.3) can be written as:

$$u(r) = A\sin k_1 r + B\cos k_1 r \quad (2.4)$$

with $k_1 = \sqrt{2m(E + V_0/\hbar^2)}$.

For $r > R$, the solution can be written as:

$$u(r) = C e^{-k_2 r} + D e^{+k_2 r} \quad (2.5)$$

with $k_2 = \sqrt{-2mE/\hbar^2}$ ($E < 0$ for bound states). To keep the wave function finite for $r \rightarrow \infty$ we must have $D = 0$, and to keep it finite for $r \rightarrow 0$ we must have $B = 0$ (Ψ depends on $u(r)/r$, hence as $r \rightarrow 0$, $u(r)$ also must go to zero). Applying the continuity conditions on u and du/dr at $r = R$, we obtain:

$$k_1 \cot k_1 R = -k_2 \quad (2.6)$$

This equation provides a relation between V_0 and R . The deuteron wave function is shown in Fig.2.2. We have mentioned in Chapter 1 that from electron scattering experiments we can estimate the rms charge radius of the deuteron ($\sim 2.1 \text{ fm}$), which provides a reasonable estimate for R . Solving eq. (2.6) numerically, a nuclear potential V_0 of about 35 MeV is calculated. This is a quite reasonable estimate of the strength of the nucleon-nucleon potential, even in more complex nuclei.

Fig.2.1 shows how close the deuteron is to the top of the well. If the nucleon-nucleon force were just a bit weaker, the deuteron bound state would not exist and we would not be here to discuss it! In fact, the formation of the deuteron from hydrogen is the first step not only in the proton-proton cycle of fusion by which our sun makes its energy, but also in the formation matter from primordial hydrogen that filled the early stages of universe.

The **nuclear spin** (total angular momentum) I of the deuteron can be expressed as the sum of three components: the individual spins S_n and S_p of the neutron and proton (each equal to $\frac{1}{2}$), and

the orbital angular momentum \mathbf{L} of the nucleons as they move about their common centre of mass:

$$\mathbf{I} = \mathbf{S}_n + \mathbf{S}_p + \mathbf{L} \quad (2.7)$$

The experimentally measured nuclear spin of the deuteron is $I = 1$. Since the neutron and proton spins can be either parallel (for a total of 1) or antiparallel (for a total of zero), there are four ways to couple \mathbf{S}_n , \mathbf{S}_p and \mathbf{L} to get a total I of 1:

- \mathbf{S}_n and \mathbf{S}_p parallel with a $L = 0$
- \mathbf{S}_n and \mathbf{S}_p antiparallel with a $L = 1$
- \mathbf{S}_n and \mathbf{S}_p parallel with a $L = 1$
- \mathbf{S}_n and \mathbf{S}_p parallel with a $L = 2$

The experimentally measured **parity** of the deuteron is **even**. In general, the parity associated with orbital motion is $(-1)^L$. Thus, even parity is obtained for $L = 0$ (*s-state*) or $L = 2$ (*d-state*), and odd parity for $L = 1$ (*p-state*). The observed even parity allows us to eliminate the combinations of spins that include $L = 1$, hence leaving only $L = 0$ and $L = 2$ as possibilities. The spin and parity of the deuteron are therefore consistent with $L = 0$ as assumed earlier, but the possibility of $L = 2$ cannot be excluded yet.

If the $L = 0$ assumption is correct, there should be no orbital contribution to the **magnetic dipole moment** in the deuteron. Thus, we can assume the total magnetic moment to be simply the combination of the neutron and proton magnetic moments:

$$\boldsymbol{\mu} = \boldsymbol{\mu}_n + \boldsymbol{\mu}_p \quad (2.8)$$

If we take the observed magnetic moment to be the z component of $\boldsymbol{\mu}$, when the spins have their maximum value ($+ \frac{1}{2} \hbar$), the calculated value for μ will be $0.879804 \mu_N$. This is in good but not quite exact agreement with the observed value ($0.8574376 \pm 0.0000004 \mu_N$). The small discrepancy can be ascribed to different contributions, such as mesons exchange between the neutron and proton, and the fact that the deuteron wave function should be expressed as a mixture of d-state ($L = 2$) and s-state ($L = 0$), thus the assumption of a pure $L = 0$ state is pretty good but not quite exact.

The bare neutron and proton have no **electric quadrupole moment**, therefore any nonzero value for the quadrupole moment of the deuteron must be due to the orbital motion. The pure $L = 0$ deuteron wave function would have a vanishing quadrupole moment. However, the experimentally observed electric quadrupole moment is $Q = 0.00288 \pm 0.00002 b$, which is obviously very small but not zero.

2.2 Properties of the Nuclear Force

This section provides an overview of the main features of the internucleon force.

*The interaction between two nucleons can be approximated (to lower order) to an **attractive central potential**.* For convenience, we have previously represented this potential with a square-well form, which simplifies the calculations and reproduces the observed data well. The key characteristics of this potential is that it depends only on the internucleon distance r and, in fact, we represent this central term as $V_c(r)$. To study $V_c(r)$ experimentally, one would measure the energy dependence of nucleon-nucleon parameters such as scattering phase shifts, and then try to choose the form for $V_c(r)$ that best reproduces those parameters.

*The nucleon-nucleon interaction is strongly **spin dependent**.* This observation follows from the failure to observe a singlet bound state of the deuteron, and from the measured differences between the singlet and triplet cross sections. Obviously, the additional term to the potential that accounts for this effect must depend on the spins of the two nucleons S_1 and S_2 , but not all possible combinations of S_1 and S_2 are permitted.

*The internucleon potential includes a noncentral term, known as **tensor potential**.* Evidence from the tensor force comes primarily from the observed quadrupole moment of the deuteron ground state. In fact, an s-state ($L = 0$) wave function is spherically symmetric, and the corresponding quadrupole moment vanishes. On the other hand, wave functions with mixed L states must results in noncentral potentials. The tensor potential must be of the form $V(r)$, instead of $V(r)$. For a single nucleon, the choice of a certain direction in space is obviously arbitrary (nucleons do not distinguish north from south, or east from west). We can express the tensor contribution to the internucleon potential as follows:

$$S_{12} = \frac{3(s_1 \cdot r)(s_2 \cdot r)}{r^2} - \mathbf{s}_1 \cdot \mathbf{s}_2 \quad (2.9)$$

which averages to zero over all angles.

*The nucleon-nucleon force is **charge symmetric**.* This means that the proton-proton interaction is identical to the neutron-neutron interaction, after the correction for the Coulomb force in the proton-proton system. Here the term “charge” refers to the character of the nucleon and not to the electric charge. This is supported by the equality of the pp and nn scattering lengths and effective ranges.

*The nucleon-nucleon force is nearly **charge independent**.* This means that the three nuclear forces nn, pp, and pn are nearly identical, again correcting for the pp Coulomb force. We note the existence of “mirror nuclei” which have the same odd number of nucleons but swap a proton for

a neutron, e.g. $^{17}\text{O}^8$ and $^{17}\text{F}^9$ ($Z = 8$ and $N = 9$, or $Z = 9$ and $N = 8$, respectively). The first few energy levels for these nuclei are shown in Table 2.1. In fact, there is a great similarity that demonstrate the independence of the inter-nucleon force.

$^{17}\text{O}^8$ [MeV]	$^{17}\text{F}^9$ [MeV]
5.08	5.10
4.55	4.69
3.85	3.86
3.06	3.10
0.87	0.50
0	0

Table 2.1 Some energy levels for $^{17}\text{O}^8$ and $^{17}\text{F}^9$

The nucleon-nucleon interaction becomes **repulsive at short distances**. This conclusion follows from qualitative considerations of the nuclear density. In fact, as we add more nucleons, the nucleus grows in such a way that its central density remains roughly constant, and thus something is keeping the nucleons from crowding too closely together. Nucleon-nucleon scattering can be quantitatively studied at high particle energies. Fig.2.3 shows the deduced singlet s-wave phase shift for neutron-proton scattering up to 500 MeV (at these energies, phase shifts from higher partial waves are also present). At about 300 MeV, the s-wave phase shift becomes negative, corresponding to a change from an attractive to a repulsive force. To account for the repulsive core, we could choose a square-well form to simplify the calculation as follows:

$$V(r) = +\infty \quad r < R_{core} \quad (2.10)$$

$$V(r) = -V_0 \quad R_{core} \leq r \leq R$$

$$V(r) = 0 \quad r > R$$

This is schematically represented in Fig.2.4. The value of $R_{core} \sim 0.5$ fm gives agreement with the observed phase shift.

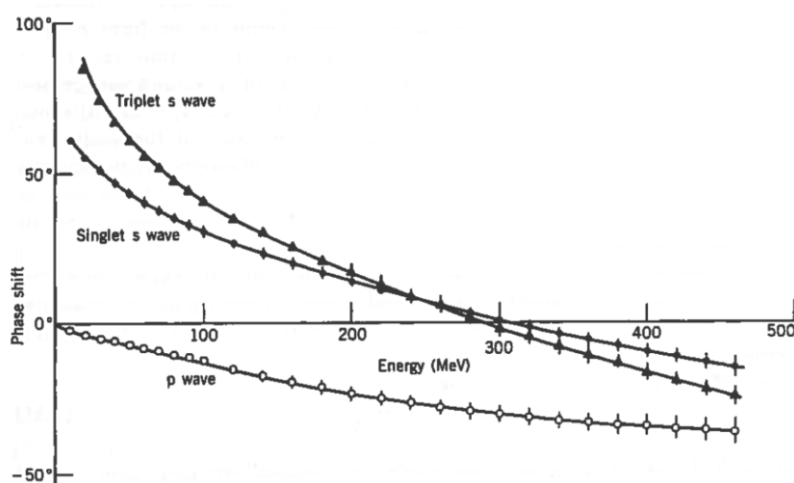


Figure 2.3 The phase shift from neutron-proton scattering at medium energies

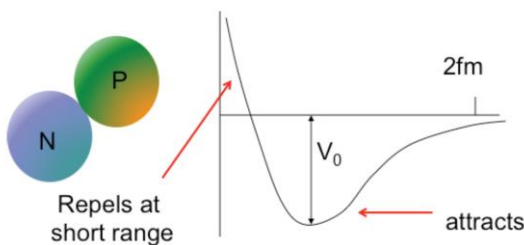


Figure 2.4 Sketch of possible potential well for internucleon force

In summary, the intern-nucleon potential is much more complicated than the Coulomb potential and has several components. This is due to the relatively complex structure of the nucleons that are, in fact, made up of other particles, quarks.

The **spin-orbit interaction** is an additional inter-nucleon interaction coming from the observation that scattered neutrons can have their spins aligned, or *polarized*, in certain directions. The polarization of the nucleons in a beam (or in a target) is defined as:

$$P = \frac{N(\uparrow) - N(\downarrow)}{N(\uparrow) + N(\downarrow)} \quad (2.11)$$

where $N(\uparrow)$ and $N(\downarrow)$ refer to the number of nucleons with their spins pointed up and down, respectively. Values of P range from +1 (100% spin-up polarized beam) to -1 (100% spin-down polarized beam). An unpolarized beam ($P = 0$) has equal numbers of nucleons with spins pointing up and down. Let us consider the nucleon scattering experiment in Fig.2.5, in which an unpolarized beam (shown as a mixture of spin-up and spin-down nucleons) is incident on a spin-up target nucleon. The nucleon-nucleon interaction causes the incident spin-up nucleons to be scattered to the left at angle θ , and the incident spin-down nucleons to be scattered to the right at angle $-\theta$.

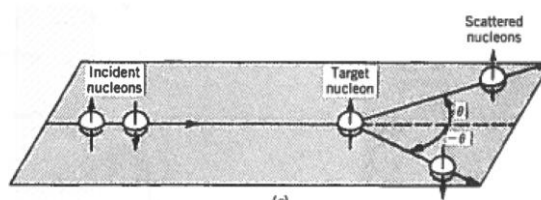


Figure 2.5 An unpolarized beam (mixture of spin-up and spin-down nucleons) is scattered from a target having spin-up.

2.3 The exchange force model

There are two principal arguments in support of the presence of an *exchange force* in nuclei. The first come from the saturation of nuclear forces. The experimental support for the saturation comes from the relatively constant nuclear density and binding energy per nucleon as we go to

heavier nuclei. A given nucleon seems to attract only a small number of neighbours, but it also repels at small distance to keep those neighbours from getting too close.

Another argument in favour of the exchange force model comes from the study of np scattering at high energies. Fig.2.6 shows the np differential cross section, where a strong peak is present at forward angles near 0° , corresponding to a small momentum transfer between the projectile and the target. In principle, we can estimate the extent of this forward peak by calculating the theoretical maximum momentum transfer. For small deflection angles, $\sin\theta \approx \theta = \Delta p/p$, where p is the momentum of the incident particle and Δp is the transverse momentum added during the collision. If F is the average force that acts during the collision time Δt , then $\Delta p = F\Delta t$. The force F is $-dV/dr$ and, in a first approximation, the average force should be of the order of V_0/R , where V_0 is the depth of the nucleon-nucleon square-well potential and R is its range. The collision time Δt should be of the order of R/v , where v is the projectile velocity. Thus:

$$\theta = \frac{\Delta p}{p} = \frac{F\Delta t}{p} = \frac{V_0}{pv} = \frac{V_0}{2T} \quad (2.12)$$

where T is the kinetic energy of the projectile. For the energies shown in Fig.2.6, this gives values of θ in the range of 10° or smaller; hence we do not expect to see a peak at 180° ! In fact, even if it is tempting to regard this backward peak in the centre of mass frame as the result of a head-on collision, our theoretical estimate above indicates such an explanation is not likely to be correct.

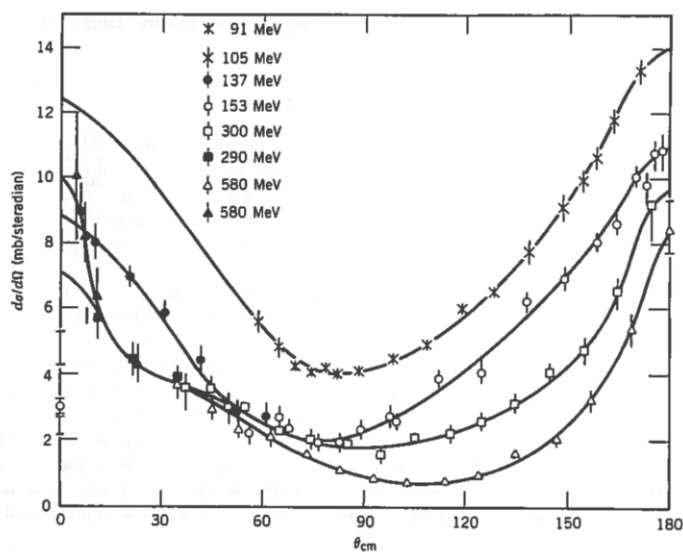


Figure 2.6 The neutron-proton differential cross section at medium energies: the strong forward-scattering peak (near 0°) is expected, while the equally strong backward-scattering peak (near 180°) is evidence for the exchange force.

A more successful explanation can be found in the exchange model if, during the collision, the neutrons and protons exchange places. In other words, the forward-moving neutron becomes a

proton, and the backward-moving proton (in the centre-of-mass system) becomes a neutron. The incident nucleon (a neutron) then reappears in the laboratory as a forward moving nucleon (now a proton), thus consistent with our estimate of the small deflection angle in nucleon-nucleon scattering.

In summary, exchange forces explain both the saturation of nuclear forces and the strong backward peak in np scattering. In the first case, “something” is exchanged between nucleons to produce a sort of saturated bond. In the second case, “something” is exchanged between nucleons and actually changes their character. According to quantum field theory, the first object (a nucleon in our case) does not setup a classical field throughout space but instead emits field quanta. The second object can then absorb those field quanta (and potentially reemit them back to the first object). The two objects interact directly with the exchanged field quanta and therefore indirectly with each other. Thus, it is natural to associate the “something” that is exchanged in the nucleon-nucleon interaction with quanta of the nuclear field. For a neutron with spin $\frac{1}{2}$ to turn into a proton with spin $\frac{1}{2}$, it is clear that the exchanged particle must have integral spin (0 or 1) and must carry electric charge. In addition, if we wish to apply the same exchange force concept to nn and pp interactions, there must also be an uncharged variety of the exchanged particle. Furthermore, based on the observed range of the nuclear force, we can estimate the mass of the exchanged particle. Let us assume that a nucleon (N) emits a particle X , and a second nucleon absorbs it:

$$N_1 \rightarrow N_1 + X$$

$$X + N_2 \rightarrow N_2$$

The fact that a nucleon emits a particle of mass $m_X c^2$ and remains a nucleon without violating the conservation of energy can be admitted only if the emission and reabsorption take place within a short enough time, Δt , that makes us unaware of energy conservation violation. This is possible since the limits of our ability to measure a given energy are restricted by the uncertainty principle; hence, if $\Delta t < \hbar/(m_X c^2)$, we will be unaware that energy conservation has been violated by an amount $\Delta E = m_X c^2$. The maximum range of the force is determined by the maximum distance that the particle X can travel in the time Δt . If it moves at speeds of the order of c , then the range R can be at most:

$$R = c\Delta t = \frac{\hbar c}{m_X c^2} = \frac{200 \text{ MeV} \cdot \text{fm}}{m_X c^2} \quad (2.13)$$

Eq. (2.13) gives a useful relation between the mass energy of the exchanged particle and the range of the force. For nuclear forces with a range of about 1 fm, the exchanged particle should have a mass energy of the order of 200 MeV.

Such particles that exist only for a very short time and allow us to violate conservation of energy are known as *virtual particles*. Thus, we can observe the force resulting from the exchange of virtual particles, but we cannot observe the particle themselves during the exchange. The exchanged particles that carry the nuclear force are called **mesons** (from the Greek “meso” meaning middle, because the predicted mass was between the masses of the electron and the nucleon). Mesons have been found in particle physics experiments in 1947. They are also found at high altitude where cosmic rays with high energy interact with the atmosphere. The lightest of the meson, known as **pion**, is responsible for the major portion of the longer range (1-1.5 fm) part of the inter-nucleon potential. To satisfy all the varieties of the exchanges needed in the two-nucleon system, there must be three pions with the electric charges of +1 (π^+), 0 (π^0), and -1 (π^-). The pions have spin 0, odd parity, and rest energies of 139.6 MeV (for π^\pm) and 135.0 MeV (for π^0), i.e. $273m_e$ and $264m_e$, respectively. At shorter ranges (0.5-1 fm), two pion exchanges is responsible for the nuclear binding. At much shorter ranges (0.25 fm), the exchange of ω mesons ($mc^2 = 783$ MeV) may contribute to the repulsive core, whereas the exchange of ρ mesons ($mc^2 = 769$ MeV) may provide the spin-orbit part of the interaction. The differing masses for the charged and neutral pions may explain the possible small violation of charge independence previously mentioned. The single pion that is exchanged between two identical nucleons must be a π^0 :

$$\begin{aligned} n_1 \rightarrow n_1 + \pi^0 & \quad \pi^0 + n_2 \rightarrow n_2 \\ p_1 \rightarrow p_1 + \pi^0 & \quad \pi^0 + p_2 \rightarrow p_2 \end{aligned}$$

The neutron-proton interaction can be carried by charged as well as neutral pions:

$$\begin{aligned} n_1 \rightarrow n_1 + \pi^0 & \quad \pi^0 + p_2 \rightarrow p_2 \\ n_1 \rightarrow p_1 + \pi^- & \quad \pi^- + p_2 \rightarrow n_2 \end{aligned}$$

The exchange force model enjoyed a remarkable success in accounting for the properties of the nucleon-nucleon system. The forces are based on the exchange of virtual mesons, all of which can be produced in the laboratory and studied directly. The pion is the lightest of the mesons and therefore has the longest range. Exploring the neutrons with higher energy probes allows us to study phenomena that are responsible for the finer details of the nuclear structure, such as those that occur only over very short distances. These phenomena are interpreted as arising from the exchange of heavier mesons. On the other hand, particle physicists are able to observe a large variety of mesons, including new particles, from high-energy collisions done with large particle accelerators. Nuclear physicists are then able to choose from this list candidates for the mesons exchanged in various details of the inter-nucleon interaction.

3. NUCLEAR MODELS

The theory used to describe the deuteron nucleus is unpractical to be applied to heavy nuclei because from a mathematical point of view we should solve a many-body problem; furthermore such a microscopic approach could obscure the essential physics of the nucleus rather than facilitate its understanding. Therefore, the strategy is to construct simplified *nuclear models* that are mathematically tractable but at the same time allow to capture the essentials of nuclear physics.

3.1 The Shell Model

Nuclear physicists use a theory similar to the atomic physics shell model. However, the *nuclear shell model* contains fundamental differences. In the atomic case, the valence electrons experience a potential that is supplied by the Coulomb field of the nucleons, while in the nucleus, the nucleons move in a potential that they themselves create. Another difference consists in the fact that in the atomic shell theory the electrons can move in spatial orbits relatively free of collisions with other electrons, while nucleons are large compared to the size of the nucleus, thus it is hard to imagine them moving in orbits without making collisions with other nucleons.

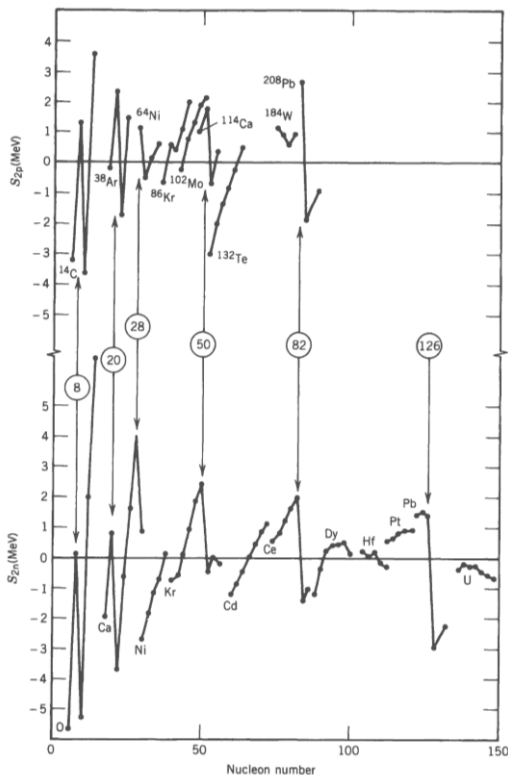


Figure 3.1 Two-proton separation energies of a sequence of isotones (top) and isotopes (bottom). The sudden change at the indicated “magic numbers” is clear (*from Krane*).

However, there are experimental evidences supporting the existence of nuclear shells. Fig.3.1 shows measured proton and neutron separation energies increasing gradually with N or Z except for a few sharp drops that occur at the same neutron and proton numbers. These so-called “magic-numbers” (Z or N = 2, 8, 20, 28, 50, 82, and 126) represent the effect of filled major shells.

The fundamental assumption of the shell model is that the motion of a single nucleon is governed by a potential caused by all the other nucleons. The existence of definite spatial orbits depends on the Pauli principle. Let us consider in a heavy nucleus a collision between two nucleons in a state near the very bottom of the potential well. When the nucleons collide, they will transfer energy to one another, but if all of the energy levels are filled up to the level of the valence nucleons, there is no way for one of the nucleons to gain energy except to move up to the valence level because the other levels (near the original one) are filled and cannot accept an additional nucleon. Such a transfer from a low-lying level to the valence band requires more energy than the nucleons are likely to transfer in a collision. Thus, the collisions cannot occur, and the shell model assumes that the nucleons orbit as if they were transparent to one another.

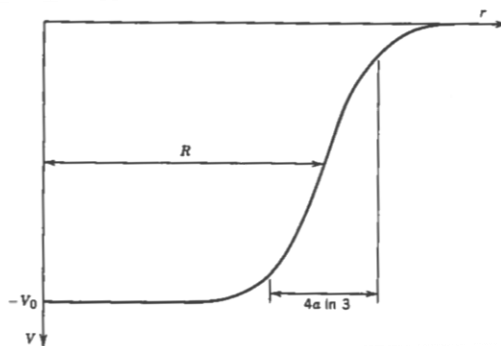
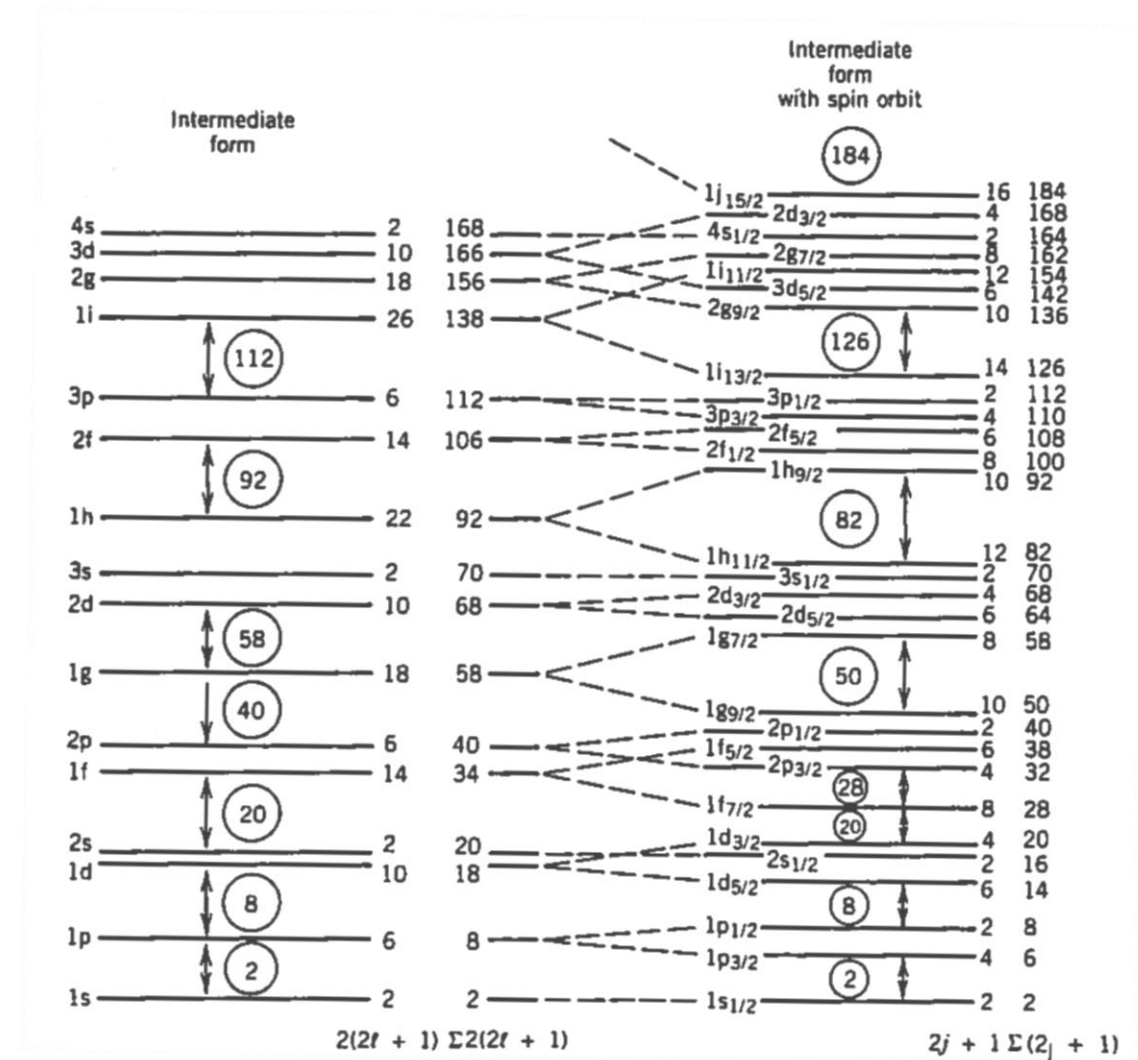


Figure 3.2 The shell-model potential (*from Krane*).

To develop this model, it is necessary to choose the **shell-model potential**. The level degeneracy represents the number of nucleons that can be put in that level, namely $2(2L + 1)$. The factor of $(2L + 1)$ arises from the m_L degeneracy, and the factor of 2 comes from the m_s degeneracy. In nuclear physics, the spectroscopic notation is different from the atomic physics one: the index n does not denote the principal quantum number, but simply counts the number of levels with a given L value. For instance, $1d$ means the first (lowest) d state, $2d$ means the second, and so on. A realistic form of the Shell model potential is sketched in Fig.3.2 and correspond to the following expression (*Woods-Saxon potential*):

$$V(r) = \frac{-V_0}{1 + \exp\left(\frac{r-R}{a}\right)} \quad (3.1)$$

where R is the mean nuclear radius and a is the skin thickness: $R = 1.2 \cdot A^{1/3} \text{ fm}$ and $a = 0.524 \text{ fm}$, and the well depth V_0 is of the order of 50 MeV. The resulting energy levels are shown in Fig.3.3. Filling the shells with nucleons according to the $2(2L + 1)$ rule, allows to obtain the magic numbers 2, 8, and 20, but the higher magic numbers do not emerge from the calculations.



which comes from the m_J values. The capacity of the $1f_{5/2}$ level is therefore 6, and that of $1f_{7/2}$ is 8, giving again 14 states (the number of possible states must be preserved, but they are grouped differently). The $1f_{5/2}$ and $1f_{7/2}$ states are known as spin-orbit pair or doublet. Considering the spin-orbit effect allows to obtain the remaining magic numbers as expected. Fig.3.4 shows a typical example of application of the shell model, considering the filling of energy levels needed to produce $^{15}_8O$ and $^{17}_8O$. The 8 protons fill a major shell and do not contribute to the structure. The extreme limit of the shell model claims that only the single unpaired nucleon determines the properties of the nucleus. In the case of $^{15}_8O$ the unpaired nucleon is in the shell $1p_{1/2}$; therefore we would predict that the ground state of $^{15}_8O$ has spin $1/2$ and odd parity ($L=1$), since the parity is determined by $(-1)^L$. Similarly, the ground state of $^{17}_8O$ should have spin $5/2$ and even parity ($L=2$), since the unpaired nucleon is in the $1d_{5/2}$ level. These two predictions are in perfect agreement with the observed spin-parity assignments.

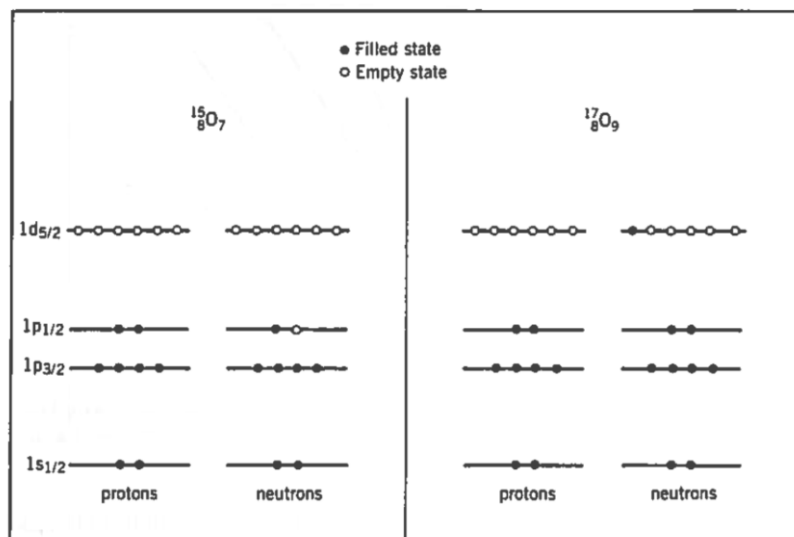


Figure 3.4 The filling of shells in $^{15}_8O$ and $^{17}_8O$ (from Krane).

In the case of **magnetic dipole moments**, the shell model still gives a reasonable (but not exact) agreement with experimentally measured nuclear properties. The magnetic moment is calculated from the expectation value of the magnetic moment operator in the state with maximum z projection of angular momentum. Including both L and S terms, we can express it as:

$$\mu = \frac{\mu_N(g_L L_z + g_S S_z)}{\hbar} \quad (3.2)$$

where $g_L = +1$ for a proton, $g_L = 0$ for a neutron, $g_S = +5.5856$ for a proton, and $g_S = -3.8262$ for a neutron. According to the Shell Model, for odd-A nuclei we expect $\langle \mu \rangle \neq 0$, and it can be expressed as follows:

$$\langle \mu \rangle = \left[g_L \left(J - \frac{1}{2} \right) + \frac{1}{2g_S} \right] \mu_N \quad J = L + \frac{1}{2}$$

$$\langle \mu \rangle = \left[g_L \frac{J(J+3/2)}{J+1} - 1/2 \frac{1}{J+1} g_S \right] \mu_N \quad J = L - 1/2 \quad (3.3)$$

Fig.3.5 shows a comparison of calculated values of the magnetic moments, using the shell-model for odd-A nuclei (known as Schmidt lines), and experimental measurements. The experimental data are generally smaller in magnitude and show a large scatter. The main reason for such disagreement lies in the oversimplified assumption that g_S for a nucleon in a nucleus is the same as g_S for a free nucleon. This is not a surprising effect if one considers that the “meson cloud” surrounding a free nucleon differs from the meson cloud of a nucleon bounded within the nucleus. Typically, this effect is considered by arbitrary reducing the g_S factor (e.g. 0.6 g_S in Fig.3.5). However the scattering of the experimental point is still large and suggests that the shell-model theory oversimplifies the calculation of the magnetic moments.

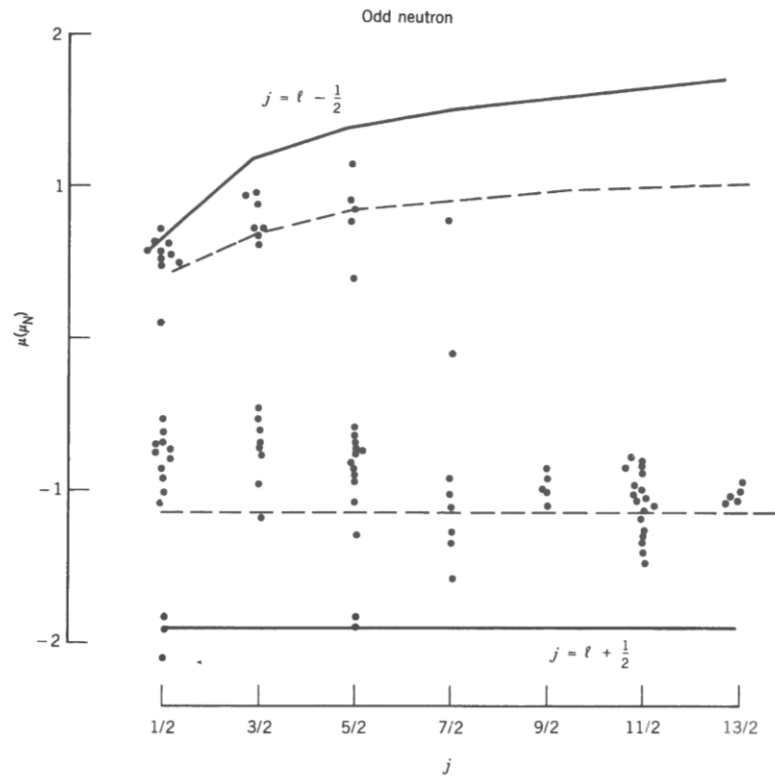


Figure 3.5 Experimental (dots) and calculated (line) values of the magnetic moments of odd-A nuclei. The Schmidt lines are shown as solid for g_S (free nucleons) and dashed for $0.6g_S$ (from Krane).

The computation of **electric quadrupole moments** in the shell-model is done by evaluating the electric quadrupole operator, $3z^2 - r^2$, in a state in which the total angular momentum of the odd particle has its maximum projection along the z axis (i.e. $m_J = +J$). Assuming that the odd particle is a proton, and that its angular momentum is aligned with the z axis, then it must be orbiting in the xy plane ($z = 0$). This would give a negative quadrupole moment of the order of $Q = -\langle r^2 \rangle$.

Calculated values are in good agreement with expectations, although a more accurate quantum mechanical computation gives the single-particle quadrupole moment of an odd proton in the state J of the shell-model as:

$$\langle Q_{sp} \rangle = -\frac{2J-1}{2(J+1)} \langle r^2 \rangle \quad (3.4)$$

where $\langle r^2 \rangle = 3/5R^2 = 3/5R_0^2 A^{2/3}$.

A less intuitive case is the one of an odd neutron. In fact, one would expect no quadrupole moment for an uncharged particle outside a filled subshell. However, odd-neutron values are not zero, even if they are generally smaller than the odd-proton case. When a subshell contains more than a single particle, all the particles in the subshell can contribute to the quadrupole moment. Since the capacity of a subshell is $2J + 1$, the number of nucleons in an unfilled subshell will range from 1 to $2J$. In this case, the quadrupole moment can be expressed as follows:

$$\langle Q \rangle = \langle Q_{sp} \rangle \left[1 - 2 \frac{n-1}{2J-1} \right] \quad (3.5)$$

where n is the number of nucleons in the subshell ($1 \leq n \leq 2J$). When $n = 2J$ (subshell lacking only one nucleon from being filled), $Q = -Q_{sp}$. These are known as “hole” states and show positive and opposite (in sign) values of the quadrupole moment compared to the “particle” states. However, the model fails to predict the extremely large quadrupole moments of certain heavy nuclei. A proper explanation requires the use of theoretical models that are different from the shell-model. Nevertheless, despite its simplicity, the shell-model is successful in accounting for the spins and parity of nearly all odd- A ground states.

3.3 The Liquid Drop Model

The liquid drop model is based on two properties that are common to all nuclei (except small- A nuclei): (i) their interior mass densities are approximately the same, and (ii) their total binding energies are proportional to their masses ($B/A \approx \text{constant}$). Both properties are compatible to the ones of macroscopic drops of an incompressible liquid: (i) the interior densities are constant, and (ii) the heats of vaporization (energy required to disperse the drop) are proportional to the masses. The liquid drop model approximates the nucleus as a sphere with a uniform interior density, abruptly dropping to zero at its surface. The radius is proportional to $A^{1/3}$, the surface area to $A^{2/3}$, and the volume to A . The mass formula consists of a sum of six terms:

$$M_{Z,A} = f_0(Z, A) + f_1(Z, A) + f_2(Z, A) + f_3(Z, A) + f_4(Z, A) + f_5(Z, A) \quad (3.6)$$

where $M_{Z,A}$ represents the mass of an atom whose nucleus is specified by Z and A. The first term is the mass of the constituent parts of the atom:

$$f_0(Z, A) = 1.007825 Z + 1.008665 (A - Z) \quad (3.7)$$

The remaining terms correct for the mass equivalents of various effects contributing to the total nuclear binding energy. The volume term is:

$$f_1(Z, A) = -a_1 A \quad (3.8)$$

This term describes the tendency to have a constant binding energy per nucleon, and since it is negative, it reduces the mass and increases the binding energy. The surface term is:

$$f_2(Z, A) = a_2 A^{2/3} \quad (3.9)$$

that represents a correction for the surface area of the nucleus. This term is positive, thus increases the mass and reduces the binding energy. In analogy with a liquid drop, this term would represent the effect of the surface tension energy. In fact, a molecule at the surface of the drop feels attractive forces only from one side, thus its binding energy is less than the binding energy of a molecule in the interior which feels attractive forces from all sides. The Coulomb term is:

$$f_3(Z, A) = a_3 \frac{Z^2}{A^{1/3}} \quad (3.10)$$

This term accounts for the effect of the Coulomb repulsion between the protons, thus increases the mass and reduces the binding energy. The next one is the asymmetry term:

$$f_4(Z, A) = a_4 \frac{(Z - \frac{A}{2})^2}{A} \quad (3.11)$$

which accounts for the tendency to have $Z = N$. This term is zero for $Z = N$, but increases with increasing departure from this condition, thus increases the mass and reduces the binding energy. Finally, the pairing term accounts for the tendency of nuclei to have even Z and even N:

$$f_5(Z, A) = -a_5 A^{-\frac{1}{2}} \quad (Z \text{ even and } N \text{ even}) \quad (3.12)$$

$$f_5(Z, A) = 0 \quad (Z \text{ even and } N \text{ odd, or } N \text{ even and } Z \text{ odd})$$

$$f_5(Z, A) = a_5 A^{-\frac{1}{2}} \quad (Z \text{ odd, } N \text{ odd})$$

This term maximises the binding energy if both Z and N are even.

Eq. (3.6) is known as *semiempirical mass formula* because the parameters a_1 to a_5 are obtained by empirically fitting the measured masses. One set of such parameters which provides accurate results for all stable nuclei, except very small A, is the following: $a_1 = 0.001691$; $a_2 = 0.001911$; $a_3 = 0.000763$; $a_4 = 0.10175$; $a_5 = 0.012$.

3.3 The Collective Model

The collective model of the nucleus combines certain features of the shell and liquid drop models. The collective model assumes that the nucleons in unfilled subshells of a nucleus move independently in a net nuclear potential produced by the *core* of filled subshells, as in the shell model. However, the net potential due to the core is not the static spherical symmetrical potential $V(r)$ used in the shell model, but it is a potential capable undergoing deformations in shape. These deformations represent the collective motion of the nucleons that are associated with the liquid drop model. As in the shell model, the nucleons fill the energy levels corresponding to such potential, which are split by the same spin-orbit interaction and lead to the same magic numbers, as well as nuclear spin and parity predictions.

There are general properties that are common to all nuclei, and it is reasonable to identify those properties not with the motion of a few valence nucleons, but instead with the entire nucleus. The origin of such properties lies in the nuclear collective motion. Fig.3.6 shows properties of even-even nuclei that reveal collective behaviour. The energy of the first 2^+ excited state seems to decrease rather smoothly as a function of A (except in regions near the filled subshells). The region from about $A = 150$ to $A = 190$ shows value of $E(2^+)$ that are very small and constant. Fig.3.7 shows the magnetic moments of the 2^+ states that are fairly constant in the range 0.7-1.0. In general, the observed nuclear properties suggest that it is convenient to consider two types of collective structures, for the nuclei with $A < 150$, and for the nuclei with $150 < A < 190$. The nuclei with $A < 150$ are typically treated in terms of a model based on vibrations about a spherical equilibrium shape, while the nuclei with $150 < A < 190$ are show structures most characteristic of rotations of a non-spherical system. Vibrations and rotations are the two major types of collective nuclear motion. This is treated with a similar mathematical approach used in the liquid drop model.

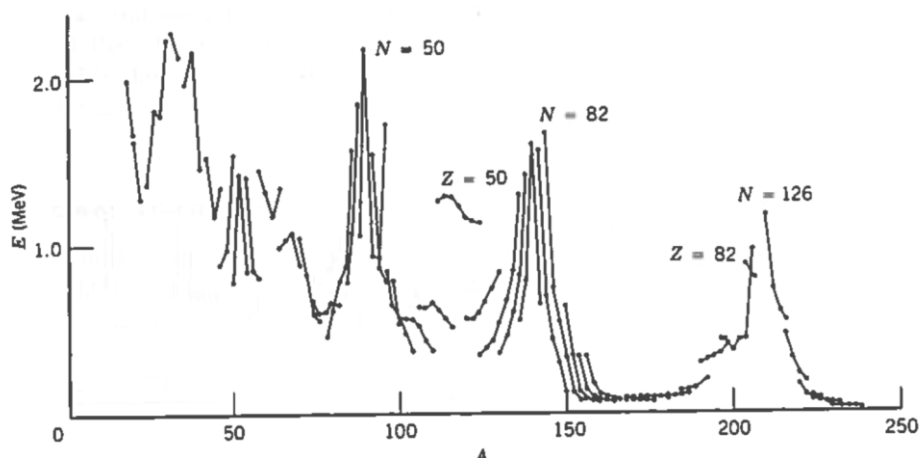


Figure 3.6 Energies of lowest 2^+ states of even- Z , even- N nuclei (from Krane).

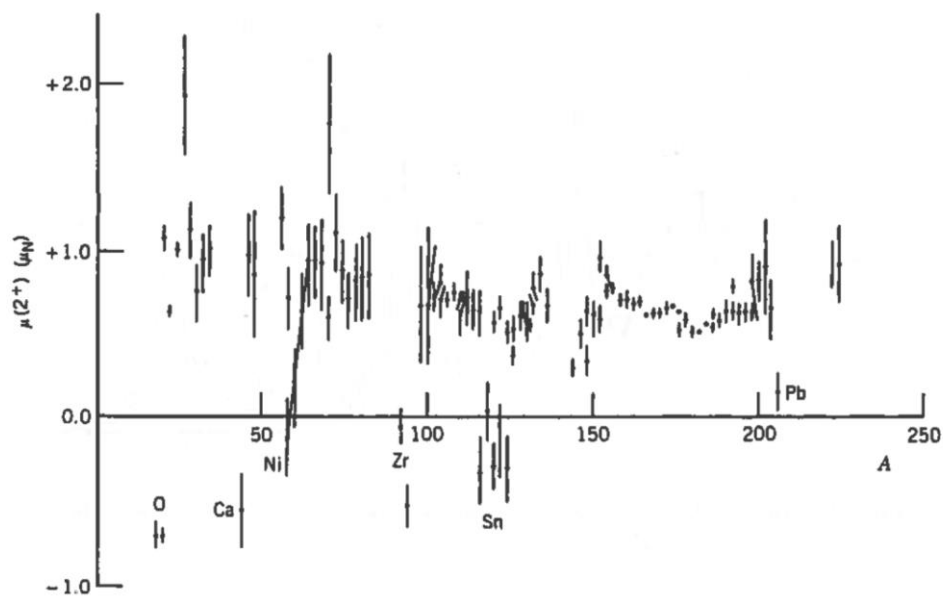


Figure 3.7 Magnetic moments of lowest 2^+ states of even- Z , even- N nuclei (from Krane).

Although the average shape of the nucleus is spherical, its instantaneous shape is not due to **nuclear vibrations**. It is convenient to define the position of a point on the nuclear surface using spherical (instantaneous) coordinates, $R(t)$ and (θ, ϕ) , as shown in Fig.3.8, in terms of the spherical harmonics $Y_{L,m}(\theta, \phi)$. Each spherical harmonic component will have an amplitude $\alpha_{L,m}(\theta, \phi)$:

$$R(t) = R_{av} + \sum_{L \geq 1} \sum_{m=-L}^{+L} \alpha_{L,m}(t) Y_{L,m}(\theta, \phi) \quad (3.13)$$

The constant ($L = 0$) term is incorporated into the average radius R_{av} , which is just $R_0 A^{1/3}$.

The $L = 1$ vibration is known as *dipole vibration*, as shown in Fig.3.9. This gives a net displacement of the centre of mass, and therefore cannot result from the action of internal nuclear forces. The next lowest mode is the $L = 2$ vibration known as *quadrupole vibration* (see Fig.3.9).

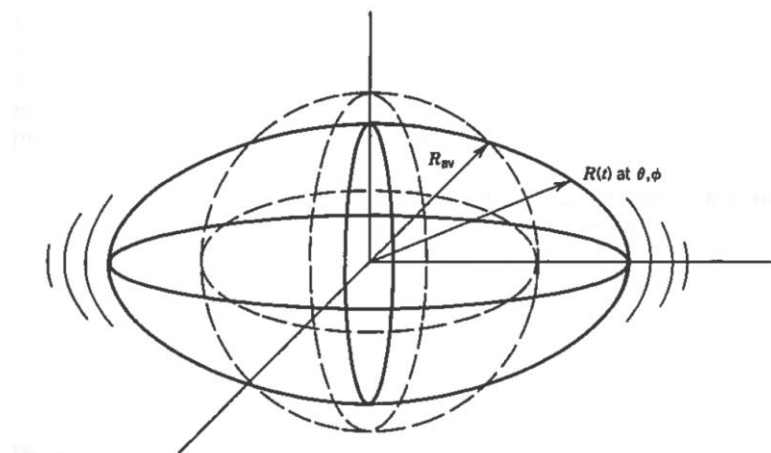


Figure 3.8 Representation of a vibrating nucleus with a spherical equilibrium shape. The time dependant coordinate $R(t)$ defines a point on the surface in the direction (θ, ϕ) (from Krane).

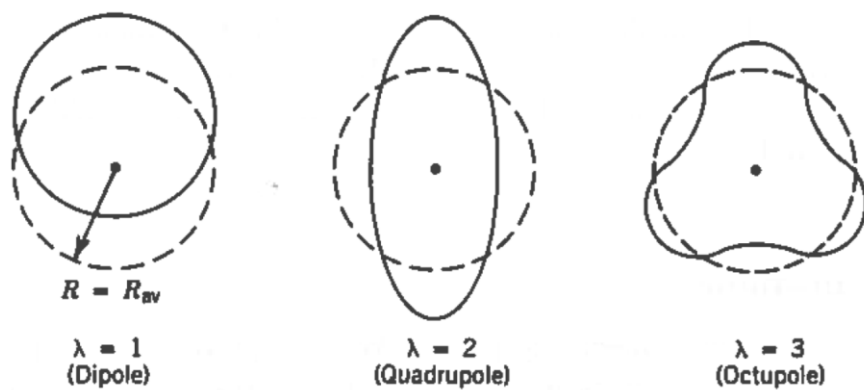


Figure 3.9 The lowest three vibrational modes of a nucleus. The dashed lines show the spherical equilibrium shape and the solid lines show an instantaneous view of the vibrating surfaces (*from Krane*).

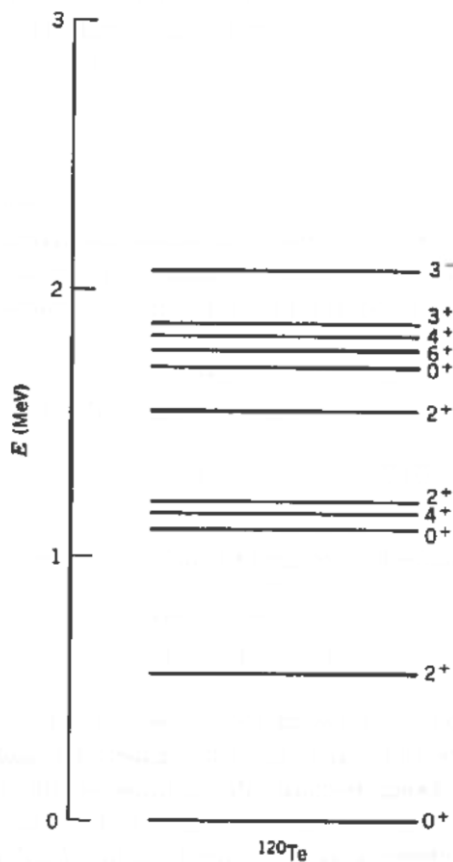


Figure 3.10 The low-lying levels of ^{120}Te (*from Krane*).

In analogy with the quantum theory of electromagnetism, in which a unit of electromagnetic energy is called photon, a quantum vibrational energy is called *phonon*. Thus, producing a mechanical vibration is equivalent to producing vibrational phonons. A single unit of $L = 2$ nuclear vibration is thus a *quadrupole phonon*. Let us consider the effect of adding one unit of vibrational energy (a quadrupole phonon) to the 0^+ ground state of an even-even nucleus. The $L = 2$ phonon carries 2 units of angular momentum and even parity (since the parity of $Y_{L,m}$ is $(-1)^L$). Thus, adding

two units of angular momentum to a 0^+ state gives only a 2^+ state, in perfect agreement with the measured spin-parity of first excited states of spherical even-Z, even-N nuclei. Let us assume to add an additional quadrupole phonon. We expect a triplet of states with spins $0^+, 2^+, 4^+$ ($L=0, L=2, L=4$, respectively) at twice the energy of the first 2^+ state, since two identical phonons carry twice as much energy as one. The next highest mode of vibration is known as *octupole vibration* mode and corresponds to $L = 3$ (see Fig.3.9). This mode carries three units of angular momentum and negative parity. Adding a single octupole phonon to the 0^+ ground state gives a 3^- state. Such states are commonly found at energies above the two-phonon triplet. An example of the vibrational states discussed above is reported in Fig. 3.10 for ^{120}Te .

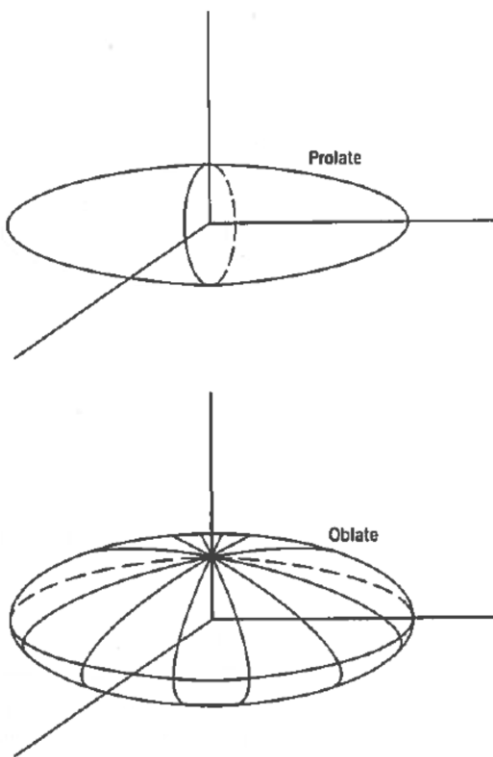


Figure 3.11 Equilibrium (static) shapes of deformed nuclei (from Krane).

Nuclei with non-spherical equilibrium shape can show **nuclear rotation** motion. These nuclei can have substantial distortions from spherical shape and are known as *deformed nuclei*. Their mass is in the range $150 < A < 190$, and $A > 220$ (rare earths and actinides). These nuclei are usually represented as an ellipsoid of revolution (see Fig.3.11). Their surface can be described as follows:

$$R(\theta, \varphi) = R_{av}[1 + \beta Y(\theta, \varphi)] \quad (3.14)$$

The deformation parameter β is related to the eccentricity of the ellipse:

$$\beta = \frac{4}{3} \sqrt{\frac{\pi}{5}} \frac{\Delta R}{R_{av}} \quad (3.15)$$

where ΔR is the difference between the semimajor and the semiminor axes of the ellipse. When $\beta > 0$, the nucleus has the elongated form of a *prolate ellipsoid*, while $\beta < 0$ implies that the nucleus has the flattened form of an *oblate ellipsoid*.

One indicator of stable deformation of a nucleus is a large *electric quadrupole moment*. Let us assume that the nucleus is rotating in the laboratory frame of reference. The kinetic energy of a rotating object is $\frac{1}{2}\mathfrak{I}\omega^2$, where \mathfrak{I} is the moment of inertia. In terms of angular momentum $L = \mathfrak{I}\omega^2$, the energy is $L^2/2\mathfrak{I}$. Taking the quantum mechanical value of L^2 , and letting I represent the angular momentum quantum number of the nucleus, gives:

$$E = \frac{\hbar^2}{2\mathfrak{I}} I(I + 1) \quad (3.16)$$

for the energies of a rotating object in quantum mechanics. Increasing the quantum number I corresponds to adding rotational energy to the nucleus, and the nuclear excited states form a sequence known as *rotational band*. The ground state of an even-Z, even-N nucleus is always a 0^+ state, and the mirror symmetry of the nucleus restricts the sequence of rotational states in this special case to even values of I . Therefore, we expect to see the following sequence of states: $E(0^+) = 0$; $E(2^+) = 6(\hbar^2/2\mathfrak{I})$; $E(4^+) = 20(\hbar^2/2\mathfrak{I})$; $E(6^+) = 42(\hbar^2/2\mathfrak{I})$; $E(8^+) = 72(\hbar^2/2\mathfrak{I})$; and so on. Indication of the lack of rigidity of a nucleus is the increase in the moment of inertia occurring at high angular momentum or rotational frequency. This effect is known as *centrifugal stretching* and is observed most often in heavy-ion reactions. In fact, the nucleus has no “vessel” to define the shape of the rotating fluid, and it is the potential provided by the nucleons themselves giving the nucleus its actual shape.

Both the vibrational and rotational collective motions give the nucleus a *magnetic moment* based on the corresponding angular momentum I :

$$\mu(I) = I \frac{Z}{A} \mu_N \quad (3.17)$$

For light nuclei, $Z/A \approx 0.5$ and $\mu(2) \approx +1\mu_N$, while for heavier nuclei, $Z/A \approx 0.4$ and $\mu(2) \approx +0.8\mu_N$.

4. NUCLEAR DECAYS AND REACTIONS

Nuclear decay can be divided into three categories. The α decay is the spontaneous emission of an α -particle (${}^4\text{He}$ nucleus) from a nucleus of large atomic number; this process is responsible for setting an upper limit on the atomic numbers of the chemical elements occurring in nature. The β decay is the spontaneous emission or absorption of an electron or a positron by a nucleus. The γ decay is the spontaneous emission of high-energy photons when a nucleus makes transitions from an excited state to its ground state.

Nuclear reactions provide information about excited states of nuclei since the residual nucleus in a reaction is typically formed in an excited state. Among the various reactions, nuclear fission and fusion are of high interest because they are used (or can be potentially used) as inexpensive sources of energy.

4.1 Decay Law

Unstable nuclei that originate from natural events are often called *radioactive*. The process occurring during a nuclear decay is typically called *radioactive decay*, or *radioactivity*. Radioactive decays are interesting for several reasons, for instance because they provide key information about the origin of the universe. Let us consider a system containing many nuclei of the same species at some initial condition (time), and that the nuclei decay at a given decay rate R . If there are N undecayed nuclei at a time t , then the number of nuclei decaying in the following time interval dt can be written as dN . Since R is the probability that a particular nucleus will decay in 1 second, Rdt is the probability that it will decay during the time interval dt , and $NRdt$ is the probability that the existing nuclei will decay in that interval. Thus, the average number of decaying nuclei is:

$$dN = -NRdt \quad (4.1)$$

where the minus sign accounts for the fact that dN is intrinsically negative since N decreases. Thus:

$$\frac{dN}{N} = -Rdt$$

$$\int_{N(0)}^{N(t)} \frac{dN}{N} = -R \int_0^t dt = -Rt$$

$$\ln N(t) - \ln N(0) = \ln \frac{N(t)}{N(0)} = -Rt$$

$$\frac{N(t)}{N(0)} = e^{-Rt}$$

$$N(t) = N(0)e^{-Rt} \quad (4.2)$$

where $N(0)$ is the number of undecayed nuclei at the initial time 0 , and $N(t)$ is the number of undecayed nuclei at the subsequent time t . Since the calculations involve probabilities, its results are correct only in the average, however fluctuations are very small when the number of nuclei involved is very large. Eq. (4.2) is known as *exponential decay law* and is plotted in Fig.4.1, which also shows the *lifetime* T characteristic of the decay (average time a nucleus survives before it decays). T is inversely proportional to the decay rate R :

$$T = \frac{1}{R} \quad (4.3)$$

hence, $N(T) = N(0)/e$.

Fig.4.1 also shows the *half-life* $T_{1/2}$ (time required for the number of undecayed nuclei to decrease by a factor of 2), and:

$$T_{1/2} = (\ln 2)T = 0.693T \quad (4.4)$$

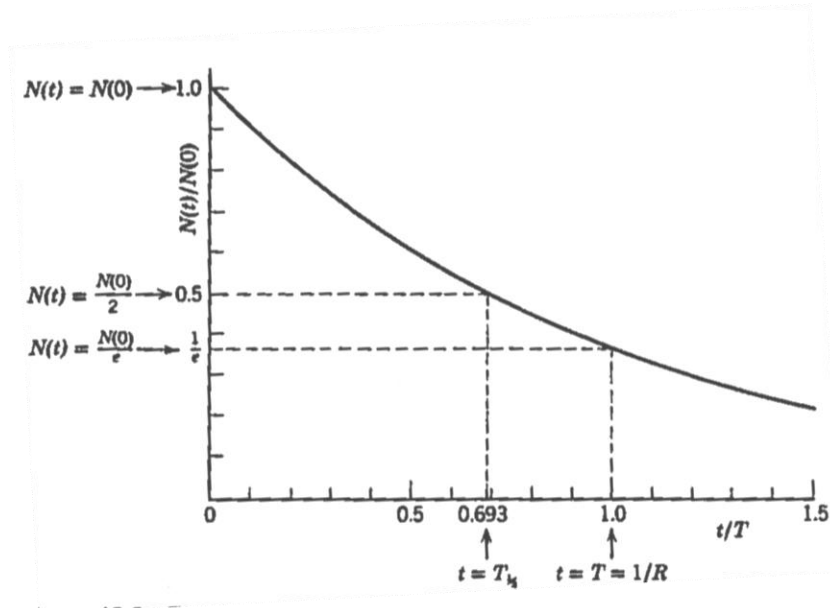


Figure 4.1 The exponential decay law (from Eisberg and Resnick).

As an example of applications of the nuclear decay law, it is worth mentioning Carbon-14 dating. This technique allows to date biological material fossils with high accuracy based on the β decay reaction of ^{14}C that has a characteristic half-life of 5730 ± 40 years. The moment of death of the living organism (e.g. a plant) can be retrieved by measuring the ^{14}C activity at the moment of the archaeological find, assuming the sample to have originally had the same $^{14}\text{C}/^{12}\text{C}$ ratio as in the atmosphere.

4.2 Alpha Decay

Alpha particles were first identified as the least penetrating radiation emitted by naturally occurring materials. In 1903 Rutherford measured their charge-to-mass ratio by deflecting α -particles from the decay of radium in electric and magnetic fields. Many heavy nuclei decay through α -emission, and only rarely any other spontaneous radioactive process results in the emission of nucleons. This is an indication of the existence of a special reason why nuclei chose α -emission over other possible decay modes.

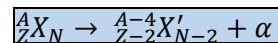
Alpha decay is the result of a Coulomb repulsion effect that becomes increasingly important for heavy nuclei because the Coulomb force increases with size at a faster rate ($\sim Z^2$) than does the specific nuclear binding force ($\sim A$). Since α decay is a spontaneous process, the emission of kinetic energy during the process comes from a decrease in the mass of the system. For a typical α -emitter ^{232}U (72 y), it is possible to compute the energy release for various emitted particles by knowing the involved masses. Table 4.1 shows the calculated values indicating that among the considered particles, spontaneous decay is energetically possible only for the α -particle. Furthermore, if a nucleus is to be recognized as α -emitter, the decay rate must also not be too small to be detected (e.g. the half-life must be less than 10^{16} y).

Emitted Particle	Energy Release (MeV)	Emitted Particle	Energy Release (MeV)
n	-7.26	^4He	+5.41
^1H	-6.12	^5He	-2.59
^2H	-10.70	^6He	-6.19
^3H	-10.24	^6Li	-3.79
^3He	-9.92	^7Li	-1.94

^aComputed from known masses.

Table 4.1 Q-values for various modes of decay of ^{232}U (from Krane).

The spontaneous emission of an α -particle can be represented by the following process:



The α -particle, as shown by Rutherford, is a nucleus of ^4He , consisting of two neutrons and two protons. To understand the decay process, we must use the conservation of energy, as well as linear and angular momentum. Let us assume the initial decay nucleus X to be at rest. Thus, the total energy of the initial system is just the rest energy of X , $m_X c^2$. The final state will consist of X' and α , both in motion due to the conservation of linear momentum. Thus, the final total energy of the system is:

$$\begin{aligned} m_X c^2 &= m_{X'} c^2 + T_{X'} + m_\alpha c^2 + T_\alpha \\ (m_X - m_{X'} - m_\alpha) c^2 &= T_{X'} + T_\alpha \end{aligned} \tag{4.5}$$

The quantity on the left side of Eq. (4.5) is the net energy released in the decay, called the ***Q-value***:

$$Q = (m_X - m_{X'} - m_\alpha)c^2 \quad (4.6)$$

and the decay will occur spontaneously only if $Q > 0$. Q-values can be calculated from atomic mass tables because even though Eq. (4.6) represents a nuclear process, the electron masses will cancel in the subtraction. If the masses are in atomic mass units (u), the Q-values can be calculated directly in MeV, expressing c^2 as 931.50 MeV/u. The Q-value is also equal to the total kinetic energy carried by the decay fragments:

$$Q = T_{X'} + T_\alpha \quad (4.7)$$

If the original nucleus X is at rest, then its linear momentum is zero. Thus, due to the conservation of linear momentum, X' and α must move with equal and opposite momenta:

$$p_\alpha = p_{X'} \quad (4.8)$$

Since α decays typically release about 5 MeV of energy, it is possible to use nonrelativistic kinematics ($T \ll mc^2$) for both X' and α . Writing $T = P^2/2m$ and using (4.7) and (4.8), it is possible to express the kinetic energy of the α -particle in terms of the Q-value:

$$T_\alpha = \frac{Q}{1+m_\alpha/m_{X'}} \quad (4.9)$$

Because the mass ratio is small compared with 1 (X' is a heavy nucleus), it is sufficiently accurate to express this ratio simply as $4/(A-4)$, which gives, with $A \gg 4$:

$$T_\alpha = Q\left(1 - \frac{4}{A}\right) \quad (4.10)$$

Typically, the α -particle carries about 98% of the Q-value, with the much heavier nuclear fragment X' carrying only about 2%. The kinetic energy of an α -particle can be measured directly with a magnetic spectrometer, and this would allow to determine experimentally the decay Q-value. This is particularly useful to measure the masses of short-lived X' nucleus that cannot be measured directly.

In 1911 Geiger and Nuttal noticed that α emitters with large disintegration energies (Q-values) had short half-lives and vice versa. The example of ^{232}Th (1.4×10^{10} y; $Q = 4.08$ MeV) and ^{218}Th (1.0×10^{-7} s; $Q = 9.85$ MeV), shows that a factor 2 in energy implies a factor 10^{24} in half life! The theoretical explanation of this effect was one of the first triumphs of quantum mechanics. A log-plot of the half-life of α decays against Q (the Geiger-Nuttal rule) for even-Z, even-N nuclei is shown in Fig.4.2. Another important systematic relationship for α emitters is shown in Fig.4.3. Considering only nuclei with $A > 212$, it is evident that adding neutrons to a nucleus reduces the disintegration energy, which in turn increase the half-life following the Geiger-Nuttal rule, i.e. the

nucleus becomes more stable. An abrupt discontinuity is present near $A = 212$ ($N = 126$). This is a clear evidence of the nuclear shell structure.

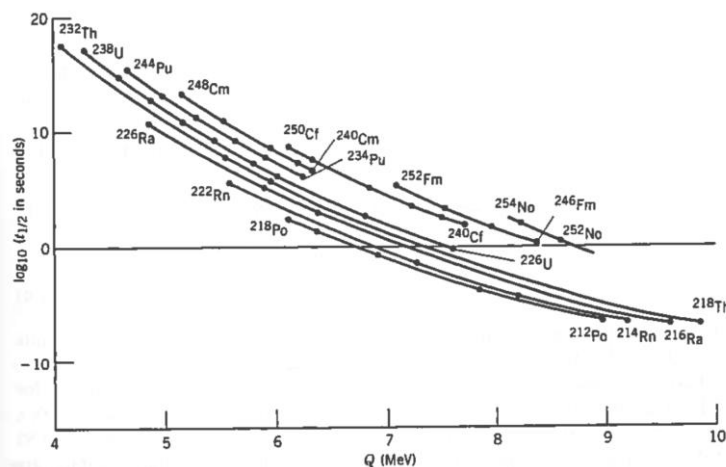


Figure 4.2 The inverse relation between α -decay half-life and decay energy, known as the Geiger-Nuttal rule. Only even-Z, even-N nuclei are shown (from Krane).

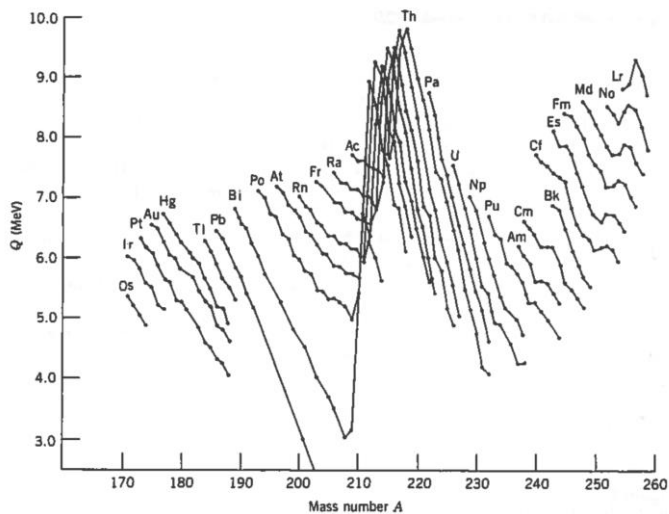


Figure 4.3 Q-values of α decay for various isotopic sequences of heavy nuclei (from Krane).

The general features of the Geiger-Nuttal rule can be accounted for by a quantum mechanical theory that was developed by Gamow and by Gurney and Condon in 1928. Based on this theory, an α -particle is assumed to move in a spherical region determined by the *daughter* nucleus. The central feature of this *one-body model* is that the α -particle is preformed inside the parent nucleus. The theory works quite well, especially for even-even nuclei. However, one should note that the theory does not prove that α -particles are preformed, but merely that they behave as if they were. The basic principles of theory are described in Fig.4.4. The potential energy between the α -particle and the residual nucleus, $V(r)$, is indicated for various distances between their centres. The horizontal line Q is the disintegration energy. The Coulomb potential is extended

inward to a radius a that can be taken as the sum of the radius of the residual nucleus and of the α -particle. Three regions of interest can be distinguished. First, the spherical region inside the nucleus ($r < a$) characterized by a potential well $-V_0$, where V_0 is taken as a positive number (classically the α -particle can move in this region with a kinetic energy $Q + V_0$, but cannot escape from it). Second, the annular-shell region ($a < r < b$) forming a potential barrier coming from the fact that the potential energy is more than the total available energy Q (classically the α -particle cannot enter this region from either directions). Third, the region outside the barrier ($r > b$) that is classically permitted. From the classical point of view, an α -particle in the spherical potential well would sharply reverse its motion every time it tried to pass beyond $r = a$. However, quantum mechanically there is a chance of “tunnelling” through such a barrier. This is justified by the fact that α -unstable nuclei do not decay immediately, but the α -particle within the nucleus must present itself again and again at the barrier surface until it finally penetrates. For example, in ^{238}U the tunnelling probability is so small that the α -particle must make $\sim 10^{38}$ tries (on the average) to escape ($\sim 10^9$ years)! The disintegration constant of an α -emitter is given in the one-body-theory by:

$$\lambda = fP \quad (4.11)$$

where f is the frequency with which the α -particle presents itself at the barrier, and P is the probability of transmission through the barrier that can be expressed as:

$$P = e^{-2G} \quad (4.12)$$

where G is known as *Gamow factor*.

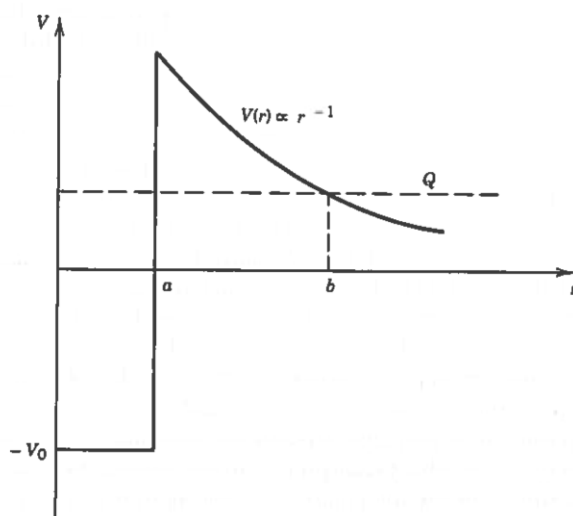


Figure 4.4 Relative potential energy of an α -particle as a function of its separation from the daughter-nucleus. The α -particle tunnels through the Coulomb barrier from a to b . (from Krane).

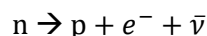
4.3 Beta Decay

The emission of electrons from the nucleus is one of the earliest observed radioactive decay processes. The capture by a nucleus of an electron from its atomic orbital was observed in 1938 by Alvarez through the detection of the characteristic X-rays emitted in the filling of the electron vacancy. The Joliot-Curie in 1934 first observed the nuclear process of positron (positive electron) emission decay. These three nuclear processes are known as β decays. In β decay processes a proton is converted into a neutron, or vice versa, thus both Z and N are changed by one unit: $Z \rightarrow Z \pm 1$, $N \rightarrow N \mp 1$ ($A = Z + N$ remains constant). The basic β decays are:

$n \rightarrow p + e^-$	negative beta decay (β^-)
$p \rightarrow n + e^+$	positive beta decay (β^+)
$p + e \rightarrow n$	orbital electron capture (ε)

The β^- decay process can be regarded as “creating” an electron from the available decay energy at the instant of decay. This electron is then immediately ejected from the nucleon. The three process above are not complete since there is yet another particle involved in each. One should note that the latter two processes occur only for protons bound in nuclei and are energetically forbidden for free protons.

β -decay electrons show a continuous energy distribution, from zero up to an upper limit (the endpoint energy) equal to the energy difference between the initial and the final states. This is because β decay is not a two-body process. In fact, a further particle is emitted in the decay process, the *neutrino*. The neutrino carries the missing energy. Conservation of electric charge requires the neutrino to be electrically neutral. Angular momentum conservation and statistical considerations require the neutrino to have a spin of $\frac{1}{2}$. Two different kind of neutrino are observed experimentally, the neutrino (ν) and the antineutrino ($\bar{\nu}$). The antineutrino is emitted in β^- decay and the neutrino is emitted in β^+ decay and electron capture. Let us demonstrate β -decay energetics considering the decay of the free neutron:



We define the Q value to be the difference between the initial and the final nuclear mass energies:

$$Q = (m_n - m_p - m_e - m_{\bar{\nu}})c^2 \quad (4.12)$$

and for decays of neutrons at rest:

$$Q = T_p + T_e + T_{\bar{\nu}} \quad (4.13)$$

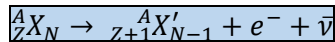
In a first approximation, we can ignore the proton recoil kinetic energy T_p (only 0.3 keV). The antineutrino and the electron will then share the decay energy, which accounts for the continuous electron spectrum. The maximum energy electrons correspond to minimum energy antineutrinos (and vice versa), and $Q \approx (T_e)_{\max}$. The measured maximum electron energy is 0.782 ± 0.013 MeV. Furthermore, using the measured neutron, electron, and proton masses, it is possible to calculate the Q-value:

$$\begin{aligned} Q &= m_n c^2 - m_p c^2 - m_e c^2 - m_{\bar{\nu}} c^2 \\ &= 939.573 \text{ MeV} - 938.280 \text{ MeV} - 0.511 \text{ MeV} - m_{\bar{\nu}} c^2 \\ &= 0.782 \text{ MeV} - m_{\bar{\nu}} c^2 \end{aligned}$$

Thus, within the precision of the measured maximum energy, it is possible to regard the antineutrino as massless, and for the following discussion we will consider the masses of the neutrino and antineutrino to be zero.

Because the neutrino is massless, it moves with the speed of light and its total relativistic energy E_ν is the same as its kinetic energy, thus we will use E_ν to represent neutrino energies. For the electron, we will use both its kinetic energy T_e , and its total relativistic energy E_e , which are related by $E_e = T_e + mc^2$. Decay energies are typically in the order of MeV, thus the nonrelativistic approximation is not valid for the decay electrons, and we must use relativistic kinematics. However, the nuclear recoil is of very low energy and can be treated non-relativistically.

Let us consider a typical negative β -decay process in a nucleus:



The corresponding Q-value would be:

$$Q_{\beta^-} = [m_N({}_{Z}^{A}X) - m_N({}_{Z+1}^{A}X') - m_e]c^2 \quad (4.14)$$

where m_N indicates nuclear masses. To convert nuclear masses into the tabulated neutral atomic masses, we can use the following formula:

$$m({}_{Z}^{A}X)c^2 = m_N({}_{Z}^{A}X)c^2 + Zm_e c^2 - \sum_{i=1}^Z B_i \quad (4.15)$$

where B_i represents the binding energy of the i^{th} electron. Thus, we can express Q_{β^-} in terms of atomic masses:

$$Q_{\beta^-} = \{[m({}_{Z}^{A}X) - Zm_e] - [m({}_{Z}^{A}X') - (Z+1)m_e] - m_e\}c^2 + \{\sum_{i=1}^Z B_i - \sum_{i=1}^{Z+1} B_i\} \quad (4.16)$$

The electron masses cancel, thus neglecting the differences in electron binding energies, we find:

$$Q_{\beta^-} = [m({}_{Z}^{A}X) - m({}_{Z}^{A}X')]c^2 \quad (4.17)$$

where the masses are neutral atomic masses. Here the Q-value represents the energy shared by the electron and the neutrino:

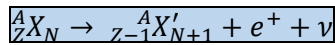
$$(T_e)_{max} = (E_{\bar{\nu}})_{max} = Q_{\beta^-} \quad (4.18)$$

In the case of the $^{210}\text{Bi} \rightarrow ^{210}\text{Po}$ decay, Eq. (4.17) gives:

$$Q_{\beta^-} = [m(^{210}\text{Bi}) - m(^{210}\text{Po})]c^2 = 1.161 \text{ MeV} \quad (4.19)$$

Fig.4.5 shows $(T_e)_{max} = 1.16 \text{ MeV}$, which is in excellent agreement with the value expected from Q_{β^-} .

In the case of positron β decay, a typical decay process is:

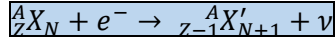


and a calculation like the previous one shows:

$$Q_{\beta^+} = [m({}^A X) - m({}^A X') - 2m_e]c^2 \quad (4.20)$$

where the electron masses do not cancel in this case.

For electron-capture processes, such as:



The calculation of the Q-value must consider that the atom X' is in an atomic excited state immediately after the electron capture. Thus, if the capture takes place from an inner atomic shell (e.g. K-shell), an electronic vacancy will be present. The vacancy is quickly filled by an electron from higher atomic shells and one (or more) characteristic X-ray is emitted. The total X-ray energy is equal to the binding energy of the captured electron. Thus, the atomic mass of X' immediately after the decay is greater than the mass of X' in its atomic ground state by B_n , the binding energy of the captured n -shell electron ($n = K, L, \dots$). The corresponding Q-value is:

$$Q_{\varepsilon} = [m({}^A X) - m({}^A X')]c^2 - B_n \quad (4.21)$$

In positron decay there is a continuous distribution of neutrino energies up to Q_{β^+} . In electron capture, however, the two-body final state results in unique values for the recoil energy and the neutrino energy. Thus, a monoenergetic neutrino with energy Q_{ε} is emitted. Table 4.2 shows some typical β -decay processes.

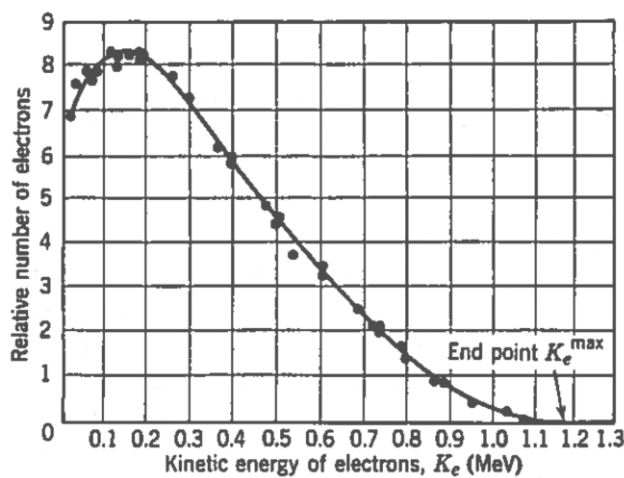


Figure 4.5 The spectrum of electrons emitted in the β decay of ^{210}Bi (from Eisberg and Resnick).

Decay	Type	Q (MeV)	$t_{1/2}$
$^{23}\text{Ne} \rightarrow ^{23}\text{Na} + e^- + \bar{\nu}$	β^-	4.38	38 s
$^{99}\text{Tc} \rightarrow ^{99}\text{Ru} + e^- + \bar{\nu}$	β^-	0.29	2.1×10^5 y
$^{25}\text{Al} \rightarrow ^{25}\text{Mg} + e^+ + \nu$	β^+	3.26	7.2 s
$^{124}\text{I} \rightarrow ^{124}\text{Te} + e^+ + \nu$	β^+	2.14	4.2 d
$^{15}\text{O} + e^- \rightarrow ^{15}\text{N} + \nu$	ϵ	2.75	1.22 s
$^{41}\text{Ca} + e^- \rightarrow ^{41}\text{K} + \nu$	ϵ	0.43	1.0×10^5 y

Table 4.2 Typical β -decay processes (from Krane).

4.4 Gamma Decay

Several radioactive nuclei emit γ -rays. These high energy photons carry away the excess energy when nuclei make γ -decay transitions from excited states to lower energy states. γ -rays have energies greater than $\sim 10^{-3}$ MeV since nuclear excited states range upward $\sim 10^{-3}$ MeV. Typically, γ decays arise when preceding β decay have produced some of the daughter nuclei in states of several MeV excitations. However, there are many other ways to produce nuclei in excited states, which subsequently γ decay. For instance, states of excitation energy around 7-8 MeV are produced following the capture of a low-energy neutron in a nucleus.

A widely used experimental technique to measure γ -ray energies is to let the photons transfer their energies to electrons by Compton effect, photoelectric effect, or pair production. The measured γ -ray energy spectrum is used to determine the energy of the nuclear excited states of the given transition. Another important information connected to γ decay is the transition rate R of each excited state. This can be measured by measuring the lifetime T of the excited state. An example of γ decay spectrum for ^{27}Al after bombardment with energetic protons is shown in Fig.4.6.

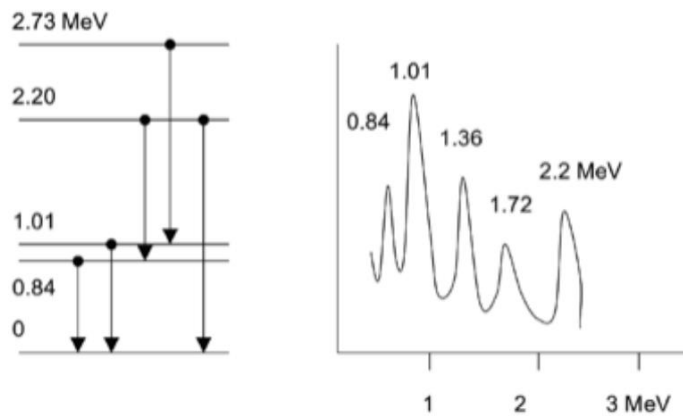


Figure 4.6 (left) Energy levels for ^{27}Al . Spectrum of γ -rays emitted after bombardment with energetic protons of ~ 5 MeV (from Krane)

In many γ decays, several groups of monoenergetic electrons are emitted along with the γ rays. In fact, if there is a preceding β decay, these groups will be superimposed on the continuous β -decay spectrum. The energy ε of these electrons is found to be related to the decay energy E :

$$\varepsilon = E - W \quad (4.22)$$

where W for the most prominent group equals the binding energy of a K-shell electron of the γ -decaying atom, and W for the other groups equal to the binding energies of electrons in the L, M, etc., atomic shells. The process involved is known as *internal conversion*. The latter consists of a direct transfer of energy through the electromagnetic interaction between a nucleus in an excited state and one of the electrons of its atom. The nucleus decays to a lower state, without ever producing a γ -ray. The internal conversion coefficient, α_K , is the ratio of the probability that a K-shell electron will be emitted, in a decay of its nucleus, to the probability that a γ -ray will be emitted. The two processes are independent alternatives, thus the total rate R_t for transition between the initial and final nuclear states is given by the following sum:

$$R_t = R + R_{ic} \quad (4.23)$$

where R and R_{ic} are the transition rates for γ -ray emission and internal conversion, respectively. This can also be written as:

$$R_t = R + \alpha_t R = R(1 + \alpha_t) \quad (4.24)$$

where $\alpha_t = \alpha_K + \alpha_L + \alpha_M + \dots$ is the total internal conversion coefficient. Thus, we can write:

$$T = \frac{1}{R_t} = \frac{1}{R(1 + \alpha_t)} \quad (4.25)$$

4.5 Nuclear Fission

In 1939 Meitner and Frisch proposed that the uranium nuclei following neutron capture are highly unstable and split nearly in half, thus called this effect *nuclear fission*. Fission results primarily from the competition between the nuclear and Coulomb forces in heavy nuclei. In fact, as already mentioned when describing the α -decay, the total nuclear binding energy roughly shows a linear increase with A , while the Coulomb repulsion energy of the protons increases faster ($\sim Z^2$). Like the α -decay case, we can consider heavy nuclei as residing very close to the top of the nuclear potential well, where the Coulomb barrier is very thin and easily penetrable. Thus, nuclear fission can occur spontaneously as a natural decay process, or it can be induced through the absorption of a relatively low-energy particle (e.g. a neutron, or a photon). Fission is an important process only for heavy nuclei (thorium and beyond) and can be applied for releasing a large total energy. This is possible thanks to the fact that every neutron-induced fission event produces, in addition to the heavy fragments, several neutrons that can in turn induce new fission events. This is known as fission “chain reaction” and can occur rapidly and without control (like in fission-based explosives), or slowly and under control (like in fission reactors).

The energetic preference for nuclei to undergo fission can be easily understood by considering the binding energy per nucleon. Let us consider the case of ^{238}U that shows a binding energy of about 7.6 MeV/nucleon. If ^{238}U were to divide into two equal fragments with $A \approx 119$, their binding energy per nucleon would be about 8.5 MeV (more tightly bound system), thus energy must be released. The extra energy can appear in a variety of forms (neutrons, β and γ emission from the fragments), but it appears primarily as kinetic energy of the fragments since Coulomb repulsion drives them apart. While the fission spontaneous decay mode does exist, it is not very probable compared to α decay (^{238}U shows a $T_{1/2} = 4.5 \times 10^9$ y and $\sim 10^{16}$ y for α decay and fission reactions, respectively), and it does not become an important decay process for nuclei with $A < 250$). The fission process is inhibited by the Coulomb barrier. In fact, if one divides ^{238}U into two identical fragments that are just touching at their surfaces, the corresponding Coulomb barrier is ~ 250 MeV, and this prevents the two fragments from separating, as shown in Fig. 4.7. However, the assumption that ^{238}U splits into two identical fragments is not very realistic, and there are certain nuclei for which the energy release puts the two fragments just below the Coulomb barrier, giving them a reasonably good chance to penetrate it. These are nuclei undergoing *spontaneous fission*, and compete successfully with other radioactive decay processes. Theoretical calculations indicate that the Coulomb barrier against fission is zero at about $A = 300$. Other nuclei maybe far enough below the Coulomb barrier and spontaneous fission is not observed, but absorption of a relatively low amount of energy (e.g. from a neutron or a photon) forms an intermediate state

that is at (or above) the barrier, thus *induced fission* occurs, successfully competing with other decay modes. The ability of a nucleus to undergo induced fission will depend on the energy of the intermediate system. Absorption of thermal neutrons can be sufficient to push some nuclei over the Coulomb barrier, while for others, fast neutrons (\sim MeV) may be required. A more realistic representation of the fission barrier for heavy nuclei is shown in Fig.4.8. Furthermore, a more detailed calculation of the energy needed to induce fission is shown in Fig.4.9, which provides the height of the fission barrier above the ground state, known as *activation energy*. Such calculation is based on the liquid-drop model that considers only average nuclear properties; however, the inclusion of effects based on the Shell model suggests that certain super-heavy nuclei ($A \sim 300$) may be more stable against fission.

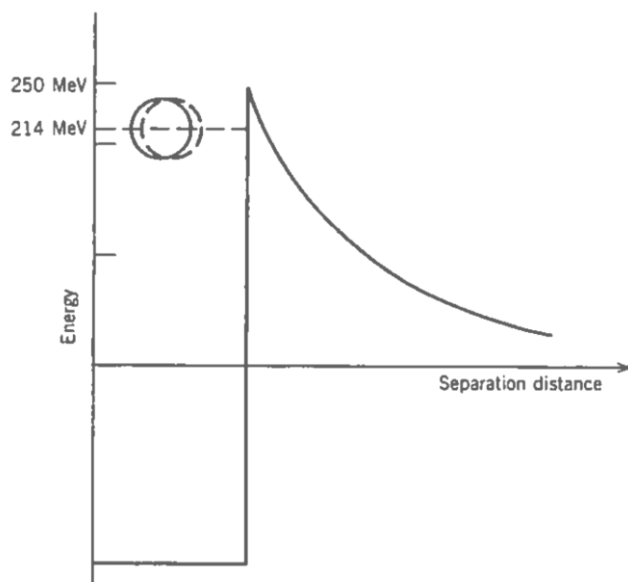


Figure 4.7 Nuclear potential well for two possible fragments of ^{238}U (^{119}Pd nuclei) (from Krane)

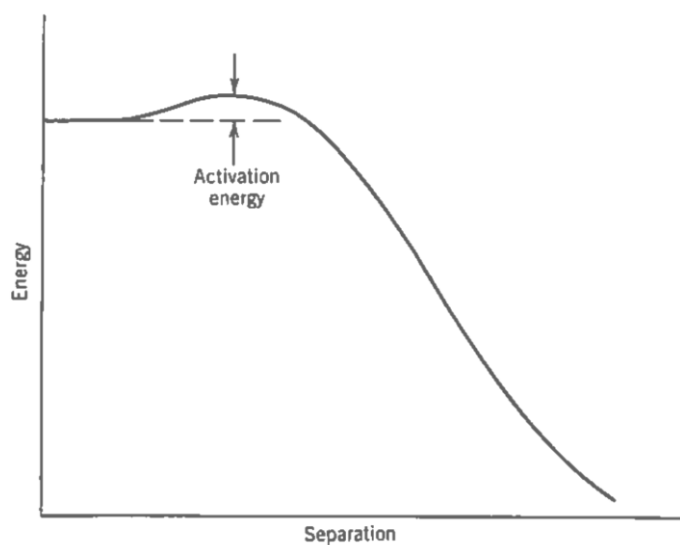


Figure 4.8 Smooth potential barrier opposing the spontaneous fission of ^{238}U (from Krane)

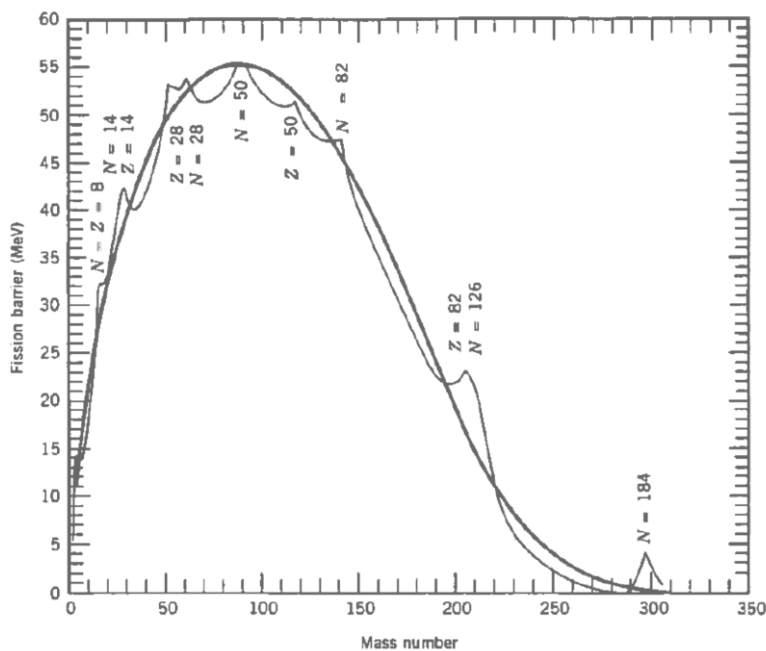


Figure 4.9 Variation of fission activation energy with mass number (from Krane)

A typical neutron induced fission reaction is:



which is possible for incident neutrons of thermal energies. The fission products are not determined uniquely, and there is a distribution of masses of the two fission products of the form shown in Fig.4.10. The mass distribution is characteristic of low-energy fission processes. In contrast, fission induced by high-energy particles show mass distributions favouring equal-mass fragments. The fission fragments must share 92 protons, and the nuclei formed will be $^{95}_{37}\text{Rb}_{58}$ and $^{140}_{55}\text{Cs}_{85}$. These nuclei are extremely rich in neutrons. In fact, most stable nuclei in this region have $Z/A \approx 0.41$, while for this fission products $Z/A \approx 0.39$. The fission fragments compensate this neutron excess through emission of one, or more neutrons at the instant of fission (within 10^{-16} s), and these neutrons are known as *prompt neutrons*. The average number of prompt neutrons, indicated with ν , is characteristic of the given fission process. For thermal neutron induced fission, the experimentally observed values of ν are 2.48 for ^{233}U , 2.42 for ^{235}U , and 2.86 for ^{239}Pu . In addition to the prompt neutrons, *delayed neutrons* are often emitted in fission. These neutrons are emitted following the β decay of the fission fragments. Typical delay times are relatively short (of the order of seconds). They play a key role in the control of nuclear reactors. In fact, no mechanical system could respond rapidly enough to prevent statistical variations in the prompt neutrons from causing the reactor to run out of control, but it is indeed possible to achieve control using the delayed neutrons. The initial fission products are highly radioactive and decay towards stable isobars by emitting β and γ radiation, which ultimately contributes to the total energy

release in fission. These radioactive products represent the waste of nuclear reactors. Many of them decay very quickly, but others have long half-lives, especially near the stable members of the series. Fig.4.11 shows the cross sections for neutron-induced fission of ^{235}U and ^{238}U . The thermal region shows the typical $1/v$ (here v is the incoming neutron velocity) dependence of the cross section for ^{235}U . The thermal cross section is 3 orders of magnitude larger than the cross section for fast neutrons. In fact, if one wants to use the fast ($\sim \text{MeV}$) neutrons emitted in fission to induce new fission events, the neutrons must first be moderated to thermal energies to increase the cross section. For ^{238}U there is no fission occurring in the thermal region, and fission can occur only for fast neutrons. This clear difference results from the relationship between the excitation energy of the compound system and the activation energy needed to overcome the barrier.

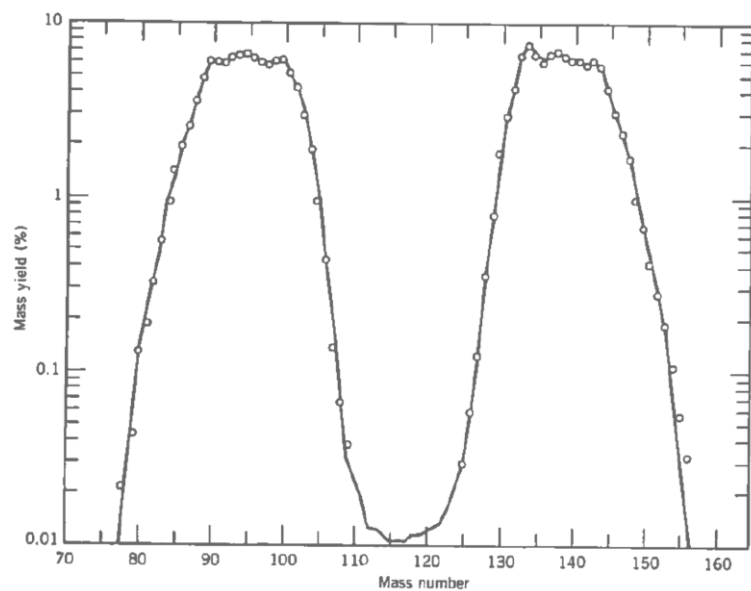


Figure 4.10 Mass distribution of fission fragments from thermal fission of ^{235}U (from Krane)

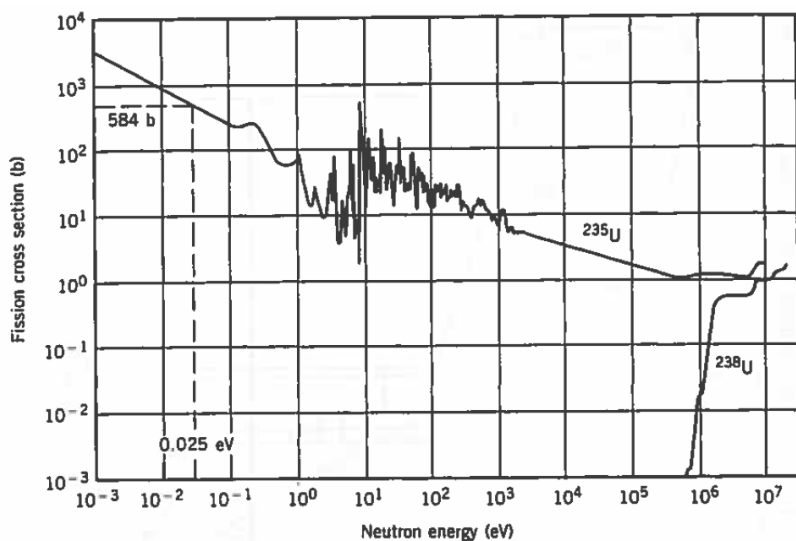


Figure 4.11 Cross-section for neutron-induced fission of ^{235}U and ^{238}U (from Krane)

When ^{235}U captures a neutron to form the compound state $^{236}\text{U}^*$, the excitation energy is:

$$E_{\text{ex}} = [m(^{236}\text{U}^*) - m(^{236}\text{U})] c^2$$

The energy of the compound state can be found directly from the mass energies of ^{235}U and a neutron, assuming that the neutron's kinetic energy is negligible (thermal neutron):

$$m(^{236}\text{U}^*) = m(^{235}\text{U}) + m_n = (235.043924 + 1.008665) u = 236.052589 u$$

Thus, we can estimate the excitation energy:

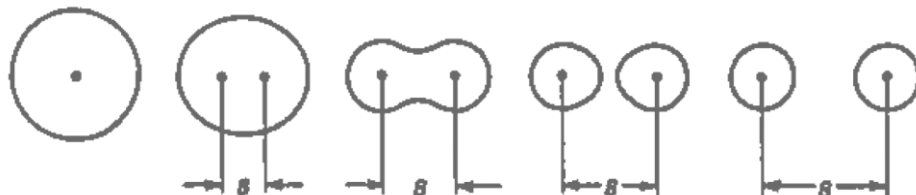
$$E_{\text{ex}} = (236.052589 u - 236.045563 u) 931.502 \text{ MeV/u} = 6.5 \text{ MeV}$$

The activation energy (energy to overcome the fission barrier) for ^{236}U is calculated also to be 6.2 MeV, thus the energy needed to excite ^{236}U into a fissionable state is exceeded by the energy we get by adding a neutron to ^{235}U . This means that ^{235}U can be fissioned with "zero" energy neutrons, which is consistent with its large fission cross section in the thermal region. A similar calculation for:



gives $E_{\text{ex}} = 4.8 \text{ MeV}$, which is much smaller than the calculated activation energy for ^{239}U (6.6 MeV). Neutrons of at least MeV energy are therefore required for fission of ^{238}U , which is consistent with the observed threshold for neutron-induced fission of ^{238}U .

The steps involved in fission are indicated schematically by the set of drawings in Fig.4.12. These define a parameter s which characterizes the progress of the fission by specifying the elongation of the fissioning nucleus, and then the separation of the two fission fragments. Fig.4.13 illustrates the reason why the fission fragments tend to have relatively too many neutrons, thus undergo a succession of β decays, or in some case *evaporation* of two or three neutrons liberating several MeV kinetic energy.

**Figure 4.12** Schematic representation of the nuclear fission process (from Eisberg & Resnick)

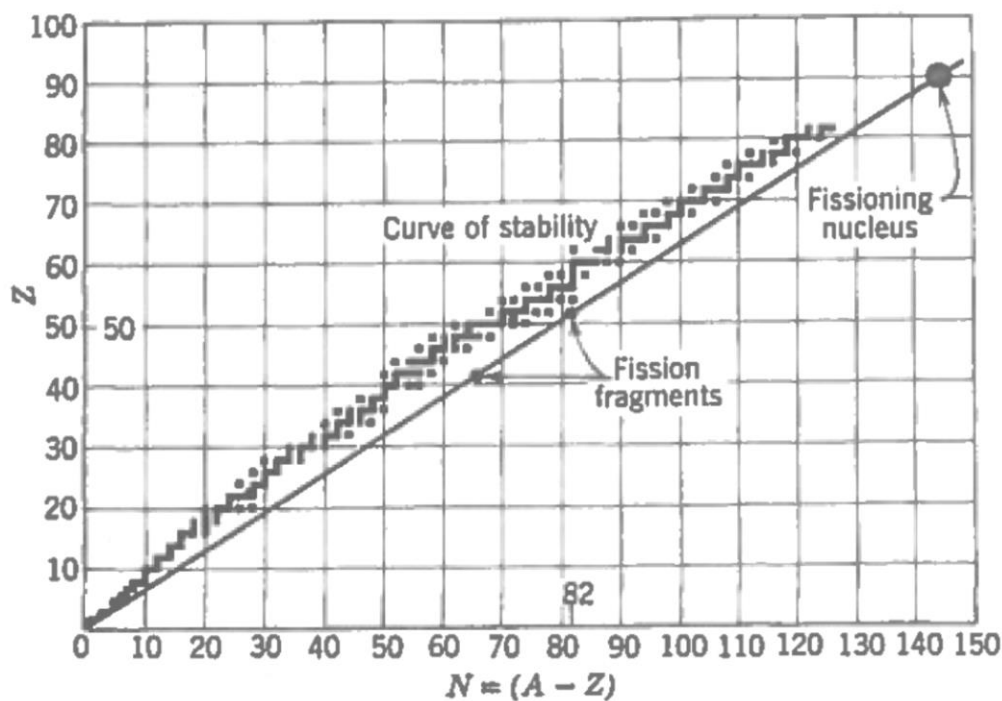


Figure 4.13 Fission fragments showing an excess of neutrons (from Eisberg & Resnick)

Let us consider an infinitely large mass of uranium in its natural isotopic composition (0.75% ^{235}U , 99.28% ^{238}U). A single fission event will produce about 2.5 neutrons on the average. Each of this “second-generation” neutrons can produce another fission event that, in turn, produces even more neutrons, and so on. This process is known as *chain reaction*. Each fission event releases about 200 MeV in the form of kinetic energy of heavy fragments, i.e. heat, and radiation. It is convenient to define the *neutron reproduction factor* k_∞ (for an infinite medium, i.e. ignoring loss of neutrons through leakage at the surface). The reproduction factor gives the net change in the number of thermal neutrons from one generation to the next. On the average, each thermal neutron produces k_∞ new thermal neutrons. For a chain reaction to continue, one must have $k_\infty \geq 1$. In fact, although we have an average of 2.5 neutrons emitted per fission, these are *fast neutrons*, for which the fission cross-section is typically small. Thus, it is convenient to moderate these neutrons to thermal velocities because of the large thermal cross sections. In the process, many neutrons can be absorbed, or lost, and the 2.5 fast neutrons per fission can easily become < 1 thermal neutron, effectively halting the reaction. Since neutrons lose energy in elastic collisions with nuclei, a popular choice for a *moderator* is carbon in the form of graphite blocks. In fact, the best choice for a moderator is the lightest nucleus, to which the neutron transfers the largest possible energy in an elastic collision. A lattice of blocks of uranium alternating with graphite is called a chain-reacting *pile*. If the reproduction factor k (for a finite pile) is exactly 1, the pile is said to be *critical*; for $k < 1$, the pile is *subcritical*, and for $k > 1$ it is *supercritical*. To maintain a steady release of energy one would like for the pile to be exactly critical.

In a nuclear reactor, fission proceeds at carefully controlled rate. A continuous source of power is obtained from the thermal energy produced when the fission fragments come to rest in the material of the reactor. All reactors consist of the same essential elements: (i) the *fuel*, or fissile material; (ii) a *moderator* to thermalize the neutrons; (iii) a *reflector* surrounding the core (fuel elements plus moderator) to reduce neutron leakage and thereby the reactor size; (iv) a *containment* vessel to prevent the escape of radioactive fission products; (v) *shielding* to prevent neutrons and γ -rays from causing biological harms to the operating personnel; (vi) a *coolant* to remove heat from the core; (vii) a *control system* allowing the operator to control the power level and to keep it constant during normal operations; and (viii) various *emergency systems* designed to prevent runaway operations in the event of a failure of the control or coolant systems. After many years of technological development, nuclear reactors have become sources of power which are economically very competitive with coal and/or oil. They are also source of unstable isotopes, not normally found in nature, that are used as tracers for diagnosing the operations of a variety of processes of interest to medicine, biology, chemistry, and engineering, or used for radiation therapy. The isotopes are produced in nuclear reactions induced by intense fluxes of neutrons present in a reactor.

4.6 Nuclear Fusion

Energy can be extracted from the nucleus in an alternative way to fission as suggested by the nuclear binding energy curve shown in Fig.4.14. In fact, it is possible to “climb” the binding energy curve toward the more stable nuclei by beginning with the very light nuclei, rather than the very heavy nuclei as in fission. Thus, if one combines two light nuclei into a nucleus below $A = 65$, energy is released. This process is called *nuclear fusion* because two light nuclei are fused into a heavier one. As an energy source, fusion has several advantages over fission. The light nuclei are abundant in nature and easy to obtain, and the end products of fusion are usually light, stable nuclei rather than heavy radioactive ones as in fission. However, nuclear fusion has a clear disadvantage over fission: to be combined, light nuclei must overcome their mutual Coulomb repulsion. On the other hand, fission induced by neutrons has practically no Coulomb barrier and very low energy incident particles can be used.

Let us consider the fusion of two ^{20}Ne nuclei to form a ^{40}Ca nucleus with a Q-value of 20.7 MeV, thus the reaction is energetically permitted. However, before the nuclear forces of the two ^{20}Ne nuclei can interact, we must move them close enough together so that their nuclear distributions begin to overlap. At the point when their surfaces are just touching, the Coulomb repulsion is 21.2 MeV. If we were to perform a nuclear reaction in which two ^{20}Ne nuclei were brought together

with a total kinetic energy of 21.2 MeV, the final energy of the system would be 41.9 MeV (the 21.2 MeV of potential energy associated with the nuclei Coulomb repulsion plus the 20.7 MeV energy released in the nuclear reaction). Therefore, the energy gain of such reaction is about a factor 2 (~ 21 MeV goes in and ~ 42 MeV comes out). Although accelerating ^{20}Ne to 21.2 MeV against a ^{20}Ne target can be easily done by particle accelerators, the overall efficiency of such induced nuclear physics experiment is not high. In fact, heavy-ion accelerators typically produce beams in the nA- μA range, and even in the totally unrealistic assumption that every particle in the beam were to react, the power output would be 20 W. This would not be enough even to run the accelerator laboratory! An alternative approach would be to heat a container of neon gas until the thermal energy is large enough to have a high probability of two nuclei approaching one another and colliding with 21.2 MeV of energy. This process is known as *thermonuclear fusion* and, in the case of Ne, would require an extremely high temperature of about 10^{11} K!

Despite the drawback mentioned above, nuclear fusion energy is currently a subject of intensive research to develop techniques allowing to heat fusible nuclei, and to increase their density to enhance the total number of fusion reactions. Fusion also powers the Sun and other stars, thus is ultimately responsible for the evolution of life on Earth. Understanding nuclear fusion is crucial to achieve a comprehensive knowledge about the end products of stellar reactions, when thermonuclear fuel is mostly exhausted and a star may pass through a nova or supernova stage, ending as an agglomerate of cosmic ash, or as a neutron star or a black hole.

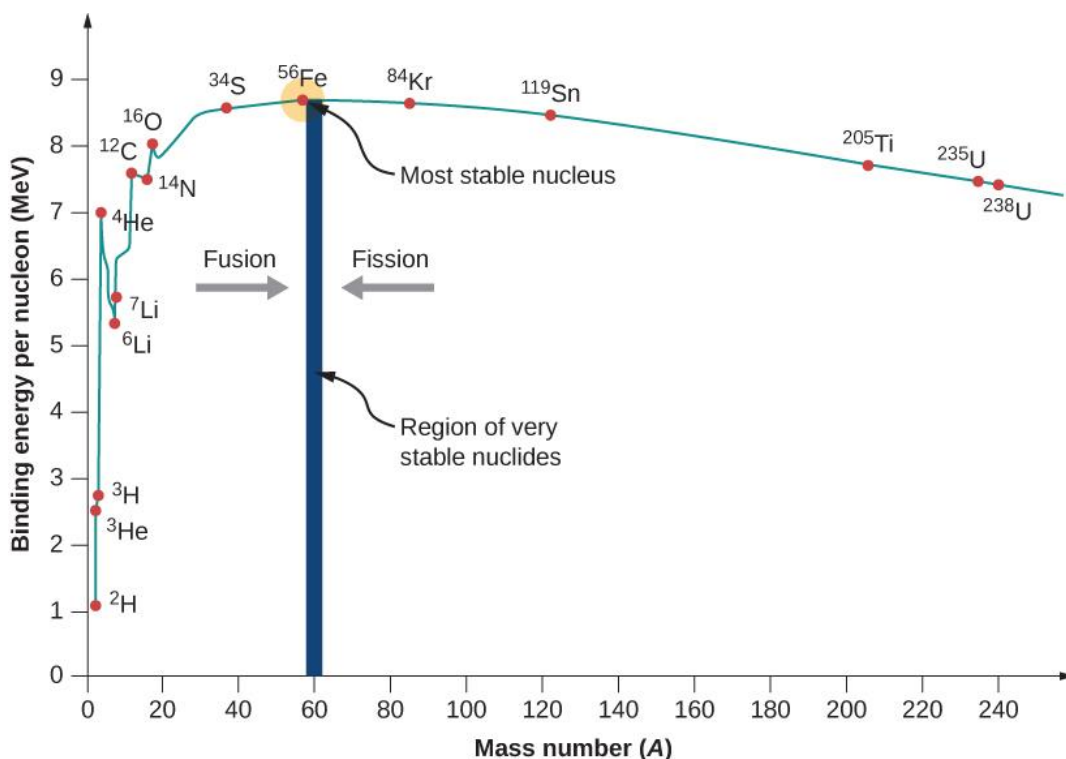
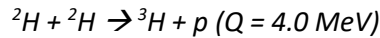
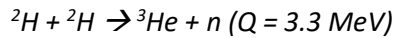
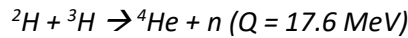


Figure 4.14 Nuclear binding energy curve

Differently from fission, nuclear fusion is not a spontaneous process on Earth because of the substantial limitations imposed by the Coulomb barrier. Typical reactions are based on *deuterium-deuterium (or D-D) fusion*:



The more stable the end product formed, the greater is the energy release in the reaction. In fact, a reaction that forms ^4He would be likely to show a large energy release, such as:



This reaction is known as *deuterium-tritium (or D-T) fusion*. Based on linear momentum conservation, and on the assumption that the incident particles have negligibly small kinetic energies, one can find that the ^4He and n share 17.6 MeV kinetic energy, and that a monoenergetic neutron with energy of 14.1 MeV emerges. Because of the large energy release, D-T fusion has been selected for its potential use in controlled fusion reactors. However, a disadvantage of such fusion reaction is that most of the energy is given to the neutron, thus it is not easy to extract. On the other hand, in nuclear fission only a small fraction of the energy is carried by the neutrons, thus the kinetic energy of the fission fragments is easy to extract.

The energy released in nuclear fusion can be estimated calculating the Q-value of the given reaction. Most of the fusion applications (including solar processes) are based on reacting particles with very small energies (1-10 keV) compared to the corresponding Q-values (several MeV). The final total energy of the product particles, again neglecting the initial motions, will then be equal to the Q-value:

$$\frac{1}{2}m_b v_b^2 + \frac{1}{2}m_Y v_Y^2 \approx Q \quad (4.26)$$

for product particles b and Y . Furthermore, the final momenta are equal and opposite:

$$m_b v_b \approx m_Y v_Y \quad (4.27)$$

and thus:

$$\frac{1}{2}m_b v_b^2 \approx \frac{Q}{1+m_b/m_Y} \quad (4.28)$$

$$\frac{1}{2}m_Y v_Y^2 \approx \frac{Q}{1+m_Y/m_b} \quad (4.29)$$

A consequence of this energy sharing is immediately apparent: the lighter product particle takes the larger share of the energy. The ratio of the kinetic energies can be calculated from Equation (4.27):

$$\frac{\frac{1}{2}m_b v_b^2}{\frac{1}{2}m_Y v_Y^2} \approx \frac{m_Y}{m_b} \quad (4.30)$$

Thus, in the D-T reaction case, the product neutron carries 80% of the total energy. In the DD reaction case, the product neutron (or proton) carries 75% of the available energy.

If R_a and R_X are the radii of the reacting particles, the Coulomb barrier is:

$$V_C = \frac{e^2}{4\pi\epsilon_0} \frac{Z_a Z_X}{R_a + R_X} \quad (4.31)$$

when the particles just touch at their surface. The product $Z_a Z_X$ will ultimately appear in an exponential barrier penetration probability. Therefore, the fusion probability decreases rapidly with $Z_a Z_X$, and the barrier is lowest for the hydrogen isotopes. For D-T fusion, $V_C = 0.4 \text{ MeV}$, thus it is still far above the typical incident particle energy (1-10 keV). However, just as in α decay, it is not necessary for the particles to be above the barrier since it is the barrier penetration probability that determines the outcome.

For particles reacting at thermal energies, it is likely that the fusion reaction will occur far from any resonance, and thus the energy dependence of the cross section comes mainly from two terms: i) the $1/v^2$ dependence, and ii) the partial reaction probability, which for two particles includes a barrier penetration factor of the form e^{-2G} , similarly to α decay:

$$\sigma \propto \frac{1}{v^2} e^{-2G} \quad (4.32)$$

where v represents the relative velocity of the reacting particles, and G is defined as:

$$G = \frac{e^2}{4\pi\epsilon_0} \frac{\pi Z_a Z_X}{\hbar v} \quad (4.33)$$

Fig.4.15 shows the cross sections of three typical fusion reactions.

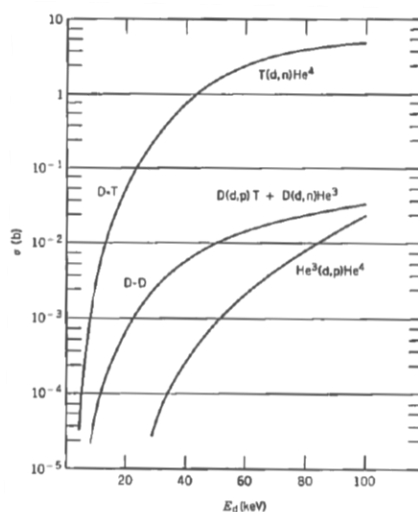


Figure 4.15 Cross sections for nuclear fusion reactions (*from Krane*)

The rate for a nuclear reaction depends on the product σv . In thermonuclear fusion there is a distribution of particle speeds described by a Maxwell-Boltzmann velocity distribution:

$$n(v) \propto e^{-mv^2/2kT} \quad (4.34)$$

In such a distribution of nuclei, it is appropriate to calculate σv averaged over all particle energies, E :

$$\langle \sigma v \rangle \propto \int_0^\infty e^{-E/kT} dE \quad (4.35)$$

Fig.4.16 shows $\langle \sigma v \rangle$ for several fusion reactions as a function of the temperature.

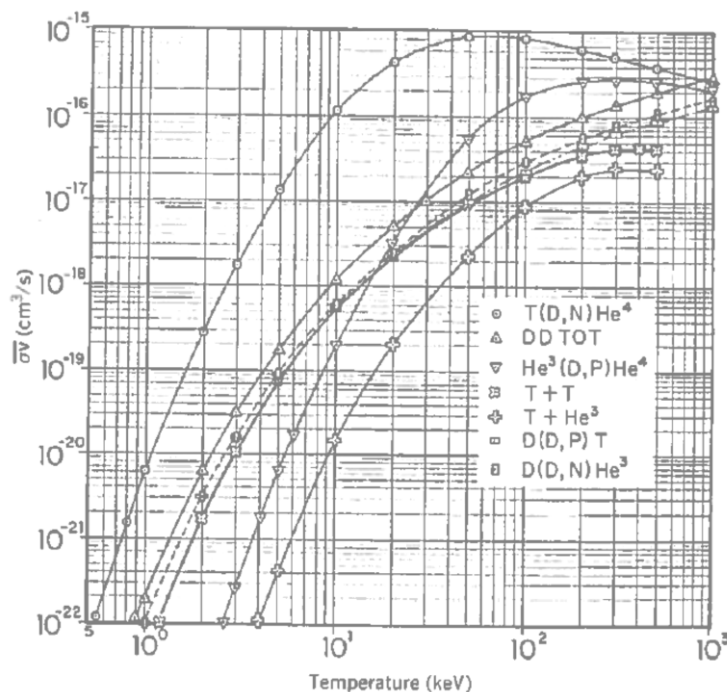
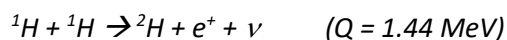


Figure 4.16 $\langle \sigma v \rangle$ averaged over a Maxwell-Boltzmann energy distribution for various fusion reactions (from Krane)

The Sun is an extremely successful prototype of a self-sustaining thermonuclear reactor. In fact, based on fossil records on Earth, the Sun's output has been nearly constant over a time scale of more than 10^9 years. The basic nuclear process in the Sun is the fusion of hydrogen into helium (H is by far the most abundant element in the universe). All fusion reactions must be two-body processes since the simultaneous collision of three particles is too improbable to be significant. The first step in the **solar fusion** process must be the combination of two protons to form the only stable two-nucleon system:

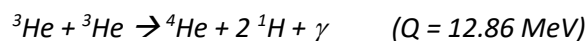


The presence of a neutrino in the final state signals a weak interaction process, which must occur to turn a proton into a neutron. The cross sections for weak interaction processes are very small,

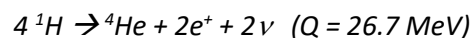
and even at the high densities at the core of the Sun ($\sim 7.5 \times 10^{25}$ protons/cm³) the reaction rate is only about 5×10^{-18} s⁻¹ per proton. However, the Sun keeps radiating thanks to the enormous number of reacting protons ($\sim 10^{56}$) that allows to have a total reaction rate of about 10³⁸ s⁻¹. This step in the solar fusion cycle is known as “bottleneck” because it is the slower and least probable one. Following deuteron formation, the following fusion reaction is very likely to occur:



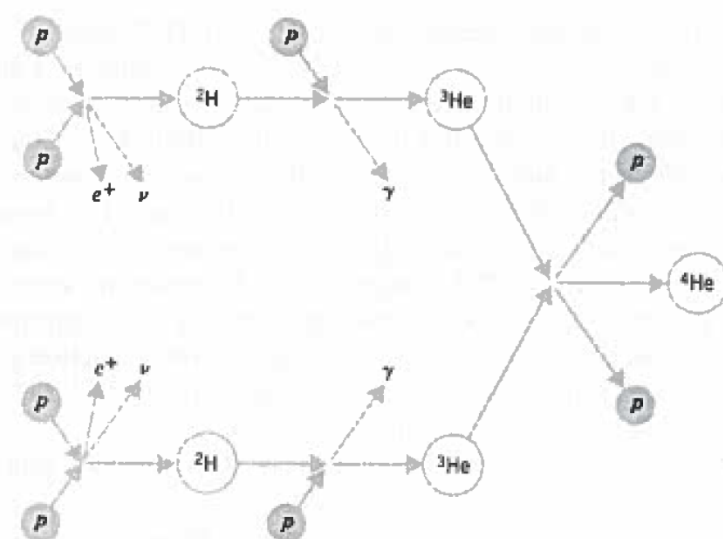
At this stage, it is very unlikely to observe D-D reactions because of the small number of deuterons present (only one ²H is formed every 10¹⁸ protons). Thus, deuterons are converted into ³He nearly as rapidly as they are formed. Reactions of ³He with ¹H or ²H are not favourable, thus ³He will interact only when it will find another ³He:



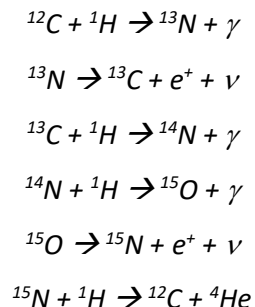
The complete process is known as *proton-proton cycle* and is schematically shown in Fig.4.17. The net process is:



The energy released in these nuclear reactions is converted to light in the *photosphere*, the outer region of the Sun. The visible light that reaches us from the Sun is characteristic of its surface and represents γ rays from reactions in the core that are scattered many thousands of times before reaching the surface. It can take millions of years for the radiation to emerge from the surface, hence the light that we see today results from solar processes that occurred millions of years ago. On the other hand, the neutrinos come to us directly from the core at the speed of light.

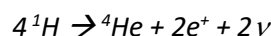


If in addition to hydrogen and helium there are heavier elements present in the interior of a star, a different series of fusion reactions can occur, e.g. the *carbon (or CNO) cycle*:



In this case ${}^{12}\text{C}$ is neither created nor destroyed, but act as a catalyst to aid in the fusion process.

The net process is:



Which is the same as in the proton-proton cycle, thus the Q-value is the same. However, the carbon cycle can proceed more rapidly than the proton-proton cycle because it does not have a process analogous to the deuterium bottleneck. Nevertheless, the Coulomb barrier is 6-7 times higher for proton reactions with carbon and nitrogen than for proton-proton reactions. Thus, the carbon cycle will be dominant at higher temperatures, where additional thermal energy is needed to increase the probability to penetrate the Coulomb barrier, as shown in Fig.4.18. Once a star has exhausted its hydrogen fuel, helium fusion reactions can take place with $3 {}^4\text{He} \rightarrow {}^{12}\text{C}$ at higher temperature needed to penetrate the Coulomb barrier. Other reactions involving fusion of light nuclei can continue to release energy, until the process ends near ${}^{56}\text{Fe}$, beyond which there is no energy gain in combining nuclei.

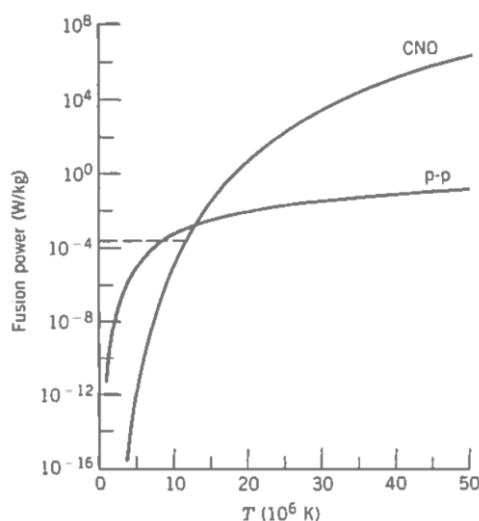


Figure 4.18 Power generation per unit mass of fuel for proton-proton and CNO processes. The dashed line indicates the Sun's power (from Krane)

Nuclear fusion can be considered as the most important phenomenon in nature. Fusion is the source of energy of the Sun and ultimately of all the natural physical and biological processes on the Earth. Furthermore, nuclear fusion is potential usable directly on Earth to produce energy in ***fusion reactors***. In fact, much of the Earth is covered by sea containing the hydrogen isotopes ^1H and ^2H , thus the fuel supply of low-A nuclei would be almost inexhaustible. However, an intense thermal fusion reactor of relatively small size would require reaching temperatures at least one order of magnitude higher than the internal temperature of the Sun. There are approaches that allow reaching such temperatures, however a “container” that would not be destroyed by the high temperature needs to be found. The Sun is so massive that gravitational fields provide a natural container. The essence of controlling fusion reactions and extracting usable energy is to heat a thermonuclear fuel to temperatures of the order of 10^8 K (mean particle kinetic energy of ~ 10 keV) while simultaneously maintaining a high enough density for a long enough time and allow to have a fusion reaction rate large enough to generate the desired power. At these temperatures the atoms rapidly become ionized (only 13.6 eV is needed to strip the electron from the hydrogen atom), and the fuel is a hot cloud of positive ions and negative electrons but electrically neutral overall. Such a system is called *plasma*. The electrostatic properties of a plasma determine a characteristic scale length called *Debye length*:

$$L_D = \sqrt{\left(\frac{4\pi\varepsilon_0}{e^2} \frac{kT}{4\pi n}\right)} \quad (4.36)$$

where n is the mean electron (or ion) density. For a rarefied plasma ($\sim 10^{22} \text{ m}^{-3}$) with a temperature of ~ 10 keV, the Debye length is $\sim 10 \mu\text{m}$, and the number of particles in a volume of dimension of one Debye length is $\sim 10^7$. It is important to mention that the physical size of the reacting plasma is much larger than the Debye length in dimension. One of the major problems is to be able to confine the plasma for a relatively long time. In fact, if the hot fuel exchanges energy with the walls of its container, it will cool down and the container will be melted. Currently there are two major schemes being explored to confine the thermonuclear fuel: *magnetic confinement fusion* and *inertial confinement fusion*. In magnetic confinement, the plasma is confined by an ad-hoc designed magnetic field system. In inertial confinement, a solid pellet is rapidly heated and compressed by being struck simultaneously from many directions with high peak-power laser beams. However, in both approaches there are many processes that cause the plasma to lose energy. The primary mechanism is *bremsstrahlung*, in which the Coulomb scattering of two particles produces an acceleration which in turn gives rise to emission of radiation. The largest accelerations are suffered by the lightest particles (electrons) but due to a local thermal equilibrium between ions and electrons, any loss by the electrons is also felt by the ions, which

become then less energetic and less effective in penetrating the Coulomb barrier. The power per unit volume radiated in bremsstrahlung is:

$$P_{br} = 0.5 \cdot 10^{-36} Z^2 n_i n_e (kT)^{\frac{1}{2}} W/m^3 \quad (4.37)$$

where kT is in keV, n_i is the ion density, and n_e is the electron density. Comparing Equation (4.37) with the fusion power density in Fig.4.19, shows a temperature at which the fusion output will exceed the bremsstrahlung loss, which is about 4 keV for D-T and 40 keV for D-D reactions. This justifies the choice of D-T for fuel of the current nuclear fusion based research reactors. It is important to note that the bremsstrahlung losses increase as Z^2 ; therefore, fusion reactions using nuclei other than hydrogen have much larger bremsstrahlung losses, along with smaller reaction rates (due to the higher Coulomb barrier). Thus, the operating temperature of a fusion reactor is chosen to obtain a power gain where fusion generated power is higher than the bremsstrahlung losses.

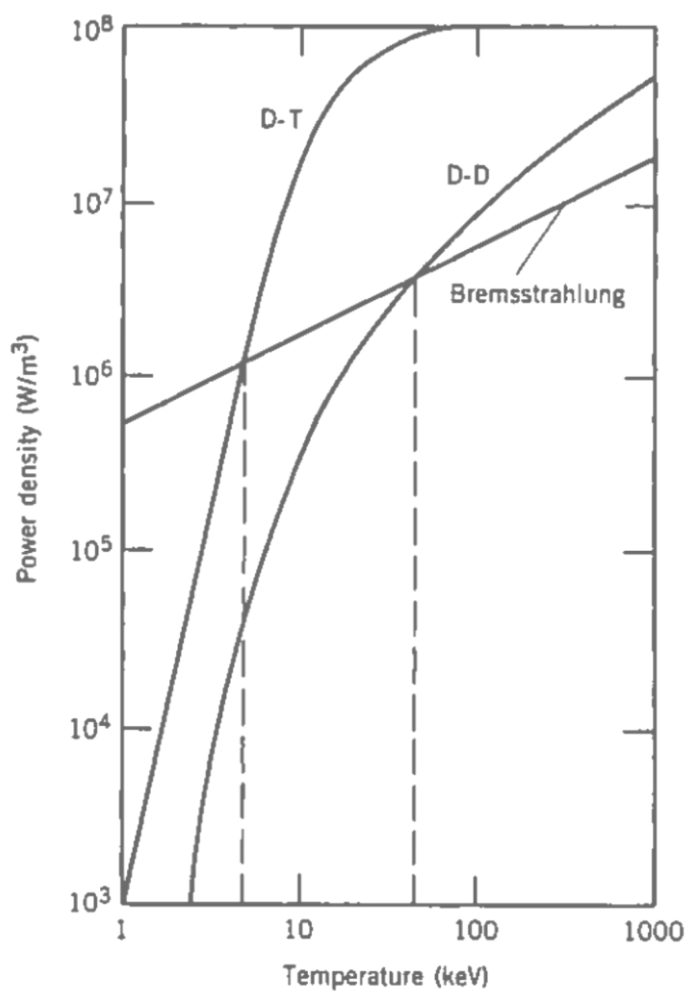


Figure 4.19 Comparison of bremsstrahlung losses with power outputs of D-D and DT nuclear fusion reactions, under the assumption of an ion density of $10^{21} m^{-3}$ (from Krane)

The fusion reactor would have a net energy gain if the energy released in fusion reactions exceeds the radiation losses and the original energy investment in heating the plasma to the operating temperature. At temperature of 4-10 keV, the D-T fusion gain is greater than the radiation losses (see Fig.4.19), thus, in first approximation, we can neglect the loss in energy due to radiation. The energy released per unit volume from fusion reactions is:

$$E_f = \frac{1}{4} n^2 \langle \sigma v \rangle Q \tau \quad (4.38)$$

where we assume that the densities of D and T are each equal to $\frac{1}{2}n$ (total n is equal to n_e for D-T), Q is the energy released per reaction (17.6 MeV for D-T), and τ is the time duration the plasma is confined during which reactions can occur. The thermal energy per unit volume needed to raise the plasma ions and electrons to a temperature T is $3/2n_e kT$ (ions) and $3/2n_e kT$ (electrons). If $n = n_i = n_e$ (local thermal equilibrium), the thermal energy is:

$$E_{th} = 3nkT \quad (4.39)$$

Thus, if we supply an energy of E_{th} to heat the plasma, and then we can confine it for a time τ , we can extract fusion energy E_f . The reactor would show a net energy gain if $E_f > E_{th}$:

$$\frac{1}{4} n^2 \langle \sigma v \rangle Q \tau > 3nkT \quad (4.40)$$

or:

$$n\tau > \frac{12kT}{\langle \sigma v \rangle Q} \quad (4.41)$$

This method allows to estimate the minimum necessary product of ion density and confinement time. This is known as *Lawson criterion* and represents the goal of a thermonuclear reactor design. For an operating temperature of 10 keV for D-T fusion, $\langle \sigma v \rangle \approx 10^{-22} \text{ m}^3/\text{s}$, and thus $n\tau > 10^{20} \text{ s/m}^3$.

A reactor design called “Tokamak”, using a magnetic confinement fusion approach, is one of the most promising candidates for the basic design of a fusion power reactor. Inertial confinement fusion uses a very different approach. A tiny pellet containing deuterium and tritium is rapidly struck with intense laser pulses ($\sim \text{ns}$) that both hit and compress it to high density. The goal of this method is to achieve densities and temperatures that are high enough to allow efficient nuclear fusion before the pellet expands and blows apart. To make a rough estimate of the requirements for such a reactor, it is important to note that the time necessary for the compressed pellet to blow apart is determined by the propagation speed of mechanical waves in the plasma medium, which is of the same order of magnitude as the mean thermal speed of the particles in the medium. At a temperature of 10 keV, the mean thermal speed is $\sim 10^6 \text{ m/s}$. If we consider a pellet compressed to a diameter of 0.1-1 mm, it is expected to blow apart in about 0.1-1 ns. Thus,

applying the Lawson criterion for a D-T mixture, with a confinement time of 0.1-1 ns, we would need a density of at least $10^{29} - 10^{30} \text{ m}^{-3}$, which is orders of magnitude greater than ordinary liquid or solid densities for hydrogen. To heat a spherical pellet of diameter 1 mm to a mean thermal energy of 10 keV per particle, the total thermal energy that must be supplied is about:

$$E_{th} \approx 4/3 \pi (0.5 \text{ mm})^3 \times 10^{29} \text{ m}^{-3} \times 10^4 \text{ eV} \approx 10^5 \text{ J}$$

This means we must supply an energy of the order of 0.1 MJ in about 1 ns, i.e. a net power of 10^{14} W ! This is the best-case scenario considering that a substantial amount of energy supplied to the pellet is absorbed through various processes, thus the estimate of the total energy we must supply to heat and compress the core of the pellet should be increased by a factor 10. Furthermore, lasers are usually inefficient to convert electrical energy into photons, and a 10% efficiency can be considered as an optimistic assumption. Therefore, the electrical power needed for the lasers can easily be $10^{16}-10^{17} \text{ W}$! Fortunately, this power would need to be provided only for a very short time interval ($\sim \text{ns}$), but the estimated peak-power value is still extremely high if one considers that the entire electrical generating capacity of the world is $\sim 10^{13} \text{ W}$. To run an inertial confinement reactor at a net energy gain, it is necessary to considerably exceed the Lawson criterion; compressions around 1000 times ordinary solid density and temperatures above 10 keV thermal energy per particle are required. The sequence of processes in laser-driven fusion can be summarised as follows: i) a pellet is injected into the machine and is simultaneously struck from many directions by intense laser pulses; ii) the outer layer of the solid pellet is immediately vaporized and forms a plasma, which continues to absorb the laser radiation; iii) the plasma itself is unconfined and rapidly “blows off”, or *ablates*, which drives a compressional shock wave back into the remaining core of the pellet (according to Newton’s third law); (iv) this shock wave compresses and heats the core to the point at which thermonuclear ignition can occur at the highest density region near the centre; (v) the α -particles resulting from the fusion events rapidly lose their energy in collisions with ions in the dense fuel, thus contributing to additional heating of the pellet; (vi) the thermonuclear burn propagates outwards, finally blowing the pellet apart and ending the nuclear fusion process. This sequence is schematically represented in Fig.4.20.

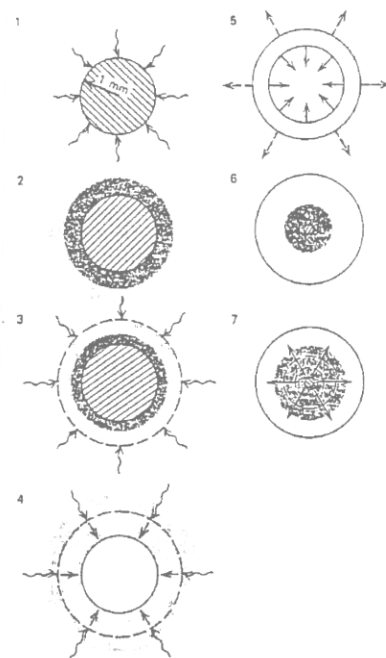


Figure 4.20 Sequence of stages in inertial confinement fusion: (1) pellet irradiation by lasers; (2) plasma formation; (3) further laser beam absorption; (4) ablation and resulting imploding shock wave; (5) shock wave compressing core; (6) ignition of core; (7) burn propagating outward (*from Krane*)

Unfortunately, nuclear fusion is also used for thermonuclear weapons. Once the first thermonuclear explosives were detonated by the United States and the USSR in the early 1950s, the fission explosives in the strategic arsenals of both nations were soon replaced with fusion-based explosive with energies 2-3 orders of magnitude greater than the early fission weapons, thus passing from a kiloton-range to a megaton-range energy. Fusion weapons includes a fission explosive as an initiator. The radiation from the fission explosion is responsible for heating and compressing the thermonuclear fuel. Present-day weapons use solid lithium deuteride as fuel. The neutrons released from the primary fission explosion (and subsequent fusions) convert the ${}^6\text{Li}$ into tritium:



Even for low-energy neutrons, the tritium carries enough energy (2.7 MeV) to easily penetrate the D-T Coulomb barrier and initiate the fusion reactions. Thus, similarly to the inertial confinement approach of controlled fusion, the heat, neutrons, and α -particles contribute to sustaining the reaction until the expansion of the fuel terminates the process. The fast neutrons released in the fusion can be used to add additional energy to the explosive by surrounding the fusion fuel with a casing of ${}^{238}\text{U}$, which fissions with fast neutrons. The operation and energy released in a thermonuclear weapon are thus dependent on a fission-fusion-fission cycle.

5. INTERACTION OF RADIATION WITH MATTER

Detectors for nuclear radiation are selected and optimized based on the type and features of radiation one needs to measure. For low energy (MeV) charged particles, e.g. from alpha decay, very thin detectors are sufficient, as the maximum range of these particles in solid state matter is typically less than 100 μm. On the other hand, gamma-rays have a large range and may require detectors with a thickness of several tens of centimetres to be converted into an electronic signal.

5.1 Ions

Coulomb scattering of charged particles by nuclei (known as *Rutherford scattering*) is an important process in nuclear physics. Nevertheless, it plays no major role in the loss of energy of charge particles interacting with solid matter, e.g. a solid state detector. In fact, since the nuclei of the detector material occupy only a very small fraction of the volume of their atoms ($\sim 10^{-15}$), it is roughly 10^{15} times more probable for the incident particle to collide with an electron rather than a nucleus. Therefore, a mechanism known as *Coulomb scattering* by the atomic electrons of the detector has the dominant effect. Conservation of energy and momentum in a head-on elastic collision between a heavy particle of mass M and an electron of mass m (at rest) allows to calculate the loss of kinetic energy of the incident particle as follows:

$$\Delta T = T \left(\frac{4m}{M} \right) \quad (5.1)$$

For a 5-MeV α-particle, the corresponding energy loss is only 2.7 keV, thus the following conclusions can be drawn:

- The incident particle can lose its energy only after several thousands of collisions, considering that most collisions will not be head-on (the energy loss in each collision will be much smaller than in equation (5.1)).
- The incident heavy particle (ion) is deflected by a very small angle in a collision with a light electron, thus the ion follows a nearly straight-line path.
- The incident particle loses energy gradually but continuously along its path, thus after travelling a certain distance (particle *range*), it has lost all its energy. The range depends on the type of particle, material, and energy of the particle. Fig.5.1 shows track of α-particles measured by a detector called *cloud-chamber*; beyond a well-defined distance no α-particle can propagate in the given material. Typically, a quantity known as “mean range” is used to indicate that one-half the particles have longer ranges and one-half shorter than this value.

- The energy needed to ionize an atom of a material is relatively low (order of 10 eV). Thus, ion-electron collisions will transfer enough energy to ionize the atom. If the energy transferred to the electron is not enough to ionize the atom, the atom is placed into an excited state. Furthermore, electrons gaining energy in the keV range (known as *delta rays*) can themselves produce ions by collisions, resulting in even more *secondary* electrons. In conclusion, the energy loss of the incident particle can be determined by including primary and secondary electrons, as well as atomic excitations.

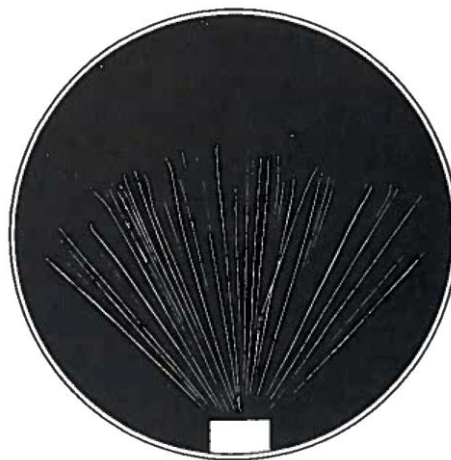


Figure 5.1 Cloud chamber tracks of α -particles from the nuclear decay of ^{210}Po (from Krane)

The range can be estimated by using a semi-empirical relation known as the *Bragg-Kleeman rule*:

$$\frac{R_1}{R_0} \cong \frac{\rho_0 \sqrt{A_1}}{\rho_1 \sqrt{A_0}} \quad (5.2)$$

where R is the range, ρ is the density, and A is the atomic mass of the material; the subscript 0 and 1 refers to the known and unknown ranges and materials, respectively.

The theoretical relationship between range and energy of the incident particle is obtained from a quantum mechanical calculation of the collision process known as *Bethe-Bloch formula*:

$$\frac{dE}{dx} = \left(\frac{e^2}{4\pi\varepsilon_0} \right)^2 \frac{4\pi z^2 N_0 Z \rho}{mc^2 \beta^2 A} \left[\ln \left(\frac{2mc^2 \beta^2}{I} \right) - \ln(1 - \beta^2) - \beta^2 \right] \quad (5.3)$$

where $v = \beta c$ is the velocity of the incident particle, ze is its electric charge, Z , A , and ρ are the atomic number, atomic mass, and density of the stopping material, N_0 is Avogadro's number, and m is the electron mass. The parameter I represent the mean excitation energy of the atomic electrons (averaged over all atomic ionization and excitation processes), which is typically regarded as an empirical constant with a value of the order of $10Z$. Equation (5.3) gives the magnitude of the energy loss of the incident ion per unit length of the given material and is also known as *stopping power*; however, it fails at low energy near the end of the range, primarily

because it does not take into account the capture of electrons by the (now) slow moving particles. The ion range can be calculated by integrating equation (5.3) over the energies of the incident particle:

$$R = \int_T^0 \left(-\frac{dE}{dx} \right)^{-1} dE \quad (5.4)$$

where T represents the initial kinetic energy of the particle.

The Stopping power as a function of the distance travelled inside matter is precisely described by a function known as **Bragg curve**. As the stopping power and the interaction cross section increase at lower energies, toward the end of the trajectory there is an increase in energy lost per unit length. This gives rise to a characteristic *Bragg peak* in the curve that occurs just before the particle comes to a complete stop. This feature is exploited for example for radiation therapy (hadron-therapy approach), since it allows a more precise spatial delivery of the dose at the desired location.

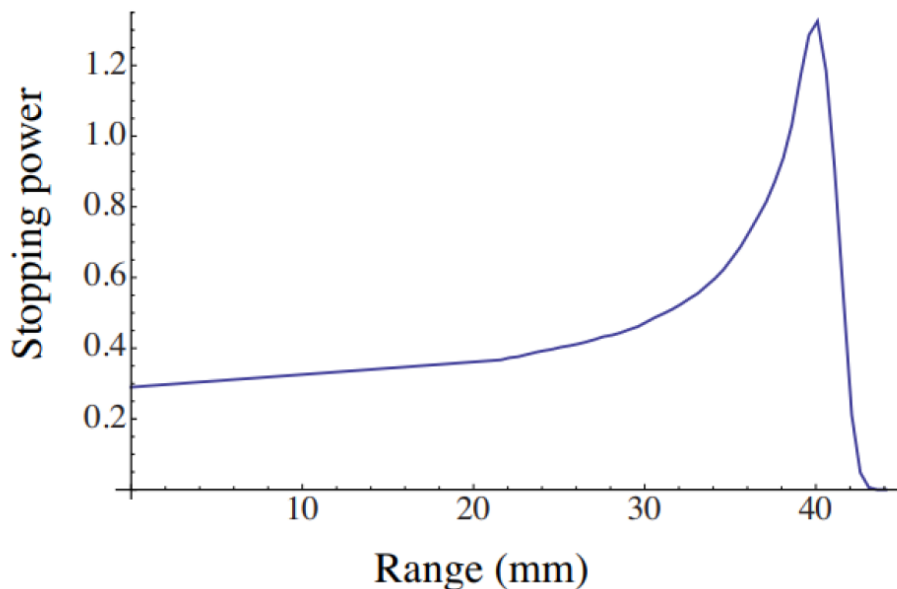


Figure 5.2 Bragg curve for protons (from Cappellaro)

5.2 Electrons

Electrons (and positrons) also interact through Coulomb scattering from atomic electrons. However, there are clear differences with respect to ion scattering in matter:

- Electrons typically travel at relativistic speed (e.g. those emitted in β decay).
- Electrons suffer large deflections in collisions with other electrons and follow unpredictable paths, thus the range is very different from the length of the path that the electron follows.

- In head-on collisions, a large fraction of the incident electron energy can be transferred to the struck electron.
- The electron is subject to large accelerations due to rapid changes in the direction and magnitude of its velocity, thus it must radiate electromagnetic energy (*bremsstrahlung radiation*)

The expressions for the energy loss per unit path length for electrons, also derived by Bethe, are the followings:

$$\left(\frac{dE}{dx}\right)_c = \left(\frac{e^2}{4\pi\epsilon_0}\right)^2 \frac{2\pi N_0 Z\rho}{mc^2\beta^2 A} \left[\ln \frac{T(T+mc^2)^2\beta^2}{2I^2mc^2} + (1-\beta^2) - (2\sqrt{1-\beta^2} - 1 + \beta^2)\ln 2 + \frac{1}{8}(1-\sqrt{1-\beta^2})^2 \right] \quad (5.5)$$

$$\left(\frac{dE}{dx}\right)_r = \left(\frac{e^2}{4\pi\epsilon_0}\right)^2 \frac{Z^2 N_0 (T+mc^2)\rho}{137m^2 c^4 A} \left[4\ln \frac{2(T+mc^2)}{mc^2} - \frac{4}{3} \right] \quad (5.6)$$

where T is the kinetic energy of the incident electron. The subscripts *c* and *r* stand for the energy losses due to collisions and radiation. The total energy loss is given by the sum of these two contributions:

$$\frac{dE}{dx} = \left(\frac{dE}{dx}\right)_c + \left(\frac{dE}{dx}\right)_r \quad (5.7)$$

The radiative term is significant only at high energy of the incident particle and in heavy materials. Although calculations of the range of electrons could be in principle done by integrating equation (5.7) over the electron path, in practice this is a very difficult process due to the random nature of this path. In practice, empirical data on absorption of beams of monoenergetic electrons are used to generate range-energy relationships for electrons.

An important effect of relativistic electrons propagating in a medium is known as ***Cherenkov radiation***. This effect occurs when a charged particle, typically an electron, travels through a dielectric (can be polarized electrically) medium with a speed greater than the speed of light in the medium. From a classical point of view, it is known that charged particles emit electromagnetic waves that will form spherical wavefronts propagating with the phase velocity of the given medium. In response, when any charged particle passes through a medium, the particles of the medium will polarize around it. Thus, the charged particle excites the molecules in the polarizable medium and then the molecules re-emit the energy given as photons. These photons form spherical wavefronts which can be seen originating from the moving particle. If the velocity of the charged particle is lower than the speed of light in the medium ($v < c/n$, where n is the index of refraction), then the polarization field which forms around the moving particle is symmetric. However, if the velocity of the charged particle is higher than the speed of light in the medium (v

$> c/n$), then the polarization field is asymmetric along the direction of motion of the particle. This results in overlapping waveforms and constructive interference leads to an observed cone-like light signal at a characteristic angle: the Cherenkov radiation. In other words, a charged particle can generate a light shock wave as it travels through an insulator. These are based on the analogue of a supersonic boom. The angle of the light wavefront is related to the speed of the particles by the relation:

$$\cos \theta = \frac{1}{\beta n} \quad (5.8)$$

Measuring this angle allows to determine the speed of the electron. This technique is extremely useful for nuclear detectors called *threshold counters*, because if one sees any light coming out from the detector, they know that the velocity of the electrons is larger than c/n .

5.3 Photons

Energetic photons (γ - and X-rays) interact with matter mainly through three different processes: (i) photoelectric effect, (ii) Compton scattering, and (iii) pair production.

In the **photoelectric effect**, a photon is absorbed by an atom and one of the atomic electrons (*photoelectron*) is released. The kinetic energy of the electron can be calculated as follows:

$$T_e = E_\gamma - B_e \quad (5.9)$$

where E_γ is the photon energy and B_e is the binding energy of the electron. Photoelectric absorption is most significant for low energy photons (~ 100 keV), increases drastically with the atomic number Z of the atoms in the absorber ($\sim Z^4$), and decreases rapidly with increasing the photon energy ($\sim E^3 \gamma$).

In **Compton scattering** a photon scatters from a nearly free atomic electron, resulting in a less energetic photon and a scattered electron which carries the energy lost by the incident photon. This process is schematically shown in Fig.5.3. Photon energies before and after the process (E_γ and E'_γ , respectively) and scattering angle (θ) are related by the Compton-scattering formula:

$$E'_\gamma = \frac{E_\gamma}{1 + \frac{E_\gamma}{mc^2}(1 - \cos \theta)} \quad (5.10)$$

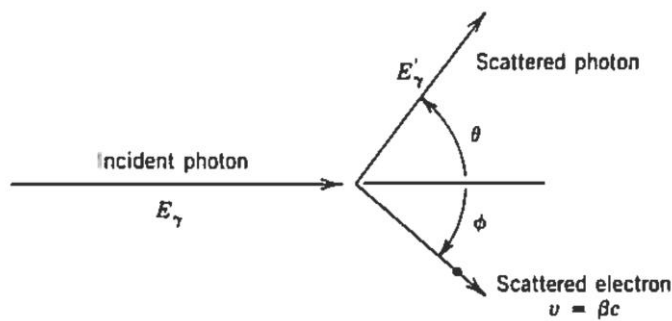


Figure 5.3 Schematic view of the Compton scattering process (from Krane)

In **pair production** a photon creates an electron-positron pair and disappears in the process. The energy balance is given by the following equation:

$$E_\gamma = T_+ + mc^2 + T_- + mc^2 \quad (5.11)$$

Where T_+ and T_- are the energies of the positron and electron produced in the process. Like photoelectric absorption, pair production requires the nearby presence of a massive atom to satisfy momentum conservation. Furthermore, pair production presents a threshold of $2mc^2$ (1.022 MeV), which is obviously the sum of the rest masses of the produced electron and positron. Fig.5.4 clearly shows that pair production is dominant only for high energy photons compared to the other two processes (> 5 MeV).

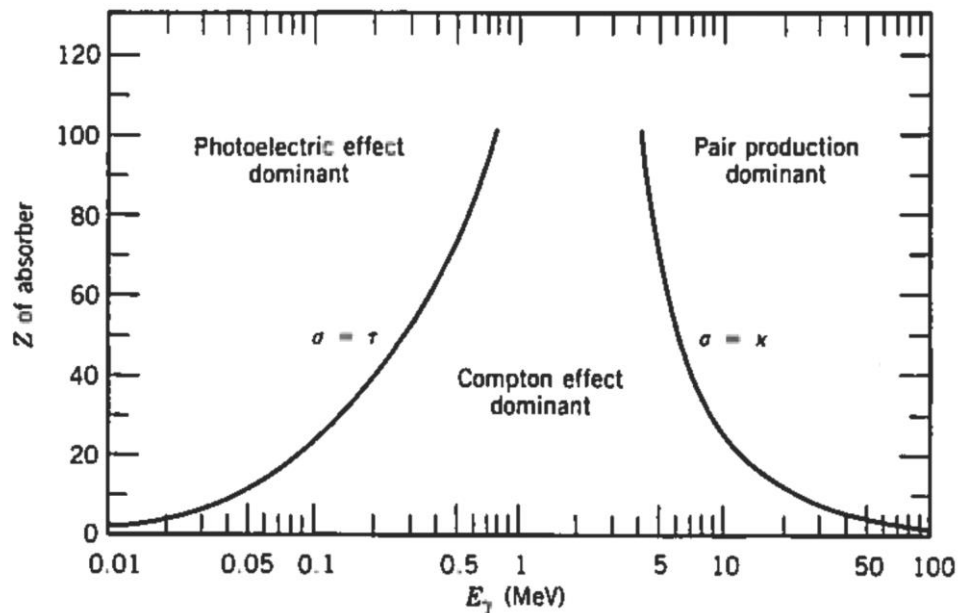


Figure 5.4 Regions of dominance of the three γ -ray interaction processes (from Krane)

Let us consider a high collimated beam of monoenergetic photons incident on a material of thickness t , as shown in Fig.5.5. The beam from the source S is collimated and then scattered or absorbed by the material. The remaining beam intensity, I , reaches the detector D . The photon may undergo photoelectric absorption or pair production (and disappear), or Compton scattering (and be deflected from reaching the detector). The photons reaching the detector are those that have no interaction at all. Thus, there must be less photons than there were in the incident beam, but with the same energy. This scenario is very different than the one occurring with high energy charged particles where, assuming a small enough material thickness t , will all reach the detector (long range), but their energy will change since they will be slowed down in the material. The total probability per unit length μ for removal of a photon is called *total linear attenuation coefficient*, and is simply the sum of the respective probabilities for photoelectric absorption (τ), Compton scattering (σ), and pair production (κ):

$$\mu = \tau + \sigma + \kappa \quad (5.12)$$

All quantities in equation (5.12) have dimensions of (length)⁻¹. The fractional loss in photon intensity when crossing any thickness dx of material is given by:

$$\frac{dI}{I} = -\mu dx \quad (5.13)$$

Thus, considering a thickness t :

$$I = I_0 e^{-\mu t} \quad (5.14)$$

Let us consider studying the intensity loss of a monoenergetic (1 MeV) beams of α -particles, electrons, and γ -rays in a geometry such as that shown in Fig.5.5. As shown in Fig.5.6, the α -particles intensity is undiminished until the thickness is very close to the mean ion range, and then it rapidly drops to zero. The electron intensity starts to decrease slowly even for material thicknesses much smaller than the particle range. However, the γ -ray intensity decreases exponentially.

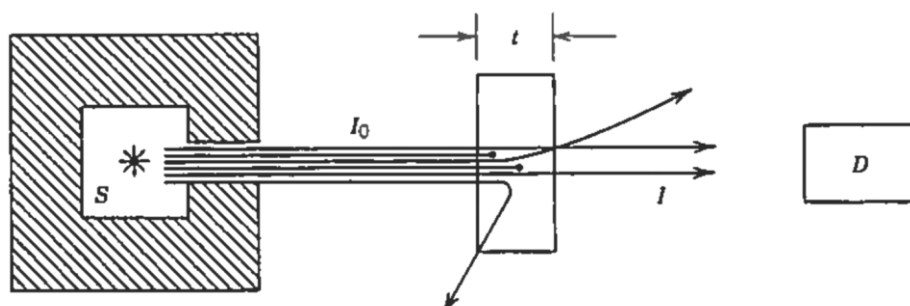


Figure 5.5 Scheme of an experiment to measure absorption of photons in a material of known thickness (from Krane)

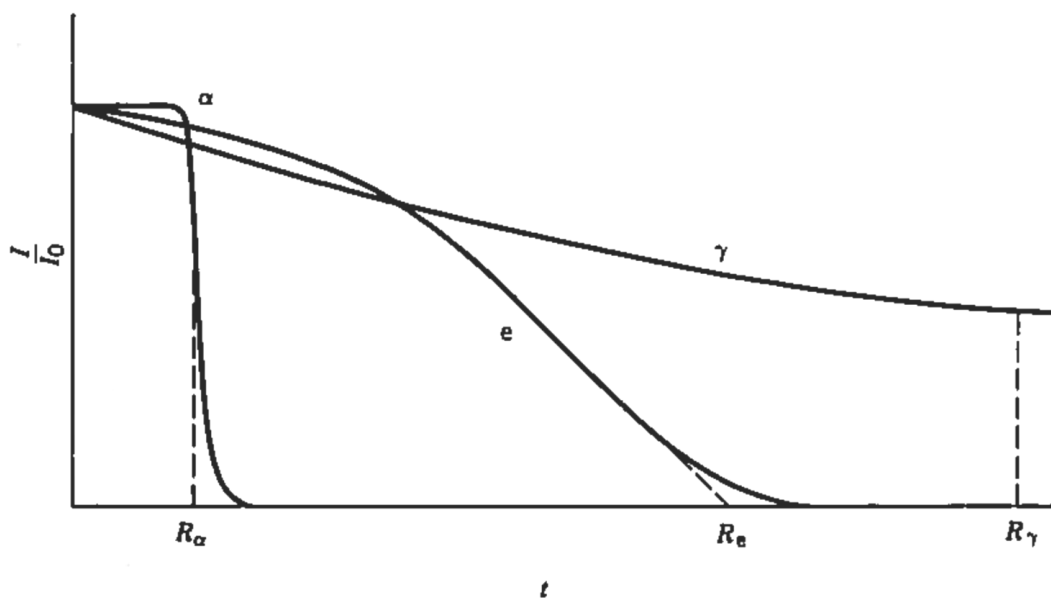


Figure 5.6 Transmitted radiation intensity measured in a setup like the one shown in Fig.5.5 (from Krane)

5.4 Radiation Detectors

A brief description of three of the most widely used detectors for nuclear radiation is reported below. The common function of many detectors is to separate and count the ions, or electrons, formed because of the incident radiation passing through the detector. The **ionization chamber** is the simplest detector accomplishing this function. It can be regarded as a parallel-plate capacitor in which the region between the plates is filled with a gas (often air). The electric field in this region keeps the ions from recombining with the electrons and allows to measure a cloud of electrons drifting toward the plate at positive potential, while the ions drift toward the plate at negative potential. The average energy to produce an ion in air is about 34 eV; thus a 1-MeV radiation produces a maximum of $\sim 3 \times 10^4$ ions and electrons. For a medium-sized chamber with a surface of 10×10 cm and a plate separation of 1 cm, the corresponding capacitance is 8.9×10^{-12} F, and the resulting signal pulse produces a voltage of:

$$\frac{(3 \times 10^4 \text{ ions})(1.6 \times 10^{-19} \text{ C/ion})}{8.9 \times 10^{-12}} \cong 0.5 \text{ mV}$$

This is obviously a small signal that then needs to be considerably amplified before being analysed with standard electronics. The signal amplitude is proportional to the number of ions formed, thus to the energy deposited by the incident radiation, and is independent of the voltage between the plates. The ionization chamber is widely used as a radiation monitor in research laboratories for radiation protection purposes. The radiation intensity is recorded as a current representing the interaction of many types of radiation during the response time of the chamber. The current output is proportional both to the activity of the source and to the energy of the radiation. As

already mentioned, to use a gas-filled detector to measure individual radiation pulses, it is necessary to provide a considerable amplification of the signal. This can be done by increasing the voltage applied on the plates to larger values (~ 1 kV). In fact, the larger electric field accelerates the electrons produced in the ionization process rather than slowly drifting them. The accelerated electrons can acquire enough energies to create new ionized atoms and, in turn, more electrons to be accelerated. This rapid amplification process that allows to produce secondary ionizations is known as *Townsend avalanche*. If the chamber is always operated such that the number of secondary events is proportional to the number of primary events, the device is called ***proportional counter***. The geometry of a proportional counter is usually cylindrical, as shown in Fig.5.7. The electric field in this geometry at a radius r is:

$$E(r) = \frac{V}{r \ln(\frac{a}{b})} \quad (5.15)$$

where b is the inner radius of the cathode and a is the outer radius of the anode wire. The avalanche occurs in the high field region near the anode wire. However, this region represents only a very small fraction of the chamber volume. Since the output signal of a proportional counter comes mainly from the avalanche process that occurs very rapidly, the timing is determined by the *drift time* of the primary electrons from the point of the original ion formation to the vicinity of the anode wire where the avalanche occurs. This time is of the order of microseconds; thus, the counter can operate in a pulse mode at a repetition rate of about 10^6 /s.

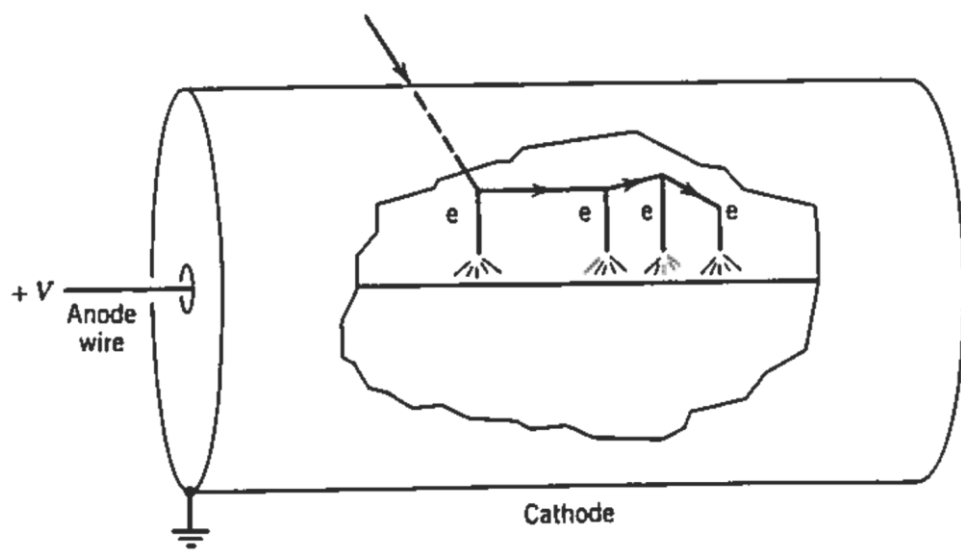


Figure 5.7 Scheme of a cylindrical proportional counter (from Krane)

If the electric field is increased to even large values, *secondary avalanches* can occur due to photons emitted by atoms excited in the original (or in subsequent) avalanche. Such photons can travel relatively far from the region of the original avalanche, and the entire tube soon participates

in the avalanche process. In this geometry, the amplification factor can be as large as 10^{10} . Since the entire tube participates for every incident event, no information on the energy of the original radiation can be retrieved, thus all kinds of incident radiation produce identical outputs if the incident beam flux is the same. Such region of operation is known as the *Geiger-Müller region* and counters based on this principle are usually known as *Geiger counters*. They are very common portable radiation monitoring systems. The output signal from a Geiger counter consists of the collected electrons from all the avalanche processes, thus the signal is of the order of 1 V and no further amplification is usually required. The collection time is still of the order of microseconds, but in this time the positive ions do not move far from the avalanche region. Therefore, there is a positively charged ion cloud surrounding the anode that reduces the electric field intensity and eventually terminates the avalanche process. The cycle would then be completed after the positive ions have drifted to the cathode and become neutralized, which takes 10^{-4} - 10^{-3} s. Fig.5.8 summarizes various regions of operation of different gas-filled counters.

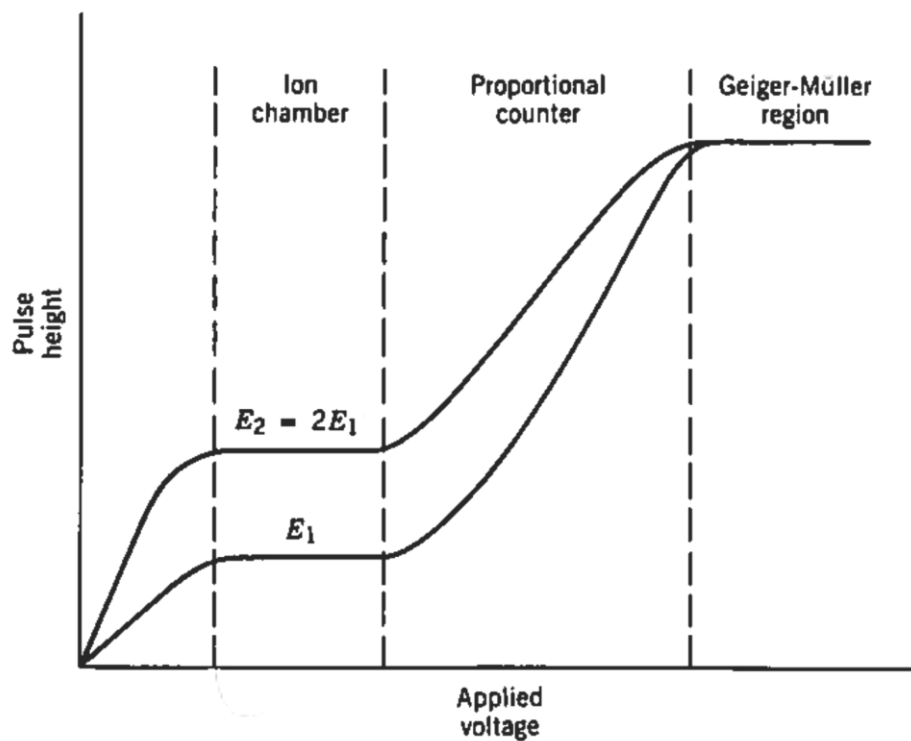


Figure 5.8 Signal amplitude produced by different gas-filled counters (from Krane)

A disadvantage of gas-filled counters is the low efficiency for many types of radiation produced in nuclear processes. This is clear if one considers that the range in air of a 1-MeV γ -ray is of the order of 100 m! Solid state detectors have higher densities, thus provide reasonable absorption probabilities for detectors of reasonable size. However, two contradictory criteria must be satisfied to build an optimized solid-state detector: (i) the material must support a large electric

field to be able to collect electrons and ions to generate an electronic pulse, also producing negligible current in the absence of radiation (low background noise); (ii) electrons must be easily removed from atoms in large numbers by the incident radiation, and they also must be able to travel easily through the material. In fact, the ions themselves do not move in a solid, but the electronic vacancy (or “hole”) is filled by successive electron transfer from one atom to the next, so that the “hole” appears to travel. The first condition supports the choice of an insulating material, while the second suggests using a conductor. Thus, the compromise is to use a semiconductor material. **Scintillation counters** are one of the best choices of materials. The electrons that are formed in the ionization process are not the same electrons generating the electronic pulse: light is the intermediary between the ionization and the pulse electrons. The basic processes in a scintillator detector are schematically shown in Fig.5.9: (i) the incident radiation enters the detector and a large number of interactions take place, resulting in excited atomic states; (ii) the excited states rapidly emit visible light, thus the material *fluoresce*; (iii) the light strikes a photosensitive surface and this process releases at most a photoelectron per photon; (iv) these secondary electrons are multiplied, accelerated, and formed into the output pulse in the *photomultiplier* tube. There are two basic types of scintillation detectors: based on organic material and based on inorganic material. In *organic scintillators* (solid or liquid) the interactions between the molecules are relatively weak, thus it is possible to discuss their properties in terms of discrete excited states of the molecules. There are two ways in which a molecule can absorb energy: (i) electrons brought to higher excited states, (ii) atoms in the molecule can vibrate against one another. Typical spacing of vibrational energies is about 0.1 eV, while the electronic excitations are of the order of a few eV. This is schematically represented in Fig.5.10. The incoming radiation interacts with many molecules, loosing a few eV at each interaction as it excites the molecule. Several possible vibrational states, as well as electronic states are excited. The molecules decay quickly (~ 1 ps) to the lowest vibrational state of the given electronic excited state, and then decays (~ 10 ns) to one of the vibrational states of the electronic ground state. It is worth noting that a scintillator must be transparent to its own radiation to be able to measure a useful signal.

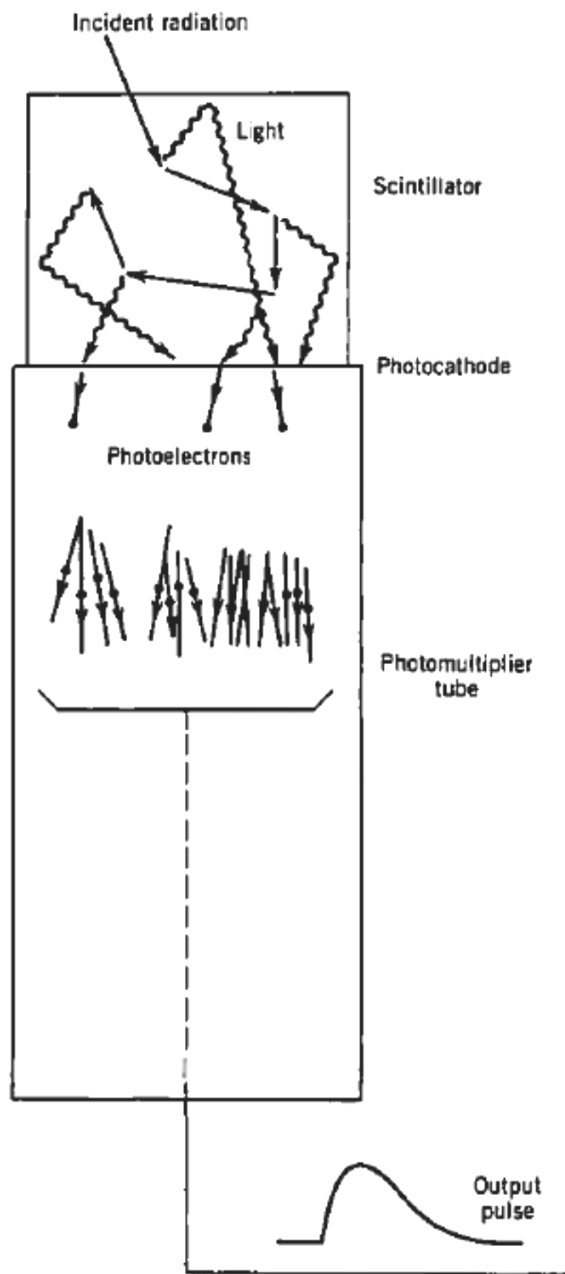


Figure 5.9 Basic scheme of a scintillator detector (*from Krane*)

The most used *inorganic scintillator* is NaI, the single crystal of an alkali halide. The single-crystal feature comes from the transparency requirement. In fact, reflections and absorption at the crystal faces would be detrimental. The collective interactions of the atoms in a crystal cause the discrete energy levels to “smear out” into a series of energy bands. The highest bands are the *valence band* and the *conduction band*, as schematically shown in Fig.5.11. In an insulating material such as NaI, the valence-band states are generally full, and the conduction-band states are empty. An incoming radiation can excite an electron across the *energy gap* (~ 4 eV) and into the conduction band. Eventually, the electron loses energy by emission of a photon and drops back into the valence band. To increase the probability for photon emission and to reduce self-

absorption of the light, small number of impurities called *activators* are added to the crystal. A commonly used activator is thallium, and these specific detectors are known as NaI(Tl). The activator provides states in the energy gap and the light emission takes place between the activator states. In the case of NaI, the wavelength of maximum emission is shifted from 303 nm in pure NaI to 410 nm in NaI(Tl). Absorption at this energy (wavelength) cannot occur in NaI(Tl) because the activator ground states are not populated; furthermore, the change in wavelength from ultraviolet to visible provides a better matching with the maximum sensitivity of most photomultiplier tubes.

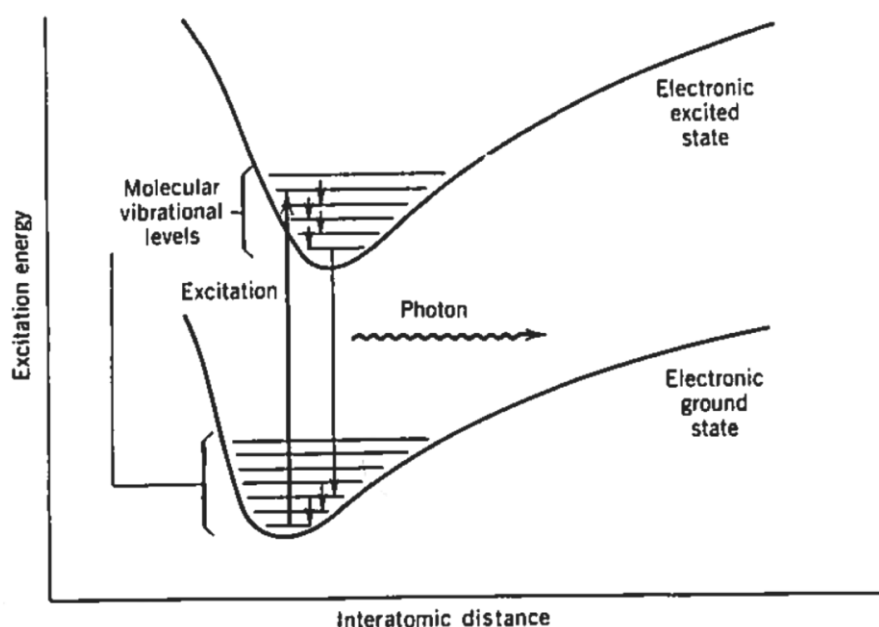


Figure 5.10 Electronic structure in an organic scintillator (from Krane)

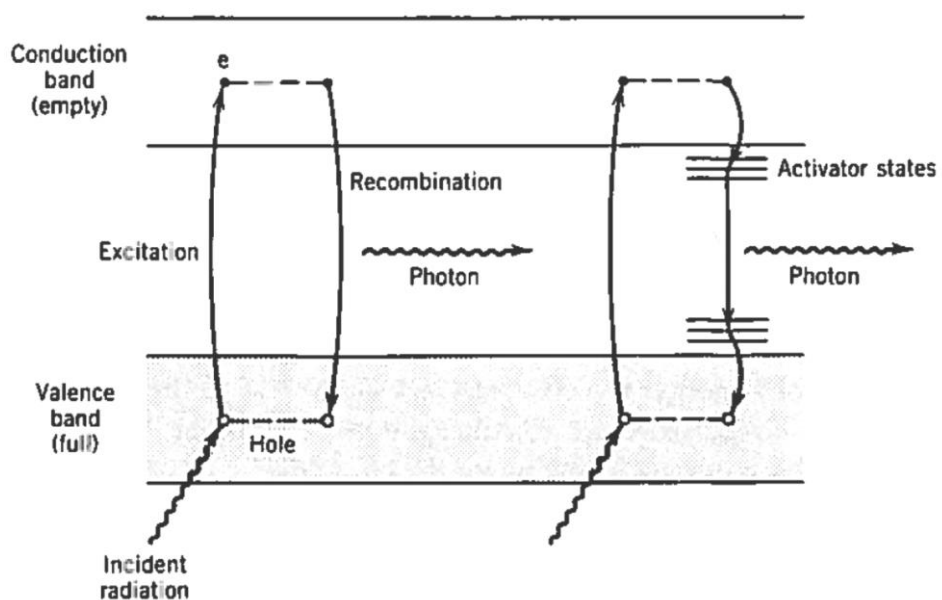


Figure 5.11 Energy bands in a crystal (from Krane)

A scheme of a photomultiplier tube is shown in Fig.5.12. The number of electrons released at the photocathode is smaller than the number of incident photons. These electrons are multiplied and focused by a series of electrodes called dynodes. The dynodes are connected to a voltage chain produced by a high-voltage supply and a series of voltage dividers. The typical potential difference between adjacent dynodes is about 100 V. Thus, electrons strike the dynodes with an energy of \sim 100 eV. The dynodes are made of material with a high probability of secondary electron emission. Considering that it takes 2-3 eV to release a secondary electron, the theoretical gain in the number of electrons is \sim 30-50. However, the practical gain is only \sim 5 because secondary electrons are released in random directions in the material, thus only a part of them will be released from the surface. Nevertheless, a photomultiplier with a 10-dynode tube will have an overall gain of \sim 5^{10} , i.e. \sim 10^7 !

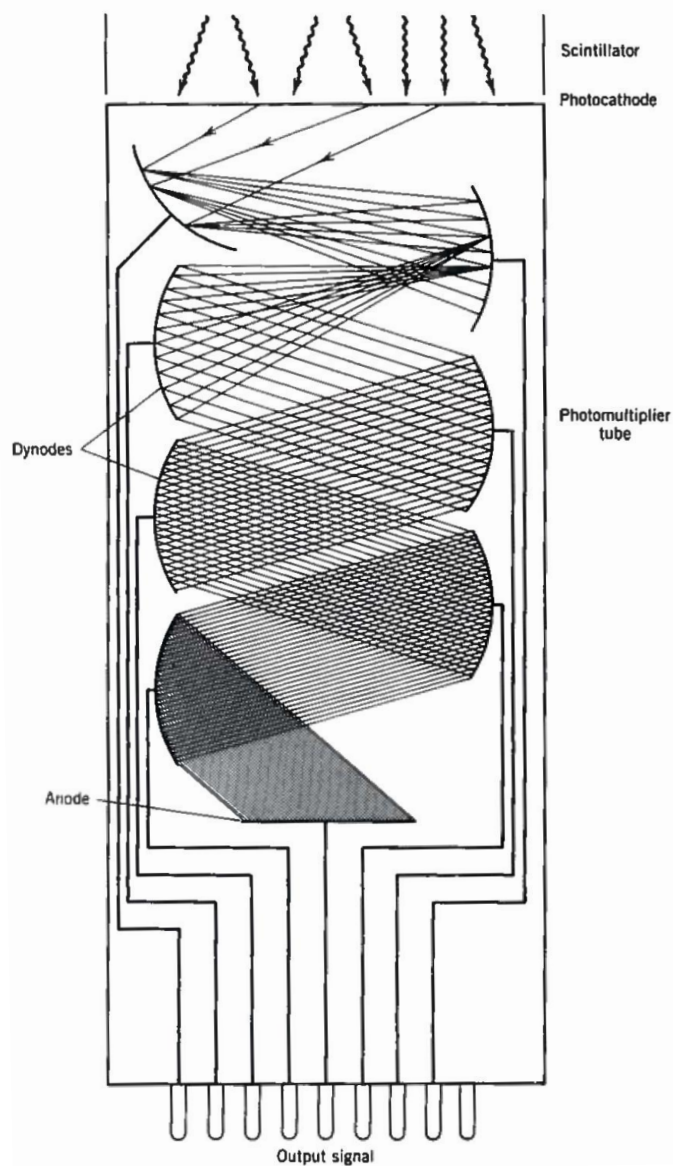
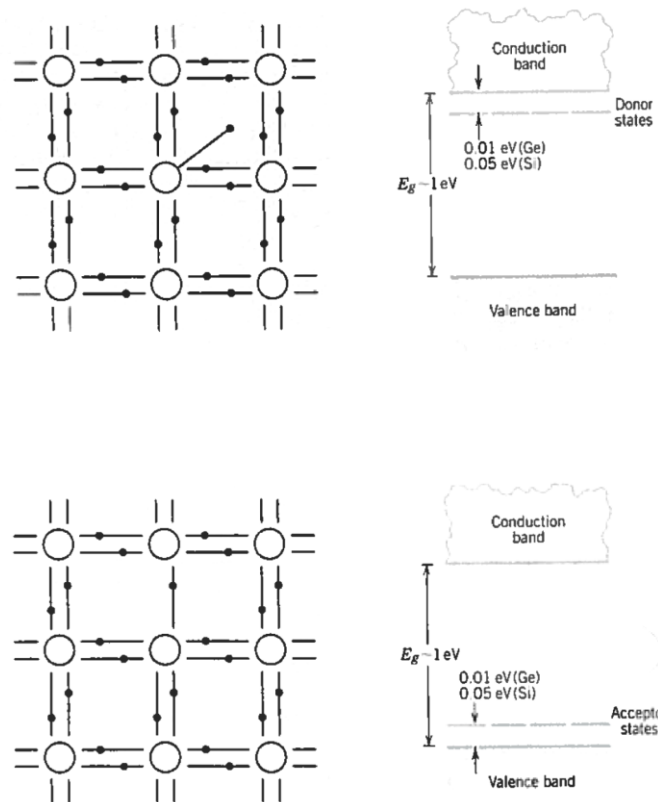
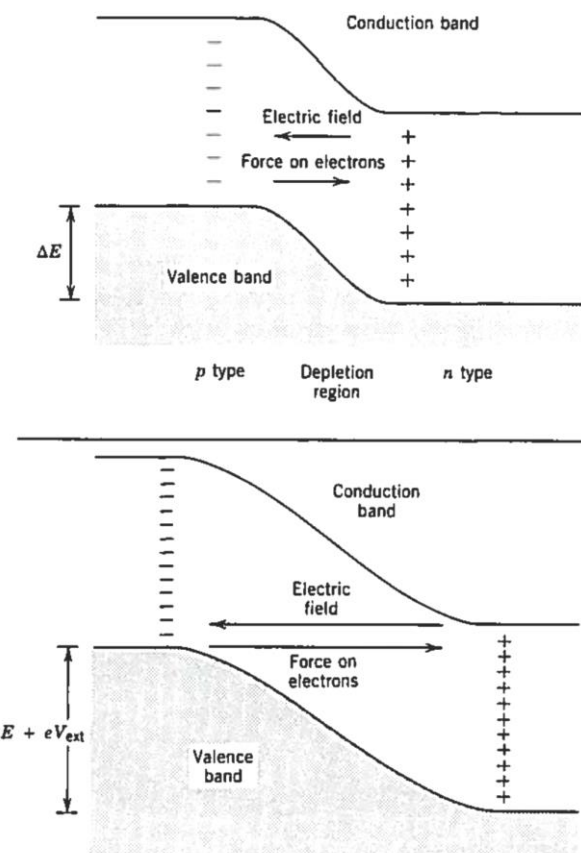


Figure 5.12 Scheme of a photomultiplier tube (*from Krane*)

Solid **semiconductor detectors** (germanium and silicon) can be used in alternative to scintillators to characterize nuclear radiation. Both Ge and Si form solid crystals with four covalent bonds formed by the valence-4 atoms. The band structure shows a filled valence band and an empty conduction band. The main difference between an insulator and a semiconductor is in the size of the energy gap, which is typically around 5 eV in an insulator and 1 eV in a semiconductor. Typically, small concentration of materials called *dopants* are added to the semiconductor to control the electrical conduction. These dopants are usually atoms with valence 3 or 5, which are introduced into the semiconductor lattice. In the case of valence-5 atoms (P, As, Sb), four of the electrons form covalent bonds with neighbouring Si or Ge. The fifth electron moves through the lattice and forms a set of discrete *donor states* just below the conduction band. Because there is an excess of negative charge carriers (electrons), this material is known as *n-type semiconductor*. Alternatively, one could use valence-3 atoms, which will form covalent bonds with four neighbouring atoms in the crystal and produce an excess of holes. These form *acceptor states* just above the valence band, and the material is known as *p-type semiconductor* because the primary charge carriers are the positively charged holes. Fig.5.13 shows the band structure of these two types of semiconductors. It is worth noting that n-type and p-type refers to the sign of the charge of the primary carriers of electric current, but the materials themselves are electrically neutral. When a p-type and an n-type material are brought into contact, the electrons from the n-type material can diffuse across the junction into the p-type material to combine with the holes. Near the junction, the charge carriers are neutralized and create a region called *depletion region*. The diffusion of electrons from the n-type region leaves behind ionized fixed donor sites, while the diffusion of holes from the p-type region leaves behind negatively charged fixed acceptor sites. The space charge from the fixed sites creates an electric field which eventually prevents further migration. The result of this process is the creation of a *junction diode*, as schematically shown in Fig.5.14. If an incident radiation enters the depletion region and creates electron-hole pairs, the result is very similar to the one described for an ionization chamber (the depletion region can be thought as a parallel-plate capacitor). Electrons flow in one direction and holes in the opposite one. The total number of collected electrons can form an electronic pulse with an amplitude proportional to the energy released by the incident radiation. Normally, these detectors are operated with large, reversed bias voltages (1-3 kV), which allows to increase (i) the magnitude of the electric field in the depletion region, thus making charge collection more efficient, and (ii) the dimension of the depletion region (forcing more carriers to drift across from one type of material to another), thus increasing the sensitive volume of the detector.

**Figure 5.13** Band structures of n-type and p-type semiconductors (from Krane)**Figure 5.14** Junction diode without (top) and with (bottom) an external reversed bias voltage (from Krane)

6. APPLICATIONS OF NUCLEAR PHYSICS

Some applications of nuclear techniques, such as fission and fusion for energy production or carbon-14 dating, have already been discussed. However, nuclear physics methods can be used in several additional applications. Some of such applications will be briefly discussed in the following.

6.1 Elemental Analysis

Nuclear physics techniques usually present advantages over traditional chemical techniques for the determination of the elemental composition of various materials. There are four techniques widely used for elemental analysis: (i) *neutron activation analysis* (NAA), (ii) *particle-induced X-ray emission* (PIXE), (iii) mass spectrometry, and (iv) Rutherford backscattering.

In ***neutron activation analysis*** (NAA), a small sample of the material under investigation is exposed to a flux of thermal neutrons from a reactor. Nuclei of stable elements can become radioactive through neutron capture (n, γ) reactions. Many of these radioactive nuclei decay through β and subsequent γ reactions, and the emitted γ -rays are characteristic of the given decay process. Thus, by means of a precise determination of the γ -ray energies, obtained when the irradiated sample is removed from the reactor and counted with a semiconductor Ge detector, it is possible to determine which isotopes are present in the sample, as well as the concentration of the isotope. NAA is a non-destructive method since, aside from a small amount of induced radioactivity, the sample is unaffected after the analysis. This is a key feature when one deals with a valuable painting or fragment of ancient pottery, since the sample can be restored in its original condition. On the other hand, ordinary chemical analysis techniques require the sample to be permanently altered. Detailed NAA of the mineral content of various ancient pottery fragments show which pieces have common origins, and systematic studies of fragments found at various archaeological excavations can help to trace the trading routes of ancient cultures. NAA has applications in any area in which a quantitative knowledge of very small amount of material present in the sample is required. For instance, atmospheric pollutants can be analysed to investigate the presence of elements that can indicate the origin of the pollution. Furthermore, NAA has application in forensic science for criminal investigations. In fact, rifle and handgun ammunitions contain Ba and Sb compounds, and firing a gun leaves residual traces of these elements in microgram quantities on the back of the hand. Additionally, arsenic and mercury poisoning can be detected in the hair.

Particle-induced X-ray emission (PIXE) is also used for analysis of small quantities of elements. In PIXE, a sample is placed in the target area of an accelerator and bombarded with protons. The

Coulomb interaction between the incident particle and the target can result in the ionization of the target atoms. Then, the vacancies are filled by the outer electrons and characteristic X-rays are emitted. The measurement of the emitted X-rays allows to deduce the element present in the sample. However, PIXE is an analysis technique limited to the surface of the sample due to the short range of charged particles in matter and to the low energy of the emitted X-rays (10-100 keV) that are absorbed by the sample itself. Furthermore, the cross section of K-shell ionization is of the order of 100 b for light elements but decreases to below 1 b for heavy elements. Thus, the sensitivity of PIXE decreases with increasing Z of the sample, as shown in Fig.6.1. The ionization cross sections also vary with the incident proton energy and present a maximum at:

$$T_p = \frac{m_p}{m_e} E_K \quad (6.1)$$

where T_p is the incident proton energy and E_K is the ionization energy. It can be demonstrated from equation (6.1) that the cross section reaches a maximum when the incident proton has a velocity equal to the Bohr orbital velocity of the electron. PIXE is a technique quite comparable to NAA in its sensitivity, but for many elements it can be superior to NAA. In fact, while NAA is limited in its selectivity by isotopes that may have small cross sections, short radioactive decay times, or no γ emission, PIXE does not present such limitations and all elements can be detected with a relatively uniform sensitivity. However, one disadvantage is that the X-ray spectrum contains many components of the K-shell and L-shell lines that can interfere, thus making the analysis difficult. A typical PIXE spectrum obtained during bombardment with 2-MeV protons is shown in Fig.6.2.

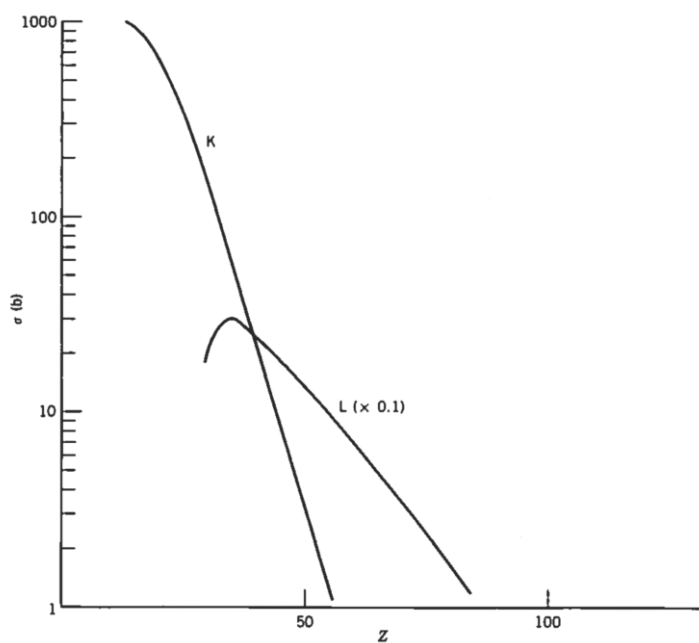


Figure 6.1 Production cross section of X-rays (K-shell and L-shell) for 5-MeV incident protons (from Krane)

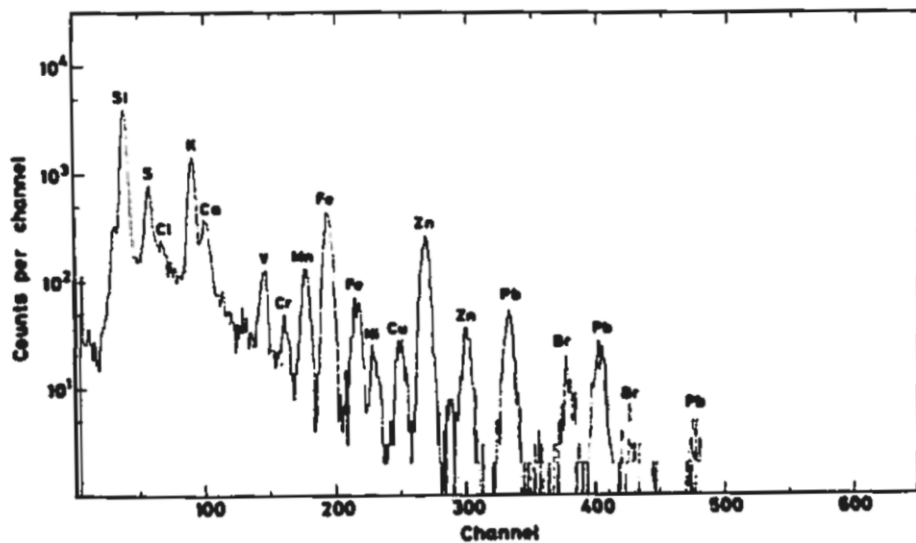


Figure 6.2 Typical PIXE spectrum from a bombardment with a 2-MeV proton beam (*from Krane*)

Nuclear techniques based on radioactive dating of ancient materials, such as C-14 dating, have fundamental limitations in terms of sensitivity of these methods. In fact, in processes involving counting long-lived radioactive decays, only a very small fraction of the atoms present in the sample are counted. This implies the use of large samples or long counting times, which become worse with the increasing age of the sample. For instance, if one considers the ^{14}C decay, its content in present-day organic material is $\sim 10^{-12}$ with respect to ^{12}C , and the decay rate is about 15 per minute per gram of total carbon sample. ^{14}C half-life is 5730 y, thus in a 1-g sample of age $\sim 10^4$ y the decay rate would be $\sim 4/\text{min}$. A statistically relevant measurement of $\sim 10^4$ decays would then take about two days, assuming a 100% efficient detection system. An alternative approach to counting the decay of ^{14}C atoms would be to directly count the atoms. In fact, a mass spectrometer would allow to distinguish ^{14}C from ^{12}C . However, a clear difficulty is present in such a measurement due to the potential presence of contaminants of other mass-14 ions in the sample. For instance, organic matter would be expected to contain ^{14}N and CH_2 . Nuclear accelerators (cyclotrons or tandem) provide the opportunity for mass and charge selection on the output beams. The combination of conventional ion momentum or velocity selectors using electric and magnetic fields, allows **mass spectrometry** to represent considerable advantages over counting of radioactive decays for material dating. In cyclotrons, the resonance condition selects for acceleration only those ions with the wanted charge-to-mass ratio. To determine the age of a sample, it is necessary to measure the amount of the rare isotope relative to the stable one. To make this comparison with a cyclotron, the resonance frequency must be changed. These accelerator-based dating techniques have a sensitivity of $\sim 10^{-15}$ in the $^{14}\text{C}/^{12}\text{C}$ ratio; thus, with only 1 mg of material, it is possible to determine sample ages to $\sim 10^5$ y.

Alpha-particle scattering is used both for qualitative and quantitative analysis. Smoke detectors contain a small quantity of the isotope ^{241}Am ($t_{1/2} = 433$ y, Q-value = 5.6 MeV). Under normal conditions, the α -particles ionize air molecules in the detector; the ions travel to the electrodes and establish a small steady-state current in the device. In case of combustion, heavy ionized atoms are present and, entering the detector, they collide with the ions responsible for the ambient current, thus causing a decrease in the steady-state current that triggers the fire alarm. On the other hand, quantitative analysis can be carried out by observing α -particles scattered at large angles, which is a technique known as **Rutherford backscattering**. Although the nucleus of an atom can often be considered infinitively heavy for an incident α -particle, a small fraction of energy is transmitted to the struck nucleus, and for backscattered α -particles ($\theta \approx 180^\circ$), the energy loss is:

$$\Delta T = T \frac{4m/M}{(1+m/M)^2} \quad (6.2)$$

where T is the incident α -particle energy, m is the α -particle mass, and M is the mass of the target. Fig.6.3 shows example of spectra of backscattered α -particles from which it is possible to deduce the presence of various elements. This technique was used for analysis of soil samples by the Surveyor spacecraft that landed on the Moon (it contained a Rutherford backscattering apparatus).

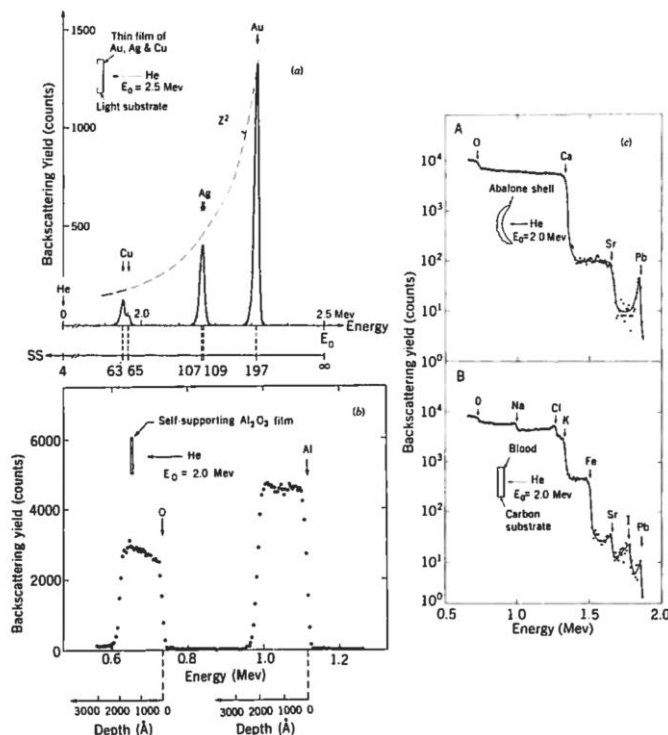


Figure 6.3 (a) Backscattering spectrum of 2.5 MeV α -particle beam from a thin Cu film; (b) in a thicker target; (c) from complex substances (from Krane)

6.2 Nuclear Medicine

The development of advanced techniques in experimental nuclear physics has permitted the implementation of such methods in medicine. This branch of research is called *nuclear medicine*, and in such a framework, nuclear physicists work in close cooperation with physicians in developing and applying these techniques.

There are techniques allowing to form images of specific areas of the body by introducing γ -emitting radioisotopes. The pattern of emitted γ -rays can then be used to produce an image of the given part of the body. The radioisotopes are ingested, and the γ -rays are detected by γ -counters. Currently there are several available pharmaceutical compounds labelled with radioactive isotopes. By choosing the proper compound that tends to accumulate in a specific organ, a local concentration of the given radioisotope can be achieved. The spatial pattern of radioactive emissions then gives a complete picture of the designated organ. One possibility is to scan over the area using a scintillation detector. A narrow collimator confines the detector to observe only a small region (2-3 mm in diameter), and the intensity is recorded by scanning back and forth through a rectangular array. One of the most common scanning techniques allows to produce an image of the brain. This is possible thanks to the so-called "blood-brain barrier". Typically, the brain has a very low absorption for impurities in normal circumstances; however, if there is a tumour the radioisotope can concentrate in the affected region and reveal itself in the scanning image. Another imaging technique is called **positron emission tomography** (PET). In this approach, positron-emitting isotopes are introduced into the area under investigation, and the two 511-keV photons emitted following electron-positron annihilation are observed in a coincidence geometry. A schematic view of this process is shown in Fig.6.4. The two photons are emitted in opposite directions and their detection serves to identify a line along which the original decay must have occurred. From many such events, it is possible to reconstruct the original distribution of radioisotopes and to map an image of the area under investigation. Among the most used isotopes are ^{15}O (2 min), ^{13}N (10 min), ^{11}C (20 min), and ^{18}F (110 min). These isotopes can be produced by a cyclotron, and because of the short half-lives the accelerator must be at the site of the hospital.

Nuclear radiation can be used in medical therapy to destroy unwanted or malfunctioning tissues in the body, such as a cancerous tumour. This method is based on the ionizing ability of nuclear radiation. In brief, the tissue destruction occurs as follows:

- the incident radiation ionizes atoms in molecules of the irradiated material (*physical* change, $t \leq 10^{-16}$ s);

- the ionized molecules participate in chemical reactions giving rise to free radicals or other excited molecules (*chemical change*, $10^{-15} < t < 10^{-3}$ s);
- the free radicals can then be incorporated into complex biological structures at the molecular level and alter their biological function (*biological change*, hours $< t <$ years).

A free radical can be a part of a biologically more complex system (e.g. a chromosome) and can alter the function of the given system, potentially causing its death if it is not able to function any more, or alternatively changing the genetic information that is passed in reproduction, thus the structure of the next generation is fundamentally different (genetic mutation). The critical factor allowing to compare the effect of different types of radiation on living tissues is known as *linear energy transfer* (LET), and measures the energy deposited per unit distance over the path of the radiation (practically the same as dE/dx). Heavy ions and α -particles are examples of high-LET radiation. They generally have short range in matter because they quickly lose their energy in collisions and present typical LET values above 100 keV/ μ m. On the other hand, electrons and photons are particles with low LET (~ 1 keV/ μ m). The main aim of ***radiation therapy*** is to concentrate the radiation damage to the area to be treated and simultaneously to minimize radiation exposure to the patient and damage to the surrounding tissues.

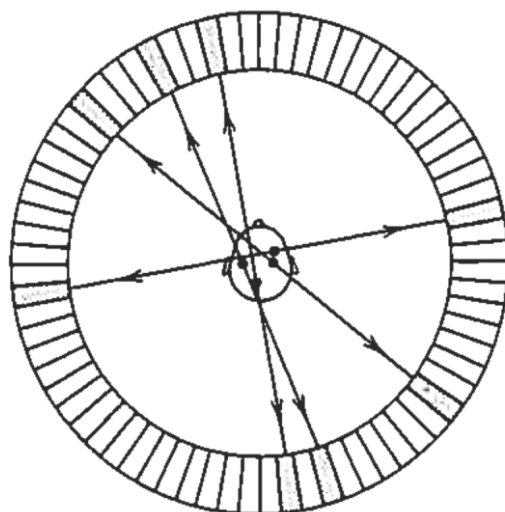


Figure 6.4 Schematic representation of the PET scanning technique (from Krane)